# Study on the membrane pore-formation mechanism of *Vibrio cholerae* cytolysin, a β-barrel pore-forming toxin

*A thesis submitted by*

**Anand Kumar Rai**

*in partial fulfillment of the requirements for the degree of*

**Doctor of Philosophy**


**Indian Institute of Science Education and Research (IISER)**

**Mohali**

February 2016

*Dedicated to My Parents*

## Declaration

The work presented in this thesis has been carried out by me under the guidance of Dr. Kausik Chattopadhyay at Indian Institute of Science Education and Research Mohali. This work has not been submitted in part or in full for a degree, diploma or a fellowship to any other University or Institute. Whenever contributions of others are involved, every effort has been made to indicate this clearly, with due acknowledgment of collaborative research and discussions. This thesis is a bonafide record of original work done by me and all sources listed within have been detailed in the bibliography.

Anand Kumar Rai
Place:
Date:

In my capacity as the supervisor of the candidate's Ph.D. thesis work, I certify that the above statements by the candidate are true to the best of my knowledge.

Dr. Kausik Chattopadhyay
Associate Professor,
Department of Biological Sciences,
Indian Institute of Science Education and Research Mohali.
Place:
Date:

# Acknowledgements

I would like to thank all the people who have contributed in their own way for the completion of this fruitful and unforgettable journey. First and foremost, I thank my supervisor, Dr. Kausik Chattopadhyay, for giving me the intellectual freedom in my work, engaging me in new ideas, and demanding a high quality of work in all my accomplishments. I appreciate all his contributions of time and ideas to make my doctoral work experience productive and stimulating. His critical and logical thinking, never say impossible attitude and disciplined behavior has helped me in growing as a better person both professionally and personally. The joy and enthusiasm he has for his research was a source of inspiration for me, even in the tough times during this work.

I express my sincere gratitude to the Director, Professor N. Sathyamurthy, for his kind help and support. I would also like to thank the doctoral committee members, Professor Purnananda Guptasarma and Dr. Sabyasachi Rakhsit for their valuable suggestions and encouragement.

I gratefully acknowledge Dr. Arunika Mukhopadhaya for her assistance with the flow cytometry-based assays. Her constant motivation and insightful suggestions helped me a lot in my Ph.D.

I am also thankful to my group members: Dr. Karan Paul and Ms. Nidhi Kundu for collaboration; Dr. Nidhi, Barkha, Reema, Nidhi, Kusum and Sachin for creating a fun-filled and cordial environment in the lab which makes research so much enjoyable. I would never forget the beautiful moments I shared with the project students Dilraaj, Anjali, Anup and Gunidhar. I would also like to thank members of Dr. Arunika's lab, Dr. Ranjai, Junaid, Sanica, Shelly, Deepinder, Aakansha and Krishna, for their help and support.

I would like to take this opportunity to thank all my teachers who have influenced my life in some way or the other.

I am indebted to MHRD, India, for providing me with a scholarship and IISER Mohali for the state-of-the-art infrastructure for my research. I thank Centre of Excellence (COE) in the Frontier Areas of Science & Technology (FAST) program of the MHRD, Govt. of India, for funding. I would like to acknowledge the Library facility of IISER Mohali and Dr. P. Visakhi, Deputy Librarian, for providing subscription to various journals. I also thank the Deans, faculty

members, non-teaching staff, research scholars and BS-MS students of IISER Mohali, for creating a very friendly environment in the campus to pursue scientific research.

Sincere thanks to my friends: Prabhat, Saurabh, Virendra and Zulfi for standing with me in all the ups and downs of my life. I especially thank to my wife Dr. Navnita Kumar for standing with me during the tough time in PhD. Finally, I express my gratitude towards my parents without whom I would not be the person that I am today. I am indebted to them for the unconditional love and the support they have showered on me throughout my life.

Last, but not the least, I thank the Almighty for giving me the courage and dedication to accomplish this journey.

**ANAND KUMAR RAI**

# List of publications

1) **Rai, A. K.,** Paul K, and Chattopadhyay K. "Functional Mapping of the Lectin Activity Site on the β-Prism Domain of *Vibrio cholerae* Cytolysin: IMPLICATIONS FOR THE MEMBRANE PORE-FORMATION MECHANISM OF THE TOXIN."**Journal of Biological Chemistry** 288 (2013): 1665-1673.
2) **Rai, A. K.**, and Chattopadhyay K. "Trapping of *Vibrio cholerae* Cytolysin in the Membrane-bound Monomeric State Blocks Membrane Insertion and Functional Pore Formation by the Toxin." **Journal of Biological Chemistry** 289 (2014):16978-16987.
3) **Rai, A. K.,** and Chattopadhyay K. "*Vibrio cholerae* cytolysin: structure-function mechanism of an atypical β-barrel poreforming toxin" **Advances in Experimental Medicine and Biology** 842 (2015):109-125.
4) **Rai, A. K.,** and Chattopadhyay K. "Revisiting the membrane interaction mechanism of a membrane-damaging β-barrel pore-forming toxin *Vibrio cholerea* cytolysin". **Molecular Microbiology** 97 (2015): 1051–1062.
5) **Rai, A. K.,** Kundu N. and Chattopadhyay K. "Physicochemical constraints of elevated pH affect efficient membrane interaction and arrest an abortive membrane-bound oligomeric intermediate of the beta-barrel pore-forming toxin *Vibrio cholerae* cytolysin". **Archives of Biochemistry and Biophysics** 583 (2015): 9-17.

# Table of Contents

## Chapter 2

**Membrane interaction mechanism of *Vibrio cholerae* cytolysin**

## Chapter 3

**Implication of the C-terminal β-prism lectin domain on the pore-formation mechanism of VCC**

**Chapter 4**

**Trapping of VCC in the membrane-bound monomeric state abrogates oligomerization, membrane insertion and functional pore-formation**

## Chapter 5

**Physicochemical constraints of elevated pH abrogate efficient membrane interaction and trap an abortive membrane-bound oligomeric intermediate of VCC**

## List of Figures

# List of Tables

# Glossary

(βME) 2-mercaptoethanol

(BSA) Bovine serum albumin

(CD) Circular dichroism

(CDC) Cholesterol dependent cytolysin

(ClyA) Cytolysin A protein

(CT/*ctx)* Cholera toxin

(CTXϕ) Filamentous bacteriophage containing CTX

(DNA) Deoxyribonucleic acid

(EDTA) Ethylenediaminetetraacetic acid

(ELISA) Enzyme- linked immunosorbent assay

(FBS) Fetal bovine serum

(FITC) Fluorescein isothiocyanate

(FRET) Fluorescence resonance energy transfer

(HA/P) Haemagglutinin protease

(HCl) Hydrochloric acid

(HEPES) 4-(2-hydroxyethyl)-1-piperazineethanesulfonic acid

(HRP) Horseradish peroxidase

(IPTG)Isopropyl β-D-1-thiogalactopyranoside

(kDa) Kilo Dalton

(LB) Luria Broth

(LDH) Lactate dehydrogenase

(LPS)Lipopolysaccharide

(NaOH) Sodium hydroxide

(NCBI) National Centre for Biotechnology Information

(Ni-NTA) Nitrilotriacetic acid

(OD) Optical density

(OMP) Outer membrane proteins

(OPD) Ortho-phenylenediamine

(PCR) Polymerase chain reaction

(PrtV) Protease of *Vibrio cholerae*

(PC) Phosphatidylcholine

(PMSF) Phenylmethylsulfonyl fluoride

(PVDF) Polyvinylidene difluoride

(SDS-PAGE) Sodium dodecyl sulfate polyacrylamide gel electrophoresis

(SPR) Surface Plasmon Resonance

(Tcp) Toxin co-regulated pilus

(UV) Ultraviolet

(VCC) *Vibrio cholerae* cytolysin

# Chapter 1

## Introduction and Literature Review

### 1. Introduction

The membrane lipid bilayer acts as a natural barrier surrounding the cells that helps in protecting the cells from the outside environment. In addition to this, a membrane lipid bilayer plays a crucial role in compartmentalization of the cells, as well as in regulation of the exchange of materials in and out of a living cell. In doing so, the membrane lipid bilayer serves as the natural permeability barrier for every living cell. It is essential for the cells to communicate with the outer environment, and regulate the transport of ions, solvents, and small molecules across the membranes. Transport and signaling through the lipid bilayer are ubiquitous processes, and these are essential for the cells to react to the changes in the environment (1-3). The cells employ many specialized membranes proteins that act as the transporters or channels for the passage of ions, solvent and small molecules across the membrane lipid bilayer. Major class of the integral membrane proteins generate aqueous channels, through which molecules are transported. For example, the membrane protein channels found in the outer membrane of the Gram-negative bacteria, known as porins, act as the molecular sieves allowing the flow of small molecules with a particular size limit across the bacterial membranes (1,2,4,5). Therefore, biomembranes are equipped with a selective permeability barrier function that is very much essential for sustaining the living cells. However, the cytolytic pore-forming protein toxins, found in the vast array of organisms starting from bacteria to humans, destroy the selective permeability barrier function of the cell membranes by making pores on the membrane lipid bilayer of the target cells (1-6).

The present thesis work deals with the structure-function relationship of *Vibrio cholerae* cytolysin (VCC), a potent membrane-damaging pore-forming protein toxin secreted by the Gram-negative bacteria *V. cholerae*, the causative agent of the severe diarrheal disease cholera.

### 1.1 Pore-forming toxins

Pore-forming toxins (PFTs) represent a unique class of membrane-damaging proteins that act by killing their target host cells by generating pores in the cell membranes. PFTs are produced by many organisms such as, bacteria, fungi, primitive metazoans, plants, and humans (7). The toxins are mostly produced as water-soluble molecules destined to generate pores in membrane lipid bilayer of target host cells. In mode of action of pore-forming toxins, proteins first associate

with membrane lipid bilayer of target cells, subsequently they undergo structural reorganization and self-assembly, and finally make pores on the membranes. This pore formation allows free diffusion of the solutes across the membranes and triggers osmotic imbalance, which further leads to the cell swelling and lysis of the cells (3,6-12). Depending on the particular members of the PFTs, the membrane-inserted pore diameters can vary from less than 1 nm up to 50 nm (8,13-15).

In some cases, transmembrane pores generated by the PFT molecules are used by the disease-causing pathogenic bacteria to inject the toxic compounds into the target host cells. Many pathogenic bacteria, towards exerting their pathogenesis process, are known to use PFTs to disintegrate the organelle membranes for the transmission into the cytoplasm. One of the most remarkable features of the PFTs is the conversion of the toxin from the water-soluble monomeric state to the oligomeric transmembrane channel with the behavior of integral membrane protein. For this, protein must undergo conformational alterations in which hydrophobic patches that remain buried in the water-soluble state become exposed to the hydrophobic environment of the membrane lipid bilayer (1,13,16). Thereby, PFTs can adopt both the water-soluble and the transmembrane structural state from the same primary structure composition. PFTs follow common mechanism of pore-formation, which involves four distinct steps: (i) Secretion of the toxin from the bacterial pathogen, (ii) Membrane interaction of the toxin with target cell membrane, (iii) Self-assembly of the toxin on the membrane surface and (iv) Membrane insertion of the toxin to generate the functional pore.

Although PFTs are predominantly virulence factors of many bacterial pathogens, they can also play significant roles in the defense mechanism of many eukaryotic organisms (1,14,17,18). One of the largest families of the mammalian PFTs includes the membrane attack complex (MAC) and perforin (PF). This MACPF superfamily plays essential roles in the defense mechanism against bacterial and viral infection in the vertebrate immune system. Sea anemones also use PFTs as venoms to kill prey.

### 1.1.1 Classification of the pore-forming toxin

Pore-forming toxin (PFTs) can be classified in many different ways. For example, they may be classified on the basis of the organisms that produce the toxin, or to a more specific characteristic that is essential for the pore-formation process on the membrane lipid bilayer of the target cells. However, the most accepted classification is on the basis of a structural requirement for the

efficient pore-formation. At the most general level, PFTs are classified as either α-PFTs, or β-PFTs. α-PFTs are anticipated to generate pores by employing α–helices (13,16,19-24). These toxin proteins tend to be high α-helical, with the bigger one having pore-forming domains consisting α-helical hairpin structure (21,25-28). This hairpin is suggested to trigger the initial steps of the membrane insertion (20-22,25). Examples of members of this class of PFTs are colicins, the insecticidal *Bacillus thuringiensis* δ-endotoxin, *Pseudomonas aeruginosa* exotoxin, and diphtheria toxin (27,29-35). Apart from the bacteria, α-PFT also produced by the eukaryotic organism. Examples include the members of the Bcl-2 and Bcl-x family of apoptotic proteins. These proteins display structural similarity with the members of the α-PFTs, and they also generate pores in the membrane lipid bilayer with similar fashion without sharing any prominent sequence and structural homology.

**Table 1.1 Structural classification of PFTs**

| **Toxin** | **Species** | **Structural features** | **Other Information** |
|---|---|---|---|
| **α-PFT** | | | |
| Colicin A | *E. coli* | All α-helical | Low pH is essential for activity |
| Exotoxin A | *P. aeruginosa* | Two α-helical domains, one β-sheet domain | Low pH induces membrane insertion |
| Cry δ-endotoxin | *B. thuringensis* | Two β-domains, one α-helical domain | Activated in midguts of insects |
| Diphtheria toxin | *C. diphtheriae* | Two β-domains, one α-helical domain | Requires low pH |
| Equinatoxin II | *Actina equina* | Mostly β with one transmembrane helix sandwiched | Interact with sphingomyelin |
| Sticholysin II | *S. helianthus* | Mostly β with helices sandwiched | |

| | | | |
|---|---|---|---|
| **β-PFT** | | | |
| Aerolysin | *Aeromonas* family | 42% b-sheet, 23 strands, eight anti-parallel sheets | Requires oligomerization |
| α-hemolysin | *S.aurens* | Three β-sheet domains, β-hairpin stem inserts | Requires oligomerization, β-barrel |
| Anthrax toxin | *B.anthracis* | Contains 3 protein exotoxins | Requires oligomerization, β-barrel |
| *Vibrio cholerae* cytolysin | *V. cholerae* | Contains four structural domains including two lectin-like domains | Requires oligomerization, β-barrel |
| | | | |
| **Cholesterol-dependent cytolysin (CDC)** | | | |
| Perfringolysin | *C. perfringens* | β-sheet and α-helical domains | |
| Pneumolysin | *S. pneumoniae* | β-sheet and α-helical domains | |
| | | | |

The other important class of pore-forming toxins, the β-PFTs, has been reported to insert into the lipid bilayer to generate β-barrel pore structure. β-PFTs have significantly different tertiary and quaternary structures compared to the α-PFTs. The water-soluble monomeric structures of the β-PFTs are more compact than the structure of α-PFTs. As suggested by their name, all β-PFTs are composed of β-sheet structures. The members of the β-PFTs include *Clostridium septicum* α-toxin, *Aeromonas hydrophila* aerolysin, *Pseudomonas aeruginosa* cytotoxin, *Vibrio cholerae* cytolysin, and protective antigen of the anthrax toxin. Unlike the oligomers of the α-PFTs, which are less stable and which dissociate when the membranes come in the contact of detergents, the

oligomers generated by the members of the β-PFT family on the membrane of the target cell are usually very stable, and remain attached to the membrane even after membrane solubilization with the detergents (36-44). For example, β-PFT oligomers are stable even in the presence of denaturing detergent sodium dodecyl sulfate (SDS) up to a temperature of 65 $^{o}$C. The mechanism of the pore-formation by the β-PFTs is explored in more detail compared to the α-PFT family members. The transmembrane pore diameter generated by the α-hemolysin, VCC, aerolysin and protective antigen of anthrax toxin is in the range of 1.5 to 4.6 nm, while the cholesterol-dependent cytolysin can generate pores having the diameter in the range of 25-35 nm with the self-assembly of up to 50 toxin monomers (20,39,45-47)

### 1.1.2 α-PFTs

Members of the α-PFT family display significant differences in the three-dimensional structures, and in the size of the pores generated in the lipid bilayer of the target host cell membranes. These protein toxins possess an elongated structure rich in α-helical domains (48,49). In the water-soluble state, the hydrophobic residues of the membrane pore-forming amphipathic α-helix are packed within the toxin core. Upon the association with the target cell membrane, the surface of these residues gets exposed and generates the pore.

#### 1.1.2.1 Cytolysin A

Cytolysin A (ClyA), a member of the α-PFT family, is responsible for the hemolytic activity of several strains of bacteria like *Salmonella enterica* and *Escherichia coli*, and it contributes to the pathogenesis process of these bacteria. The crystal structure of the water-soluble monomeric ClyA displays an elongated, mostly α-helical molecule (48,50). A bundle of four α-helices constitutes the central core of the toxin. At the tail of the molecule, an extra helix bundle generates a five-helix bundle with the longer helices (Figure 1.1). A β-hairpin, the 'β-tongue', which is connected by two small helices and lying against the four-helix bundle, forms the 'head' domain of the molecule (51). The pore structure of the ClyA displays an octameric pore structure with an inner pore diameter of about 25-30 Å. Interestingly, it reveals the molecular structural reorganization of the toxin needed for the conversion of a water-soluble monomeric form to the membrane inserted oligomeric pore structure (48).

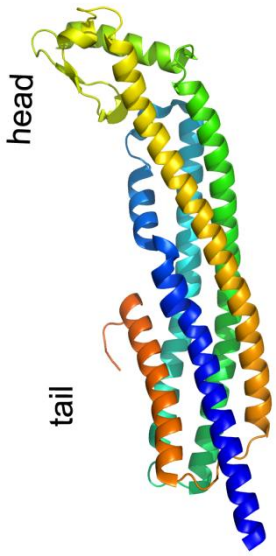


**Figure 1.1: Crystal structure of α-PFT, Cytolysin A (PDB ID: 1QOY).** ClyA is organized as a four-helix bundle from αA, B, C and F. At the tail of the molecule this bundle is extended by αG. The head region of the protein comprises a hydrophobic β-hairpin, which is flanked by two helices.

### 1.1.2.2 Cry toxins

The insecticidal crystal protein Cry toxins produced by *Bacillus thuringiensis* (Bt) have been a subject of intensive research for its potential in the economical importance in the agricultural applications (51,52). Each toxin of Cry toxin family is typically specific to only one or few insect species, depending on the aminopeptidase N (APN) and cadherin-like receptor molecule present on the mid-gut epithelial cells of the target insect (51,53,54). In the mode of action of the Cry toxin, the toxin is ingested by a susceptible insect, and is solubilized by high pH conditions present in the midgut of insect, subsequently causing the proteolytic removal of the carboxy terminal region, thus activating the toxin. Solubilization and proteolytic activation of the toxin leads to membrane interaction with APN and cadherin-like receptor molecule, and insertion into the epithelial cell membranes generating ion channels or membrane pores leading to the insect death (50,52,53,55).

The molecular structure of the Cry1Aa toxin suggests that the toxin harbors three structural domains. Domain 1 is composed of seven α-helices generating a bundle around the α-helix 5, and α-helix 1 is proposed to be cleaved during the membrane insertion (51,53). Experimental evidence indicates the critical role of the Domain 1 in membrane insertion and pore-formation of

the toxin. Domain 2 structure is a β-Prism fold and it acts as a receptor-binding domain of the toxin (Figure 1.2).

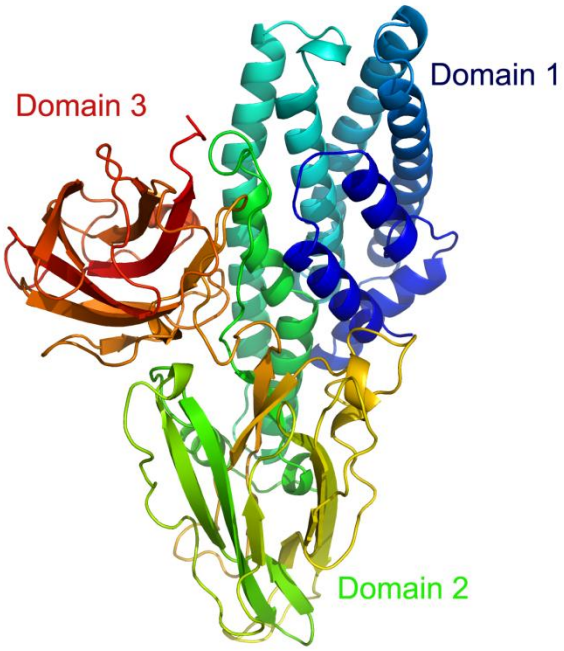


**Figure 1.2: Structure of Bt toxin Cry protein (PDB ID: 1CIY)**

Domain 3 generates a β-sandwich 'jelly roll' topology of antiparallel β-sheets, and is responsible for the receptor interaction of the toxin. Some portion of both domain 2 and 3 can be inserted into the brush border membrane vesicles of the target insect (51,53).

### 1.1.3 β–PFTs

#### 1.1.3.1 *Staphylococcus aureus* α-hemolysin

*Staphylococcus aureus* α-hemolysin is secreted as a water-soluble single-chain polypeptide with 293 amino acid residues (without any cysteine). The toxin interacts with the cell membranes to generate the transmembrane pore structure (56,57). The molecular mechanism of pore-formation has been studied significantly in case of α-hemolysin (58-60). The molecular structures of monomeric form and transmembrane heptameric form have been well resolved (59,61-66).

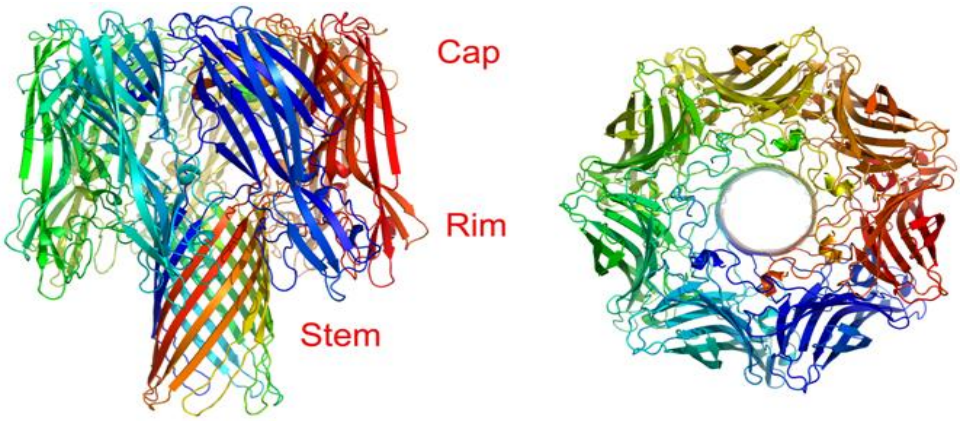


**Figure 1.3: Structure of α-hemolysin heptamer (PDB ID: 7AHL)**

The transmembrane oligomer generated by the α-hemolysin has a mushroom-shaped structure harboring the cap, rim, and a stem domain. The cap of the toxin has a diameter of nearly 10 nm, and is generated by β-sandwich structure (Figure 1.3). Together with the rim domain it forms the central core of the toxin. The stem region or transmembrane domain is composed of 14-strand β-barrel generated from 7 β-hairpins, with each of the hairpin shared by a single protomer of the toxin (4,28,61,66-69). Many studies have suggested the differences in the susceptibility of different mammalian cells toward the α-hemolysin. For example, rabbit erythrocytes are lysed by a nanomolar concentration of the protein, while lysis of human erythrocytes needs 200-fold higher concentration of the toxin; this has been attributed to the presence of specific receptor in the case of rabbit erythrocytes. A recent study on the membrane binding of the toxin has suggested that the clustered phosphatidyl choline head-groups act as the binding sites for the α-hemolysin (57,62,70-73). After the initial membrane interaction of the toxin, the α-hemolysin first self-assembles to generate a non-functional 'pre-pore' oligomeric complex, which further inserts its pore-forming stem-loop into the membrane lipid bilayer, and generates a functional transmembrane pore structure (58,67,68,70,74-76). Hence, the pore-formation by the toxin involves multiple steps involving the reorganization of the N-terminal region as well as the structural reorganization of the rim and central domain of the toxin. Deletion of the N-terminal region of the toxin arrests the toxin in the pre-pore stage, suggesting the significance of this region in the conversion of pre-pore to functional pore in the toxin (74,75,77). The α-hemolysin pore is slightly anion selective. In past few years, three-dimensional toxin structure of many other members of the β-PFT family have been determined, which reveals high similarities in the

structural part as well as in the molecular mechanism of the functional pore-formation observed with the α-hemolysin (33).

### 1.1.3.2 Anthrax toxin protective antigen

*Bacillus anthracis* generates three monomeric states of the proteins that are collectively known as anthrax toxin. This A-B type of toxin harbors two A-components, known as the edema factor (EF) and the lethal factor (LF). The B-component is a 83 kDa pore-forming toxin known as the 'protective antigen (PA)'. The PA helps in delivery of the EF and LF to the target host cells. Invasion of the host cells is triggered when the PA interacts with the membrane receptor present on the surface of target host cells, subsequently leading to the proteolytical activation of the protein and pore formation (Figure 1.4). EF and LF compete for the interacting site on the PA heptamer, resulting in the generation of a complete anthrax complex with 1 to 3 EF and/or LF molecule(s) per oligomer (45,78-81). The resulting complexes of the anthrax toxin are transported to the endosome of the target cells. Under the effect of low pH condition, the PA pre-pore converts into a mature active transmembrane pore structure, and EF and LF open and cross the endosomal lipid bilayer via the transmembrane pores, moving into the cytosol (40,45,79).

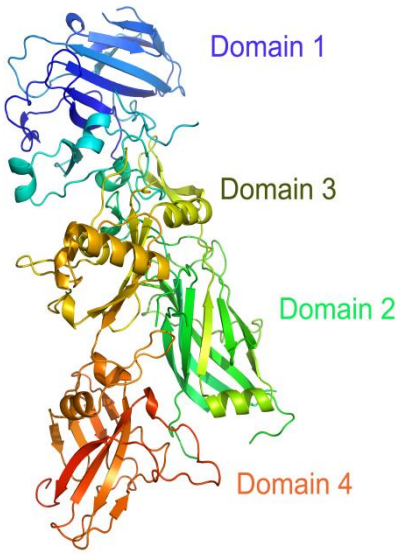


**Figure 1.4: Structure of anthrax toxin protective antigen monomer (PDB ID: 1ACC)**

The molecular structure of the monomeric form of PA suggests four structural domains. Domain 1 harbors the protease cleavage site for furin, as well as an interacting site for the calcium ions (82). The calcium ions are essential for the maintenance of the structural organization of the

oligomer and the ligand-interacting site after the proteolysis. Domain 2 contains many long β-strands. The most important function of this domain is to generate a transmembrane pore to act as a gateway for the entry of LF and EF into the cytosol. Recent studies have suggested that the domain 2 also participates in the membrane interaction of PA. Domain 3 is believed to participate in the self-assembly of PA, and alteration in this domain significantly abrogates the oligomerization of PA (83). Domain 4 is involved in the association of the toxin with the cellular receptor. This domain makes a little connection with the rest of the toxin (45,80,84). The conversion of the pre-pore oligomeric species to the functional transmembrane pore structure depends on the presence of an acidic pH condition and a specific receptor on the surface. Consistent with the observation with the α-hemolysin, the PA pore is SDS-stable and heat resistant (Figure 1.5).

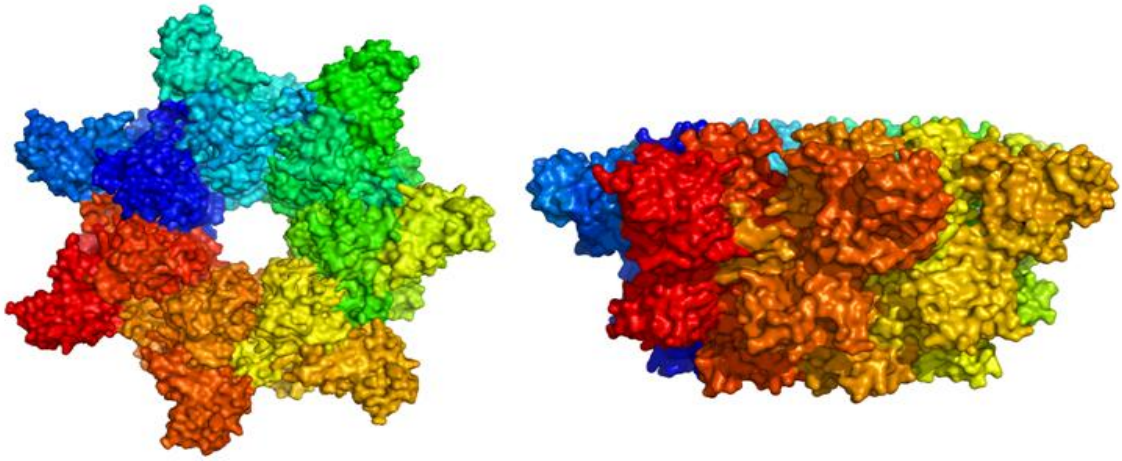

**Figure 1.5: Heptameric pore structure of Protective Antigen (PDB ID: 1TZO)**

### 1.1.3.3 Aerolysin

Aerolysin is an important virulence factor of the *Aeromonas* family, responsible for the gastrointestinal diseases, wound infections, meningitis and septicaemia in human. Aerolysin is a well-studied member in the family of β-PFTs. Aerolysin is produced as a 52 kDa protoxin form containing an N-terminal signal peptide. Protoxin is secreted into the extracellular medium through the type II secretion system (39,82,85-87). The inactive proaerolysin is proteolytically converted into the active form by proteases such as trypsin, furin or chymotrypsin, and this leads to the deletion of 41-43 long peptide at the carboxy-terminal end of proaerolysin, thus generating

the mature aerolysin, which assembles as a dimer in solution (82,88-92). However, for the binding to the target cell membranes, the dimer of the toxin dissociates into monomers (85,93,94). Many GPI-anchored proteins act as the interacting target for the aerolysin toxin (88,95). The pore generated on the membrane of the target cells leads to cell death by triggering membrane depolarization (96-98).

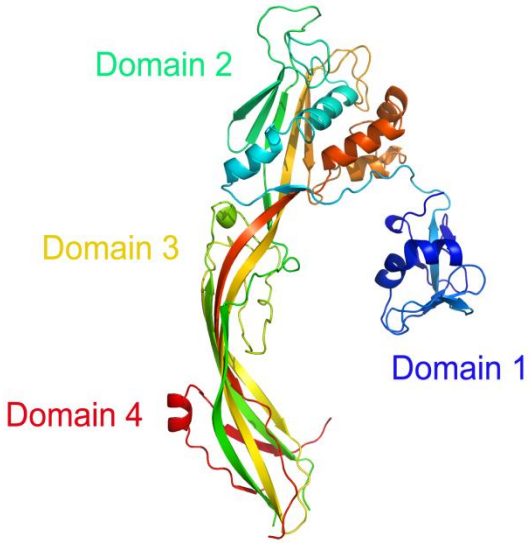


**Figure 1.6: Crystal structure of proaerolysin (PDB ID: 1PRE)**

The monomeric structure of the aerolysin appears as an L-shaped molecule with an N-terminal lobe (domain 1) and, a large lobe constituted from the domains 2-4. Domain 1 and 2 play a significant role in the membrane binding and receptor interaction, whereas domain 3 and 4 are essential for membrane oligomerization and the insertion of the toxin into the lipid bilayer of the membrane (72,85,99). The pore-forming loop is present in the domain 3, and it consists of an amphipathic loop of approximately 20-25 amino acid residues (Figure 1.6). For the membrane insertion of the toxin, the amphipathic hairpin extends away from the toxin core towards the lipid bilayer, and associates with the neighboring loops for the generation of the transmembrane β-barrel architecture. Despite sharing the limited amino acid sequence homology with the other members of the β-PFT family, the three-dimensional structure of aerolysin displays high degree of structural similarity.

### 1.1.3.4 Cholesterol-dependent cytolysin

The cholesterol-dependent cytolysins (CDCs) constitute a major group of the water-soluble monomeric toxins with a molecular weight of 50-80 kDa. The members of the CDC family are widely distributed over many Gram-positive bacteria (100-104). The well-studied members of CDC family are perfringolysin O from *C. perfringens*, pneumolysin from *S. pneumonia*, streptolysin O from *S. pyogenes* and listeriolysin O from *L. monocytogenes* (102,105-118). More recently CDCs have also been reported in the Gram-negative bacteria. The two major properties make the CDC family so unique: (i) CDCs critically depend on the presence of cholesterol in the target cell membranes for their activity, leading to the generation of very large, membrane inserted, transmembrane complexes with a pore diameter of up to 350 Å (101,103,106-109,113,119); (ii) the members of the CDC family toxins display very high amino acid sequence similarity with each other (40-80%). In particular, the sequence similarity is high within the C-terminus where the so-called 'undecapeptide' is positioned (an eleven amino acid-long region rich in tryptophan residues (ECTGLAWEWWR) that is critically important for the association towards the target cell membranes) (102,104-106,120).

The molecular structure of the three members of the CDC family (intermedilysin from *Streptococcus intermedius*, perfringolysin O from *Clostridium Perfringens* and anthrolysin O from *Bacillus anthracis*) highlights that each of the water-soluble toxin folds into four discontinuous domains (103,115,118,120-124). The structural similarity between these three CDCs suggests a probable similar structural arrangement of the other members of the CDC family, and similar functional pore-formation mechanisms as well (106,121,122,125).

Studies on perfringolysin O (PFO) further elucidate our knowledge regarding the mechanism of functional pore-formation. The water-soluble toxin monomers secreted by the bacteria first interact with the surface of the target host cells through the domain 4 of the toxin. As the monomers associate, only the tip of domain 4 inserts into the membrane. In each protein monomer, domain 3 has two sets of three short α-helices (Figure 1.7). The initial interaction events of domain 4 induces a movement of a short β strand in domain 3 of each toxin monomer, followed by blocking any hydrogen bonding interactions between the short α-helix and short β strand (118,121,126,127).

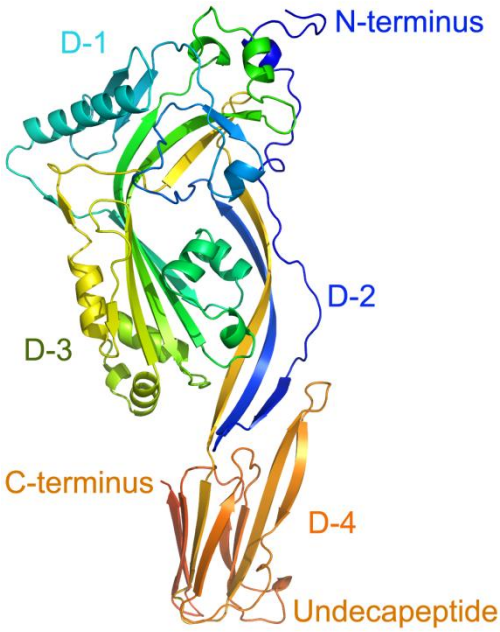


**Figure 1.7: Structure of the perfringolysin O (PDB ID: 1PFO)**

This movement in domain 3 allows exposure of the interface through which toxin monomers can interact. The conformational rearrangement of three short α-helices initiates a process in which they become two transmembrane-β-hairpins. The β1 strand of the β-hairpin from one monomeric unit interacts with the β4 strand of the β-hairpin of the neighboring monomer unit. The monomers generate the hydrogen bonds between each other on the lipid bilayer of the membrane and form the pre-pore oligomeric assembly (112,120,128,129). The insertion of the domain 3 pore-forming transmembrane-β-hairpins involves reorientation of domain 1 closer to the lipid bilayer, bending of the β sheets in domain 2, and a 40 Å vertical insertion of the pre-pore complex into the membrane, which result in the formation of a transmembrane β-barrel pore structure. Recent studies suggest that the domain 4 of each toxin interacts with cholesterol present in the lipid bilayer of the target cells. In all cases, membrane pore-formation either by PFO, streptolysin O or intermedilysin (ILY) requires the presence of cholesterol in the membranes (130,131).

## 1.2 *Vibrio Cholerae*

### 1.2.1 Microbiology

*Vibrio cholerae,* the causative pathogen of the human disease cholera, is a highly motile flagellated bacterium, found in lakes, brackish water, rivers, ponds and other water bodies. *V. cholerae* is a member of the *Vibrionaceae* family. The *Vibrio* genus composed of 63 species and 11 of them are known to be highly pathogenic for the human including *V.cholerae* (O1 and O139), *V. vulnificus, V. parahaemolyticus, V. mimucus, V. hollisae, V. fluvialis, V. alginolyticus, V. damsela, V. metschnikovii, V. cincinnatiensis and V. furnissii.* Among these, the first three species can induce severe human diseases (132-135). *V. cholerae* can be classified on the basis of lipopolysaccharide in the outer membrane, most importantly the O-antigen responsible for the classification of the O serogroups. Presently, 206 O serogroups are identified, but only O1 and O139 have been shown to cause epidemics of cholera (136-138). The O1 serogroup can be classified into three subtypes based on the presence of three antigens known as A, B, and C. The combinations of these three antigens generate the serotypes, similar to serogroup with extra specific antigens as shown by serological testing, Ogawa (A and B), Inaba (A and C), and Hikojima (A, B, and C). The O1 serogroup can also be subclassified into two distinct biotypes called "classical and E1 Tor." (136,139).

### 1.2.2 Key virulence factors of *Vibrio cholerae* and their biological function

#### 1.2.2.1 Cholera toxin

The CTX Φ phage plays a critical role in the evolution of the *V. cholerae* since it contains the genes *ctx*AB that encode the cholera toxin (CTX). The CTX Φ lysogenizes *V. cholerae* by employing the site-specific integration into the host chromosome. Cholera toxin (CT; 84 kDa) is a typical AB5 type of toxin consisting of a pentameric ring of B subunits (11.6 kDa) and an A subunit (29 kDa) (140,141). Before the entry of the CT into the target host cells, the A subunit is proteolytically converted into a catalytic A1 subunit and A2 subunit, whose role is to regulate the non-covalent interactions with the B subunits. First, B subunits associates with the ganglioside GM1 receptor, and the retrograde transporters on the lipid rafts transfers CT to the endoplasmic reticulum. The A1 subunit then detaches from the protein complex, and activates G-protein in a way that it continuosly keeps on stimulating adenylyl cyclase (140,141). The levels of the cAMP in the intestinal epithelial cells significantly increase when adenylyl cyclase is present in the active form. Diarrhea results in the flow of $Cl^-$ and water via the apical surface of the epithelial

cells into the intestinal lumen through the opening of cAMP-responsive $Cl^-$ channels (Figure 1.8).

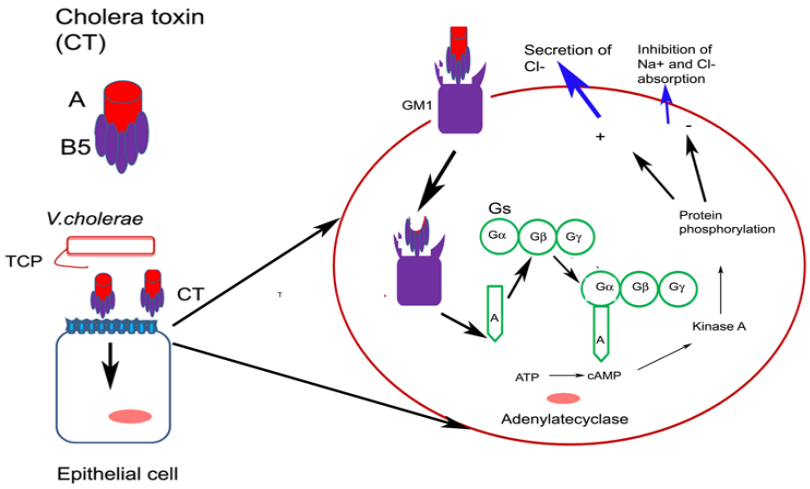


**Figure 1.8: Schematic diagram of the mode of action of cholera toxin (CT).** First, bacteria colonises the cells through the toxin co-regulated pilus (TCP). CT is produced, and is transported into the cells via the binding of the B subunits with the GM1 receptor. Subsequently, the A subunit ADP-ribosylates the Gs protein (GTP-hydolysing protein) and triggers the conversion of the ATP into cyclic AMP (cAMP). cAMP mediates phosphorylation of CFTR, which leads to loss of ions from within the cells.

### 1.2.2.2 Toxin co-regulated pilus (TCP)

The pathogenesis of cholera requires the *V. cholerae* to colonize in the host. The colonization of bacteria depends upon the toxin co-regulated pilus (TCP) which is related to the type 4 bundles generating the pilus of enteropathogenic *E.coli*. The association of pilli units into type 4 pilli produces a polymeric system, which allows distinct cellular functions, including biofilm formation, cell signaling, host-cell adhesion and surface motility (142). In many Gram-negative bacteria, blocking of this pilus association results into a severe decrease in the virulence, indicating a critical role of the pilli in the pathogenesis process. This crucial colonization factor is believed to trigger bacteria-bacteria associations and assembly of the microcolonies. *V. cholerae* TCP biogenesis system acts as a secretion apparatus for a soluble colonization factor TcpF, which is considered to be necessary for the mouse intestinal colonization of the *V. cholerae* strains, even though the molecular mechanistic detail remain unexplored (132). Apart from that, TCP has been shown to protect *V. cholerae* from complement-mediated cytolysis.

Albeit CT and TCP are the major virulence factors of *V. cholerae*, many other accessory factors have been reported to play important role in the pathogenesis of the *V.cholerae (143)*. These factors include the additional pilli, such as fucose-interacting and mannose-interacting hemagglutinins that might play significant roles in the colonization process by classical and E1 Tor biotypes (144,145). Apart from that, the E1 Tor biotype strains produce many minor toxins that play some part in the pathogenesis of cholera. The CTXΦ also encode zonula occludens toxin (ZOT) (which probably acts as an enterotoxin and morphogenetic phage protein), the S-CEP (Chinese hamster cell-elongating protein) cytotoxic protein, and the actin-crosslinking RTX toxin (146).

#### 1.2.2.3 RTX toxin

The RTX (repeats-in-toxin) is a multifunctional toxin encoded precisely downstream of the CTX element in the *V. cholerae* genome. The RTX gene cassette is constituted of the *rtxA*, *B*, *C*, *D* and *E* genes. *rtxA* encodes for the toxin, *rtxC* encodes for a putative toxin activator acyltransferase, *rtxB* and *rtxE* encodes for putative secretory ATPases, and *rtxD* encodes for the periplasmic linker of type 1 secretion system thus mediating the RtxA export. The *rtx* gene cassette is present in the disease-causing pathogenic strain of the *V. cholerae* O1 E1 Tor and O139 and many of the non-O1, non-O139 environmental and clinical isolates (146-148). The actin cross-linking is a major activity of the RTX toxin, and the toxin has been involved in the pathogenesis of cholera disease (147). The toxin is nearly 485 kDa in molecular mass and harbors a series of glycine-rich repeat regions at the N- and C-terminal, while the activity modules are positioned within the core region of the toxin. Additionally, RTX toxin harbors a cysteine proteinase module, which is activated by the GTP interaction, probably in the host cell cytoplasm. The RTX toxin undergoes autoprocessing by its protease module after the transfer into the cytoplasm, and it is essential for the actin crosslinking activity of the toxin.

#### 1.2.2.4 Mannose-sensitive hemagglutinin

*V. cholerae* is mainly present in the aquatic coastal environment. Many factors including pH, temperature, and natural habitat affect the survival of bacteria. Interaction and adherence with the planktonic organism is poorly elucidated at the molecular level, however it has been suggested that the interaction between chitinaceous surfaces, including those found in the copepods can provide bacteria with protective environment and nutrients. The mannose-sensitive hemagglutinin (MSHA) pilus has been found to play an essential role in *V. cholerae* adherence to

a crustacean copepod, *Daphnia pulex*. Within the mammalian host, MSHA has been reported to play a limited role in the pathogenesis because *V. cholerae* deficient in MSHA shows no loss of the virulence as compared to the wild type bacteria in the mouse model experiments (149-152). MSHA has been reported to associate with glycosylated S-IgA. *V. cholerae* associates with S-IgA in a MSHA-dependent manner, and that association of S-IgA blocks bacteria from crossing the mucus barriers and attaching to the surface of epithelial cells. MSHA repression for evasion of the immune response appears to be crucial during the initial stage of the infection because the bacteria crosses the mucous layer and starts to express the virulence factors essential for colonization (153).

**1.3 Regulation of *V. cholerae* virulence factors**

*V. cholerae* needs to respond to many environmental conditions by regulating the genes that are necessary for those specific conditions. Nutrient composition, temperature, pH, $CO_2$ concentration, bile, bile salts and other environmental conditions are well known to influenec the expression and the maintainance of the virulence factors of bacteria. The major transcriptional activator of virulence genes comes from the AraC family member, ToxT, which directly regulates CT, TCP, and other necessary virulence factor expression by regulating the promoters, including *ctx*A, *tcp*A, *tcp*I, *tcp*C, *acf*A. The *toxT* gene is located in the same pathogenicity island, *Vibrio* pathogenicity island (VPI), as the TCP-biogenesis machinery (154). Its gene product results from the activity of the two promoters, either its own promoter located at a position directly upstream of the gene, or the tcpA-F promoter. Two membrane OmpR family transcriptional activators TcpP and ToxR associate with the *toxT* promoter to cooperatively drive its expression and the production of major virulence determinants. Although ToxR is essential, it is not sufficient for the activation of *toxT*. ToxR triggers the transcription of *OmpU*, the primary envelope protein gene, however, represses *OmpT*, encoding the other outer membrane protein OmpT. The *tcpPH* operon expression is mainly dependent on a LysR transcriptional regulator *aphB* with its partner *aphA*. The promoter activity of *aph*A has been reported to be suppressed by HapR, a quorum sensing governing transcription factor, in the *V. cholerae* E1 Tor strains (154). The ToxT pathway also contributes to the mannose-sensitive hemagglutinin (MSHA) pili formation, which is involved in the evasion of secretory IgA (SlgA)-mediated innate immune responses in a mouse model of *V. cholerae* pathogenesis. The cAMP receptor protein (CRP) is a major transcription factor that regulates metabolism in pathogenic enteric bacteria. The

alterations in the adenylate cyclase gene *cya* and *crp* gene activate the transcription of critical virulence factor genes *ctx* and *tcp* for their production (155).

### 1.4 Secreted *V. cholerae* peptidases

#### 1.4.1 Hemagglutinin/protease

The zinc metalloprotease of *V. cholerae* known as hemagglutinin/protease belongs to the family of M4 metalloproteases. The peptidases of this family harbor the conserved HEXXH motif implicated in the catalytic zinc ion complex. The zinc present in the core is tetrahedrally coordinated and other zinc ligands are positioned in the C-terminal to the HEXXH. The proteases of this family from species *V. anguillarum, V. vulnificus, V. proteolyticus* and *V. cholerae* are known as vibirolysin (144). The vibriolysin produced by the *V. choleare* has been identified as hemagglutinin that agglutinates a specific type of responder in erythrocytes. Hemagglutinin/protease, also named as mucinase or detachase, is a secreted *V. cholerae* metalloprotease which displays activity for ovomucin, fibronectin and lectoferrin. *V. cholerae* is mostly found on many surfaces in its natural aquatic environment, hence extensively secreted hemagglutinin/protease is believed as a critical factor involving in bacterial detachment and spreading from its natural habitats (144).

#### 1.4.2 *Vibrio* aminopeptidase

*Vibrio* aminopeptidase also known as bacterial leucyl aminopeptidase, has been initially purified from the culture supernatant of *Vibrio proteolyticus*. The enzyme possesses specificity in removing the N-terminal residue of oligo and polypeptides. It specifically cleaves the large hydrophobic residue without affecting the glutamyl or aspartic acids. The functional form of the peptidase is nearly 30 kDa, and harbors two zinc ions in its core catalytic site. The *lap* gene in *V. choleare* produces an aminopeptidase, a 54 kDa protein that after the processing results in the 34 kDa active enzyme (156).

#### 1.4.3 The PrtV protease

*V. cholerae* PrtV (protease of *V. cholerae*) protease belongs to a metallopeptidase M6 family, a well known member in the family of an immune inhibitor A produced from *Bacillus thuringiensis*. The M6 metallopeptidase family contains a structural motif HEXXHXXGXXD, where the two histidines and the aspartic acid bind with the zinc ligands, and the glutamate is presumed to be the catalytic residue. The *V. cholerae prtV* gene is positioned at the monocistronic operon within a pathogenicity island encoding an 120 kDa protein (157-159).

Inactivation of the prtV gene by insertion of the kanamycin cassette displays no effect on colonization or cytotoxic properties and virulence potential.

### 1.5 *Vibrio cholerae* cytolysin

*V. cholerae* cytolysin (VCC) is a pore-forming toxin secreted by many pathogenic strains of the Gram-negative bacteria, *V. cholerae,* the causative pathogen of the diarrheal disease cholera. VCC displays potent cytotoxic activity against the erythrocytes and mammalian cells. It is also reported to possess enterotoxin activity in terms of inducing fluid accumulation in the rabbit ileal loops (159-167). Based on these observations, VCC has been suggested as a potential virulence factor of *V. cholerae*. VCC is secreted by the pathogenic strains which lack the 'cholera toxin'(159,160,163,165,168,169).

VCC is encoded by the *hlyA* gene present in *V. cholerae* chromosome number two. VCC is synthesized as a ~81 kDa protein known as Pre-Pro-VCC. During the secretion of the toxin, the N-terminal signal peptide composed of 25-residues is removed to generate a non-functional precursor form of the VCC molecule (Pro-VCC) (Figure 1.9). Further, this Pro-VCC undergoes a proteolytical deletion of the ~15 kDa N-terminal sequence, which results in the formation of a functional form of the toxin (Mature-VCC). Proteolytic activation of the toxin is mediated by the HA/protease, which is the major extracellular protease of *V. cholerae* (170,171). The conversion of Pro-VCC into the mature state of the VCC can also be obtained in vitro by other proteases like trypsin, chymotrypsin, and subtilisin (172,173). In addition to this, proteolytic activation of the Pro-VCC by the proteases present on the surface of the target host cell membranes is also reported (167).

The functional mature form of the toxin induces lysis of the erythrocytes and other eukaryotic cells by generating a heptameric pore with a diameter of 1-2 nm (38,167,173-178) (Figure 1.10). The membrane pore-formation ability of the toxin is also seen in case of the membrane lipid bilayer of the synthetic liposomes (179). Along with its membrane permeabilization activity, VCC toxin also displays a prominent lectin-like activity by binding to the complex glycoproteins and glycolipids with the terminal β1-galactosyl group (180). VCC is characterized as a member of the β-PFT family, and follows the generalized scheme of β-PFT membrane pore-formation mechanism (178,181-186).

### 1.5.1 Structural features of VCC

The high-resolution structure of the water-soluble, monomeric precursor form of the toxin, Pro-VCC (187) as well as that of the heptameric transmembrane pore state of VCC have been determined (174). Many previous studies confirm that the VCC is a β-PFT family member, and the toxin induces the pore-forming activity by generating transmembrane heptameric β-barrel pores on the target cell membranes (169,182,188-191). Consistent with the β-PFT transmembrane pore structure, pore complex of VCC represents a mushroom-shaped organization, which can be divided into two parts: (a) transmembrane β-barrel structural, and (b) membrane-interacting rim domain. Structural analysis of the VCC molecule highlights many unique features that are not reported in the archetypical member of β-PFT family. Similar to the archetypical β-PFTs, VCC also contains a central cytolysin domain (174,187,189,190,192).

Apart from this cytolysin domain, VCC also contains three additional structural domains (an N-terminal Pro-domain in the inactive Pro-VCC precursor state of the toxin, and the two lectin-like domains, namely β-Trefoil domain and β-Prism lectin-like domain at the C-terminal side of the cytolysin domain), which are not commonly documented in any other member of the β-PFT family (181,187,189).

#### 1.5.1.1 Cytolysin domain

The VCC molecular structure contains 325 amino acid-long cytolysin domain that is structurally similar to the cytolysin domains present in the other β-PFTs, like *S. aureus* α-hemolysin. Cytolysin domain of the VCC harbors a 'pre-stem' motif that inserts into the membrane and generates a β-barrel structure which gives rise to a central scaffold of the transmembrane pore state (174,175,183,189,193). Notably, the majority of the rim-domain is also generated by the cytolysin domain.

As mentioned above, cytolysin domain of VCC harbors the 42-residue 'pore-forming loop', which is involved in the formation of the transmembrane β-barrel pore structure. In the water soluble monomeric form of the toxin, this region remains completely folded within the cytolysin domain, in the form of a 'pre-stem' loop.

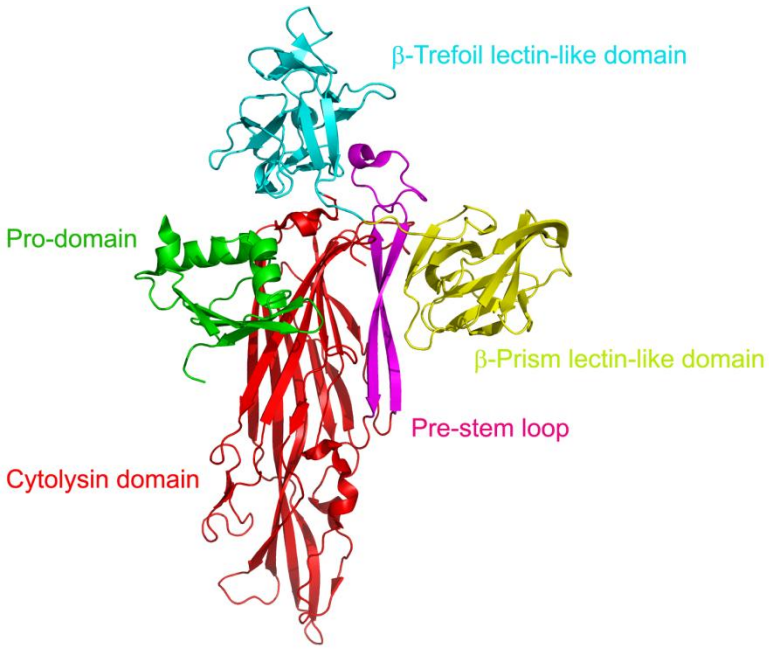


**Figure 1.9: Crystal structure of Pro-VCC (PDB ID: 1XEZ)**

During the process of the functional pore-formation, the 'pre-stem' loop from each of the participating protomers undergoes structural reorganization to obtain a 'stem' configuration, and gets inserted into the lipid bilayer of the membrane. Stem region from each of the protomers contributes two β-strands towards the formation of the stem region of the heptameric β-barrel pore structure (194). The crystal structure of the transmembrane oligomer highlights the contribution of the extensive interactions between the stem regions and the neighboring protomers, towards the robust stability of the oligomeric assembly (174). Apart from the pore-forming stem-loop segment, another part of the cytolysin domain constitutes the membrane-proximal rim-domain of the transmembrane pore structure. The structural analysis of the β-PFT pores suggest an important role of the membrane-proximal rim-domain as a structural scaffold that mediates the interaction of the protein with the lipid head-group of the target membrane lipid bilayer (181).

#### 1.5.1.2 Pro-domain

VCC toxin is secreted by the bacteria as a water-soluble inactive precursor known as Pro-VCC. The high-resolution three-dimensional structure of Pro-VCC shows the presence of ~15 kDa Pro-domain, connected to the the N-terminal side of the core cytolysin domain through a 29-residue long flexible linker. The linker region harbors a ~15 amino acid long sequence that act as the cleavage site(s) for a group of proteases. The proteolytic removal of the Pro-domain generates

the mature form of the toxin (195). The presence of the Pro-domain in the precursor form of the toxin is critical for the efficient secretion and the appropriate folding of the VCC molecule. An earlier study has shown that the *V. cholerae* cells, containing the recombinant truncated *hlyA* gene lacking the sequence for the Pro-domain is unable to secrete the protein (196,197). In vitro denaturation/renaturation assay has demonstrated that without the Pro-domain, VCC fails to refold back to its active conformation. The recent study suggests that the presence of the Pro-domain increases the unfolding property of the Pro-VCC molecule in response to many denaturing conditions, whereas active mature form of the toxin displays considerable resistance towards the unfolding of the toxin (198). The Pro-domain shows an intramolecular chaperone-like activity in terms of providing significant level of structural plasticity in the VCC structure, which probably is essential for the efficient secretion of the toxin in its precursor form across the bacterial membrane (196). However, it's not clear so far how the presence of the Pro-domain keeps the protein in its inactive precursor form.

#### 1.5.1.3 β-Trefoil lectin-like domain

VCC harbors a β-Trefoil lectin-like domain (~15 kDa) at the C-terminal edge of the central cytolysin domain. This β-Trefoil lectin-like domain is also found in related cytolysin from *Vibrionaceae* bacteria, but is not reported in the archetypical β-PFTs like *S. aureus* α-hemolysin. The β-Trefoil lectin-like domain is associated with the cytolysin domain through a short linker sequence constituted of Gly-Gly-Arg-Pro. The β-Trefoil lectin-like domain of VCC displays a structural similarity with the carbohydrate-interacting domain of the plant toxin ricin. The QXW conserved carbohydrate-interacting motif (s) present in this domain is homologous to those found in the the archetypical β-Trefoil lectins (199). However, the carbohydrate binding property of the β-Trefoil domain of VCC has not yet been elucidated. The implications of the β-Trefoil domain in the structure-function mechanism of VCC also need to be explored.

#### 1.5.1.4 β-Prism lectin-like domain

The VCC harbors a ~15 kDa domain that is linked to the C-terminal end of the β-Trefoil domain through a long linker sequence. This domain is not found in any other member of the β-PFT family, including the pore-forming cytolysin secreted by *V. vulnificus* and *Aeromonas hydrophilia*. This C-terminal domain of the VCC displays structural similarity to several β-Prism lectins including jacalin and *Maclura pomifera* agglutinin (MAP) (181,187,200,201). The β-

Prism lectin-like domain of VCC possesses a binding pocket similar to the carbohydrate-binding pocket of the jacalin and MPA lectin. The specific role of the β-Prism lectin-like domain toward the carbohydrate-binding property of VCC has not been explored earlier. During the process of functional pore-formation in the lipid bilayer of the target host membranes, VCC molecule undergoes a profound structural reorganization. The β-Prism domain of the VCC obtains two different structural positions with respect to the central cytolysin domain, in the monomeric precursor form (Pro-VCC) and in the membrane-inserted transmembrane pore state. In the monomeric water-soluble inactive precursor Pro-VCC, the β–Prism domain is positioned on the opposite side of the Pro-domain and masks the pre-stem region (187). In the transmembrane pore state, it is relocated at the place of the Pro-domain (174). This structural rearrangement of the β-Prism domain appears to be mandatory for the membrane insertion and the functional oligomeric pore-formation procedure. In absence of such a structural reorganization of the β-Prism domain, a steric hindrance would be generated between the contributing protomers, and that would subsequently block the oligomerization of the toxin. In addition to this, without such reorganization of the β-Prism domain, the pre-stem loop would not be able to open up for the membrane insertion.

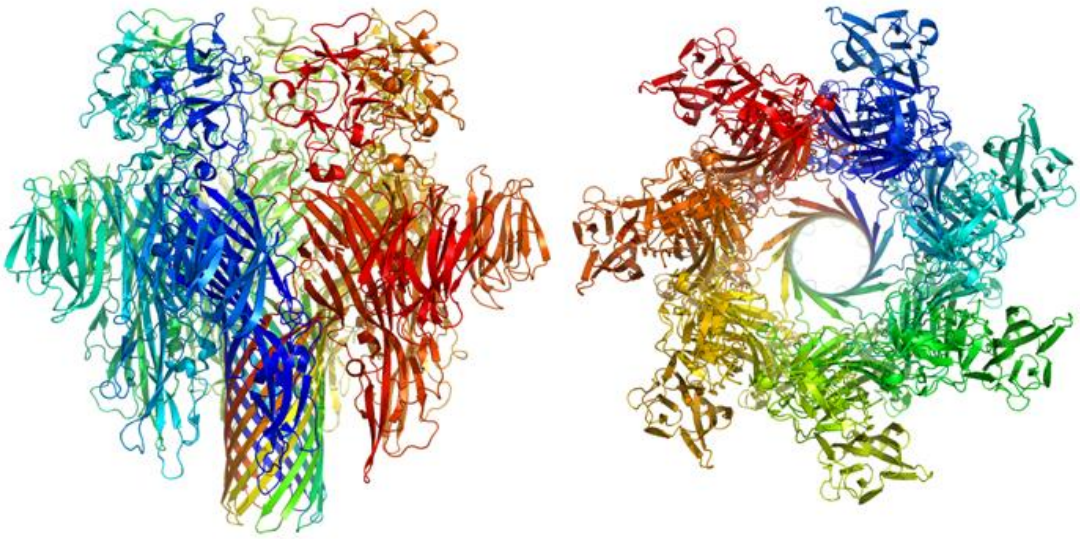

**Figure 1.10: Structure of VCC transmembrane oligomer (PDB ID: 3O44)**

### 1.5.2 Structural features of the VCC β-barrel pore

Earlier study based on the transmission electron microscopy (TEM) has characterized the transmembrane oligomer of VCC as a typical ring-like structure with an inner diameter of ~1-2 nm. The inhibitions of the cytotoxic ability by the osmoprotectants of specific molecular sizes have also suggested similar pore diameter of the VCC oligomer (202). The single channel conductance measurement study on the VCC oligomeric pore generated in the synthetic lipid bilayer has suggested that VCC produces anion-selective diffusion channels (203). This analysis also indicates that the VCC pore has an asymmetric geometry, a larger opening in the '*cis-side'* than that in the '*trans-side'* with a narrow region at the central part of the lumen. The high-resolution structure of the VCC oligomeric pore also shows the 'cup-shaped' lumen geometry of the pore. The analysis of the oligomeric pore structure shows the narrow constriction near the center of the pore lumen, and it is created by the aromatic ring of a tryptophan residue contributed from each of the participating toxin protomers.

### 1.5.3 Structural reorganizations during oligomeric pore-formation

The structural analysis of the water-soluble monomeric form and the transmembrane oligomeric pore form of VCC reveals that VCC undergoes structural reorganization within the toxin monomer during the process of the oligomeric transmembrane pore formation. The most critical structural change is the opening up of the 'pre-stem' region from within the cytolysin domain, and its insertion into the membrane lipid bilayer to generate the 'stem' configuration. In the water soluble monomeric structure of Pro-VCC, the 'pre-stem' region remains packed between the β-Prism domain and the cytolysin domain of the toxin (175). Hence, the movement of the β-Prism domain is essential for the conversion of 'pre-stem' to the 'stem' region of the toxin. During the formation of the functional pore of the toxin on the membrane, the β-Prism domain of the toxin reorients with respect to the central cytolysin domain by almost $180^{o}$ angle, and attains the same location where the Pro-domain is located in the Pro-VCC structure. This reorganization of the β-Prism domain of the VCC represents the second most critical structural change involved in the membrane pore-formation process of VCC. The structural change in the position of the β-Prism domain allows the 'pre-stem' to undergo reorganization for the membrane insertion and the functional heptameric pore-formation process.

### 1.5.4 Mechanism of membrane pore-formation

The pore formation by the β-PFT family members on the membrane lipid bilayer of the target cells involves three distinct steps: (i) interaction of the water-soluble monomeric form of the toxin with the target cell membranes, (ii) self-assembly of the membrane-associated monomeric toxin to generate the intermediate 'pre-pore' oligomeric assembly on the membrane surface, (iii) conversion from the transient 'pre-pore' oligomeric assembly to the functional transmembrane pore structures (128,181,192,204). During the process of the pore-formation, the pore-forming 'stem-loop' of the toxin is inserted into the membrane lipid bilayer, thus generating the transmembrane β-barrel structure.

Many structural studies have reported that most of the members of the β-PFT family follow a similar mechanism of pore formation on the membranes (Figure 1.11). However, each member of the β-PFT family differs from each other in the specific details of the pore-formation process. The membrane interaction step displays an enormous range of variation in terms of receptor specificity. The role(s) of different lipid components and presence of specific receptor(s) on the membrane have been documented. The molecular mechanisms that involve the discrete steps for the functional pore-formation are not properly elucidated for most of the β-PFT members. The pore-formation by VCC can be triggered in the synthetic lipid vesicles or liposomes, indicating that the membrane association step does not critically require any particular non-lipid components. However, the membrane pore-formation is reported to be more efficient in the biomembrane compared to the synthetic lipid bilayer of the liposomes, indicating the possible role of the accessory receptor molecules in the pore-formation process of VCC. For example, erythrocytes are more susceptible towards the toxin as compared to the liposome. VCC toxin shows a different level of hemolytic activity towards the erythrocytes of the different species. The rabbit erythrocytes are found to be more sensitive as compared to the human erythrocytes. Earlier studies have suggested the role of cell surface protein(s) (e.g., glycophorin B on the human erythrocytes) as the potential receptor for the VCC toxin (205).

VCC also exhibits potent lectin-like activity which may aid in its interaction with the target cell membranes. However, the specific receptor for VCC has not been identified. A previous study suggested that the binding of the VCC molecule with the liposomes is mainly driven by the global amphipathicity of the toxin.

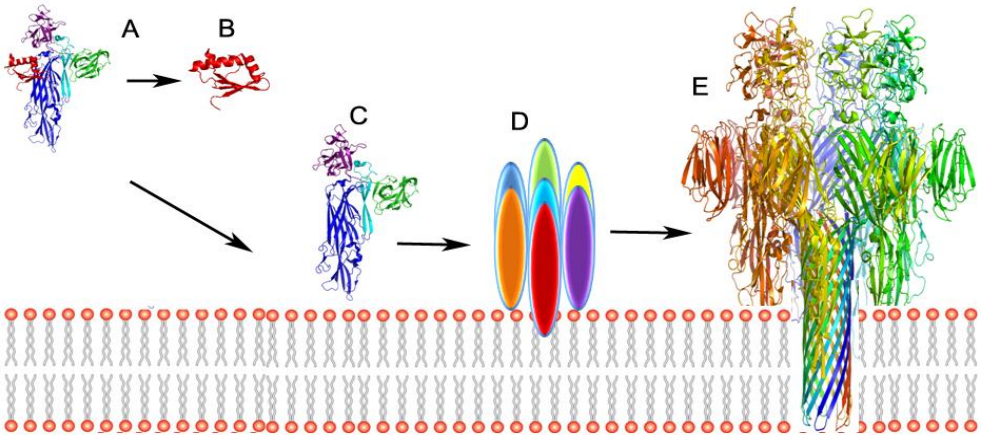


**Figure 1.11: Proposed mode of action by *Vibrio cholerae* cytolysin**. (A) Secretion of the protein as a water-soluble monomer, (B) proteolytic removal of the N-terminal Pro-domain, (C) Interaction of the mature form of the protein with the host cell membrane, (D) self-assembly of the seven monomers to form a non-functional SDS-labile pre-pore oligomer, (E) conversion of the pre-pore oligomer into the SDS-stable functional transmembrane β-barrel channel.

Presence of the cholesterol in the lipid bilayer of the membranes has been suggested to play a critical role in the membrane pore-formation mechanism of the toxin (114,119,192,206-209). In the pore-formation process of VCC, the 'pore-forming loop' of the toxin unfolds and inserts into the membrane toward the generation of the functional pore. It is indicated that the trapping of the pore-forming stem-loop in its pre-stem configuration through engineered disulfide linkages could arrest the toxin in its pre-pore oligomeric assembly. Also, a VCC variant without the pre-stem loop is found to remain arrested in the pre-pore oligomer configuration on the membrane surface. Overall these studies suggested that the VCC follows a similar mechanism of pore-formation as that for the archetypical β-PFTs (208,210). A previous study indicated that the membrane interaction of the VCC precedes membrane oligomerization. Many physicochemical factors also affect the binding and oligomerization events of the toxin. For example, membrane association can occur even at a low temperature of 4 $^{o}$C, while the membrane oligomerization and functional pore-formation gets abrogated under the similar condition. This observation clearly indicates that the association of the toxin with the target cell membrane is a distinct step from its subsequent oligomerization and pore-formation steps. Whatsoever, membrane pore-formation mechanism employed by VCC highlights wide numbers of unsolved issues that remain to explored in detail.

## 1.6 Specific objectives

The present thesis work investigates the structure-function relationship of *Vibrio cholerae* cytolysin (VCC) with special emphasis on the following objectives:

A. To investigate the molecular mechanism of membrane interaction and identify the specific structural motif responsible for the binding to the membrane lipid bilayer of the target cells.

B. To explore the implications of the β-Prism lectin-like domain-mediated lectin property of the toxin.

C. To delineate the sequence of events for the pore-formation on the membrane by VCC.

D. To elucidate the importance of the physicochemical constraints on the membrane pore-formation mechanism of the toxin.

# Chapter 2

## Membrane interaction mechanism of *Vibrio cholerae* cytolysin

### 2.1 Abstract

The pore-formation mechanism of VCC follows a sequence of events that includes interaction of VCC with the target cell membranes, generation of the pre-pore oligomeric intermediate, membrane insertion of the pore-forming stem-loop, and generation of the functional oligomeric pore structure. However, the mechanisms of membrane association, membrane oligomerization, and subsequent pore-formation process are still not understood fully. In this study, we have identified the distinct loop sequences within the membrane-proximal rim region of VCC that supposedly play crucial roles in allowing the interaction of VCC with the target membrane lipid components. Even though any alteration in this loop sequences does not affect the amphipathic-driven partitioning of the VCC towards the target membrane lipid bilayer, such alterations abrogate the more specific association of VCC with the lipid components of the membrane, and block the membrane pore-formation mechanism of the toxin. This structural motif in VCC appears to be necessary for its efficient interaction with the lipid component of the membrane, that in turn, play a critical role toward the membrane pore-formation mechanism of the toxin, thus probably acting as the primary mediator to trigger the successive steps in the functional β-barrel pore formation and cytotoxic responses.

### 2.2 Introduction

VCC is considered as a potent virulence factor of *V. cholerae* due to its efficacy to display enterotoxic activity and cytotoxicity (211). VCC generates transmembrane heptameric β-barrel pores in the target cell membrane, thus leading to the colloid-osmotic lysis of the cells. In accordance with the pore-forming mechanism of the β-PFTs, VCCs follows the same sequence of events: (i) interaction of the water-soluble monomeric toxin to the membrane lipid bilayer of the target cells, (ii) generation of the pre-pore oligomeric intermediate by the membrane-associated toxin molecules, (iii) insertion of the pore-forming stem-loop into the membrane lipid bilayer, (iv) formation of the functional heptameric transmembrane pore structure on the membrane.

Association of the toxin to its target cell membranes represents the most critical steps towards the membrane pore-formation mechanism of the toxin. It has been suggested that the global

amphipathicity of the protein may act as the possible driving force triggering the association of VCC with the membrane lipid bilayer. However, more specific interactions of VCC with the membrane-associated receptor (s) or receptor-like molecule (s) have already been indicated in previous studies (212,213). For example, VCC harbors a specific carbohydrate-binding site within its structure which can be responsible for its interaction with the cell-surface glycan receptors. The association of the toxin with the membrane, followed by the membrane pore-formation processes of the toxin can be mimicked in the membrane lipid bilayer of the liposomes as well (186). Hence, it is evident that the membrane binding and pore-formation mechanism of VCC does not strictly require any non-lipid component(s) present in the membranes. However, the details of the multiple aspects of the VCC: membrane interaction is still unclear.

In order to explore the specific association events of VCC with the membrane lipid bilayer of the target cells, we have examined the structural basis of the lipid-mediated membrane binding mechanism of VCC. Our study identified the distinct structural motif present in the VCC structure that is critically involve in the functional membrane interaction mechanism of the toxin followed by the functional pore-formation process.

## 2.3 Materials and methods

### 2.3.1 Cloning and expression of recombinant VCC mutants

The nucleotide sequence encoding the wild type Pro-VCC protein was amplified by a PCR-based procedure using the *V. cholerae* chromosomal DNA as the template. Regions-specific alterations and site-specific mutations within the nucleotide sequence were introduced by the PCR-based method. The amplified products obtained after PCR were cloned into the expression vector pET14b (Novagen), between the restriction digestion sites of Nde1 and BamH1. The pET14b expression vector allows the addition of six histidine tag at the N-terminal end of the recombinant protein. All the recombinant constructs were verified by DNA sequencing. The recombinant pET14b vector harboring the nucleotide constructs for the Pro-VCC variants were transformed into *E. coli* Origami B cells.

### 2.3.2 Purification of wild type and the mutant variants of Pro-VCC

*E. coli* Origami B cells transformed with the cloned constructs in the pET14b expression vector was grown in the LB medium supplemented with 50 μg/ml of ampicillin. The transformed *E.coli* Origami cells were inoculated in a small-scale seed culture and were grown for overnight at 37 ˚C. The overnight culture of bacteria was inoculated into 1 liter of LB broth medium (2% of the

LB medium volume), the culture was allowed to grow up to $A_{600}$ = 0.6 at 37 $^{o}$C with continuous shaking of 200 rpm. The expression of the recombinant protein was induced by using 1 mM IPTG (Isopropyl β-D-1-thiogalactopyranoside), and the culture was grown for additional three hours at 30 $^{o}$C in continuous shaking conditions. The bacterial cells were pelleted by centrifugation at 2700 x g for 30 minutes in a hanging bucket centrifuge, subsequently the cells were resuspended in 10 ml PBS (20 mM sodium phosphate buffer containing 150 mM NaCl (pH 7.4)) supplemented with bacterial protease inhibitor cocktail (Sigma) (198).

The cells were lysed by employing the ultrasonication by using a Mesonix Ultra sonicator with twenty pulses of thirty seconds each, with ten seconds interval between each pulse, at amplitude of 20, followed by centrifugation at 11,500 x g for 20 minutes at 4 ˚C. The supernatant fraction after the centrifugation was collected, and 20 mM imidazole (prepared in PBS) was added into that fraction, followed by passing through the Ni-NTA column (Qiagen) pre-equilibrated with PBS. The Ni-NTA column was washed with the 50 ml of the 20 mM imidazole in PBS. The recombinant protein of interest was eluted by using 300 mM imidazole in PBS.

The eluted protein from the Ni-NTA column was diluted with a buffer containing 10 mM Tris-HCl and 1 mM EDTA (pH 8.0), and subsequently was loaded onto the Q-sepharose column (GE Healthcare Life Sciences) pre-equilibrated with the same buffer. The bound protein was eluted using a linear gradient of 0 to 500 mM NaCl in 50 ml buffer using an FPLC system (AKTA purifier, GE Healthcare), at a flow rate of 2 ml/minute. Eluted fractions of the protein were examined by SDS-PAGE (10% of gel) and Coomassie staining (198). The concentration of the protein was determined by recording the absorbance at 280 nm, based on the theoretically calculated extinction coefficients obtained from the corresponding amino acid compositions.

### 2.3.3 Generation of mature-VCC

The mature form of the VCC variants were generated by the treatment of trypsin from the Pro-VCC variants, usning a protein: trypsin ratio of 2000:1 for 10 minutes at room temperature. The reaction was stopped by using 1 mM Phenyl Methyl Sulfonyl Fluoride (PMSF). The mature forms of the VCC variants were purified by passing through the Q-sepharose column. Purity of the proteins were examined by SDS-PAGE and Coomassie staining analysis (198). The concentration of the protein was estimated by recording the absorbance at $A_{280}$ using the theoretically calculated absorbance value as predicted from the protein amino acid compositions.

### 2.3.4 Assay of the pore-forming activity in the erythrocytes membranes

The hemolytic activity of the VCC variants against the human erythrocytes was monitored by recording the decrease in the turbidity of the human erythrocytes suspended in PBS. In each experimental setup, concentration of the human erythrocytes was adjusted to OD ~0.9 at $A_{650}$. The concentration of the VCC variants used was 100 nM in each setup, and the lysis of the human erythrocytes was monitored over a period of 1 hr.

### 2.3.5 Binding to the human erythrocytes by flow cytometry

Interaction of the VCC variants with the human erythrocytes was monitored by employing the flow cytometry-based experiment. A previous report suggested that the low temperature (4 $^{o}$C) affects the membrane oligomerization and functional pore-formation efficacy of the toxin without significantly affecting the membrane interaction ability of the protein towards the human erythrocytes. Therefore, we examined and compared the binding ability of the VCC variants to human erythrocytes at 4 $^{o}$C. The human erythrocytes ($10^6$ cells) were incubated with VCC variants (concentration of 75 nM) in a reaction volume of 100 µl at 4 $^{o}$C for 30 minutes in ice-cold PBS buffer. We observed that under this concentration of the protein, VCC could not display any pore-forming ability. Cells were pelleted, and resuspended in 50 µl of PBS buffer containing the rabbit anti-VCC antiserum (1:100 v/v dilution and 0.1% w/v BSA; Sigma-Aldrich), and incubated at 4 $^{o}$C for 30 minute. Cells were treated with the fluorescein isothiocyanate (FITC)-conjugated goat anti-rabbit IgG (1:100 v/v dilution; Sigma-Aldrich) in 50 µl of PBS containing the 0.1% BSA at 4 $^{o}$C for 30 minute. Cells were pelleted, washed twice with ice-cold PBS and resuspended in 500 µl ice-cold PBS and analyzed by using FACSCalibur (BD Biosciences, San Jose, CA, USA) flow cytometer. The FITC fluorescence was recorded using the excitation wavelength 488 nm and emission wavelength of 530 nm in the FL1 channel. Geometric mean fluorescence (GMF) values were calculated by FLOWJO software (www.flowjo.com). The interaction data were calculated using the equation:

$$\%Binding = [(GMF_{test}-GMF_{control})/(GMF_{maximum}- GMF_{control})] \times 100$$

Where, $GMF_{control}$ = GMF for the cells that were not incubated with toxins, but incubated in presence of anti-VCC and anti-rabbit-FITC; $GMF_{maximum}$ = GMF for the cells treated with the highest concentration of WT-VCC used in the assay (75 nm), followed by treatment with anti-VCC and anti-rabbit-FITC.

### 2.3.6 Enzyme-linked immunosorbent assay (ELISA)

Interaction of the VCC variants with the immobilized asialofetuin (Sigma-Aldrich) was examined by employing the ELISA-based assay. 100 μl of asialofetuin (10 μg/ml) in PBS was added into each well of the 96-well flat-bottom microtiter plates (Nunc) and incubated at 4 $^{o}$C for overnight. Next morning the plate was taken out and washed with the PBS containing 0.05% Tween 20 (TPBS). For reducing the nonspecific binding, 200 μl of 3% of nonfat dry milk prepared in PBS was treated for 1 hour. After washing three times with TPBS, VCC variants were incubated at 25 $^{o}$C for 2 hour and subsequently treated with the 100 μl of rabbit anti-VCC antiserum (1:5000 dilution v/v) for 90 minute, washed thrice with TPBS, and subsequently treated with horseradish peroxidase-conjugated goat anti-rabbit IgG (1:10000, v/v) at 25 °C for 1 hour. Interaction of the VCC mutants towards the asialofetuin were observed by color development with mixing of o-phenylenediamine (10 mg/ml) in 0.1 M sodium citrate buffer (pH 4.5) containing $H_2O_2$ (2 μl/ml of 30% (v/v) $H_2O_2$), reaction were quenched by adding 2 N $H_2SO_4$, and absorbance values were recorded at 490 nm in a microplate absorbance reader (iMark, Bio-Rad).

### 2.3.7 Surface plasmon resonance (SPR)

The interaction of the VCC variants with the membrane lipid bilayer of the Asolectin-cholesterol liposomes was monitored by surface plasmon resonance (SPR)-based assay on a Biacore 3000 platform (GE Healthcare Life Sciences) using L1 sensor chip at 25 $^{o}$C. The L1 sensor chip was preconditioned with HBS (20 mM HEPES and 150 mM NaCl, pH 7.5). The L1 sensor chip was prepared for the binding experiment by injecting the Asolectin-cholesterol liposomes (0.5 mM lipid concentration) for 10 minute at a flow rate of 1 μl/minute. After that, washing was performed by using 20 mM NaOH, at a flow rate of 100 μl/ml for 12 seconds. To block the non-specific binding, bovine serum albumin (BSA; 0.1 mg/ml) was injected for 5 minutes at a flow rate of 10 μl/min. VCC variants (with three different concentrations, 250, 500, and 1000 nm) were injected for 600 seconds at the flow rate of 5 μl/min. Additional washing was performed with HBS for additional 60 seconds. The binding sensogram plots were prepared with the BIAevaluation 4.1.1. Software (GE Healthcare Life Sciences). Endpoint response units (corresponding to the irreversibly bound protein on liposome membranes) were obtained from the corrected sensogram plots at the 60 second time-point of buffer injection after the protein injection was complete. After each interacting experiment, L1 chip was regenerated by removing

the liposomes and the associated proteins by using one injection of 40 mM octyl β-D-glucopyranoside at a flow rate of 10 μl/minute for 5 minutes (214). No loss of the Asolectin-cholesterol liposomes binding ability was observed after regeneration.

### 2.3.8 Protein amphipathicity by Triton X-114 partitioning

The amphipathicity of the toxin mutants were estimated by monitoring their partitioning into the detergent-rich phase of Triton X-114. Triton X-114 is a non-ionic detergent that generates a single phase with water-based buffer at a low temperature of 4 $^{o}$C, and separates into detergent-rich phase and water-rich phase at or above the 22 $^{o}$C. VCC mutants (100 μg/ml) were mixed with 2 % (volume/volume) Triton X-114 in PBS (20 mM sodium phosphate buffer containing 150 mM NaCl (pH 7.4)) at low temperature 4 $^{o}$C in a reaction volume of 500 μl. When the temperature of the reaction mixture increased to 25 $^{o}$C, the two different phase of the reaction mixture separate to each other, aliquots of 100 μl were collected from each phase, proteins were precipitated by using the 9-volume ice-cold acetone. The acetone precipitated samples obtained from the reaction setup were analyzed by SDS-PAGE (10 % of gel) and Coomassie staining.

### 2.3.9 Pull-down assay with liposomes

The binding of the VCC mutants with the lipid bilayer of the Asolectin-cholesterol liposomes was monitored by using the pull-down-based assay. VCC mutants (1 μM) were incubated in the presence of Asolectin-cholesterol liposomes (6.5 μg) in a reaction volume of 100 μl for 30 minutes at 25 $^{o}$C. After the completion of the incubation, the reaction mixture was subjected to ultracentrifugation at 105,000 × g at 4 $^{o}$C for 30 minutes. The supernatant fraction was collected carefully after the ultracentrifugation and the pellet fraction was washed with PBS and then resuspended in 100 μl PBS. For examining the liposome-bound VCC mutants and free VCC variants, equal volume of aliquots of the supernatant and the pellet fraction of the protein were boiled for 10 minutes in the presence of the SDS-PAGE loading buffer (62.5 mM Tris-HCl pH 6.8, 2.5 % SDS, 0.002 % Bromophenol Blue, 0.7135 M (5%) β-mercaptoethanol, 10 % glycerol ) and analyzed by SDS-PAGE/Coomassie staining.

For probing the formation of the SDS-stable oligomers in the presence of the lipid bilayer of the Asolectin-cholesterol liposomes, VCC mutants (1μM) were treated with the liposome suspensions (6.5 μg) in a reaction volume of 100 μl for 30 minutes at 25 $^{o}$C as mentioned above. Asolectin-cholesterol liposome-associated fractions of the VCC mutants were pelleted by using

ultracentrifugation at 105,000 × g at 4 $^{o}$C for 30 minutes. The pellet fractions were washed with the PBS and further dissolved in 50 μl SDS-PAGE loading sample buffer and divided into two equal aliquots. One part was incubated at room temperature, whereas the other half part was boiled for 10 minutes. The oligomerization propensity of the toxin was analyzed by SDS-PAGE/Coomassie staining. The unboiled protein sample allowed the detection of the SDS-stable oligomers of the liposome-associate VCC mutants.

For the trapping of any SDS-labile pre-pore oligomers formed by the VCC mutants in the presence of the Asolectin-cholesterol liposomes, $BS^3$ [bis(sulfosuccinimidyl) suberate; Thermo Pierce a homobifunctional N-hydroxysuccinimide ester (NHS ester)crosslinker] was used for the covalent cross-linking of the pre-pore oligomer. Protein variants (1 μM) were incubated with the Asolectin-cholesterol liposomes (6.5 μg) in a reaction volume of 100 μl for 30 minutes at 25 $^{o}$C, subsequently by ultracentrifuge at 105,000 × g for 30 minutes at 4 $^{o}$C. The pellet fraction was washed and resuspended in 50 μl of PBS in the presence and the absence of 5 mM $BS^3$ and was incubated for 30 minutes at 25 $^{o}$C. The reaction was terminated by the addition of 50 mM Tris-HCl (pH 8.0) for 15 min. The reactions were subjected to ultracentrifugation at 105,000 × g for 30 minutes at 4 $^{o}$C. The pellet fractions were boiled for 10 minutes. The generation of the SDS-labile pre-pore oligomer was analyzed by SDS-PAGE/Coomassie staining.

### 2.3.10 Preparation of the liposomes

Asolectin, cholesterol, 1,6-Diphenyl-1,3,5-hexatriene (DPH) and calcein were obtained from Sigma-Aldrich. For the preparation of the Asolectin-cholesterol liposomes, equal amounts (5 mg) of asolectin and cholesterol were dissolved in 2 ml chloroform in a round-bottom flask. The chloroform was evaporated at room temperature under constant shaking for generation of a lipid film. The lipid film was dried under vacuum for 4 hours, followed by resuspension in PBS at 37 ˚C for 4 hours. For preparing uniform large unilamellar vesicles (LUVs), liposomes were continuously extruded through a 0.1 μm polycarbonate membrane using a Mini-Extruder apparatus (Avanti Polar Lipids, Inc., Alabaster, AL, USA). For preparing dansyl-PE-containing Asolectin-cholesterol liposomes, 1% dansyl-PE (w/w) was mix to the initial lipid mixture.

For the preparation of the calcein-trapped Asolectin-cholesterol liposomes, the dry lipid film was resuspended in HBS (20 mM HEPES, 150 mM NaCl, pH 8.0) containing 50 mM calcein dye for 2 hours at 37 $^{o}$C with continuously shaking condition. The untrapped calcein dye was removed by ultracentrifugation. The calcein entrapped liposomes were pelleted at 105,000 × g for 20

minutes at 4°C. The supernatant containing untrapped calcein was removed, and calcein containing liposome pellet was washed 5-6 times with HBS. To obtain a homogenous mixture of large unilamellar liposome vesicles, the calcein trapped liposomes were repeatedly extruded through a 0.1 μm polycarbonate membrane using a Mini-Extruder apparatus. After extrusion, untrapped calcein dye was removed by passing through Sephadex G-50 (GE Healthcare Life Sciences) size-exclusion chromatography column equilibrated with HBS. The calcein-release assay was performed on a Perkin-Elmer LS 55 spectrofluorimeter. Protein (1 μM) was incubated in the presence of 100 μM calcein-trapped Asolectin-cholesterol liposomes in a 2 ml reaction volume. The calcein fluorescence was recorded at 520 nm upon excitation at 488 nm, using 1 cm cuvette, with the excitation and emission slit widths of 2.5 nm and 2.5 nm, respectively. The 100% calcein release was obtained by treating liposomes with 6 mM sodium deoxycholate.

For the preparation of 1,6-Diphenyl-1,3,5-hexatriene (DPH)-labelled Asolectin-cholesterol liposomes, the DPH stock of 1 mg/ml was made in 1,2-Dioxane. The liposomes resuspension in PBS were incubated with DPH (1:200, w/w) for 1 hour at 25 ˚C.

**2.3.11 Fluorescence resonance energy transfer (FRET) assays**

Fluorescence resonance energy transfer (FRET) from the tryptophan residue (Trp318) located in the stem region of the VCC to DPH (Diphenylhexatriene) incorporated in the lipid bilayer of the Asolectin-cholesterol liposomes was examined to qualitatively probe the membrane insertion event of the VCC (194). The Asolectin-cholesterol liposomes (50 μg/ml) labeled with DPH was incubated with VCC mutants (1 μM) in 10 mM Tris-HCl buffer containing 150 mM NaCl at 25°C. FRET signal from the tryptophan-to-DPH was recorded on a Perkin-Elmer LS 55 spectrofluorimeter by recording the intensity of the fluorescence at 470 nm upon excitation at 290 nm, with the excitation and emission slit widths of 2.5 nm and 5 nm, respectively.

FRET from the tryptophan residue of VCC to the dansyl-PE incorporated in the Asolectin-cholesterol liposomes (outer leaflet of liposome labeled with dansyl-PE) was monitored to assess the intimacy of VCC with the membrane. The dansyl-PE labeled Asolectin-cholesterol liposomes were incubated with the VCC mutants (1 μM) in 10 mM Tris-HCl buffer containing 150 mM NaCl at 25°C. FRET signal from the tryptophan-to-dansyl was recorded on a Perkin-Elmer LS 55 spectrofluorimeter by recording the intensity of the fluorescence at 512 nm upon excitation at 280 nm, with the excitation and emission slit widths of 2.5 nm and 5 nm, respectively. The data

were corrected using the control experiment with the Asolectin-cholesterol liposomes labeled with dansyl-PE in the absence of any protein treatment.

### 2.3.12 Association and cytotoxicity assay with the human colorectal adenocarcinoma cells HT-29

The HT-29 cells were grown in DMEM culture medium containing 10% fetal bovine serum (FBS), 100 μg/ml streptomycin and 100 units/ml penicillin (Invitrogen Life Technologies), and were maintained in a humidified atmosphere of 5% $CO_2$ at 37 $^oC$.

Interaction of the VCC mutants towards the HT-29 cells was monitored by employing the flow cytometry-based experiment as mentioned above. Briefly, HT-29 cells ($0.5\times10^5$ cells) were treated with the VCC mutants (100 nM) at 25 $^oC$ for 1 hour in PBS with a reaction volume of 100 μl, followed by staining with anti-VCC antiserum and FITC-conjugated goat anti-rabbit antibody. The cells that were not treated with protein but stained with the anti-VCC and anti-rabbit-FITC served as a control experiment. Percentage of interaction with the HT-29 cells was calculated as described above.

The cytotoxic effect of the VCC variants toward the HT-29 cells was monitored by the LDH (lactate dehydrogenase)-release assay. Briefly, HT-29 cells ($10^5$ cells) were treated with VCC mutants (100 nM) in a reaction volume of 100 μl at 37 $^oC$ for 24 hr. After the incubation, the culture medium was collected and was examined for the LDH-release by using the CytoTox 96® Non-Radioactive Cytotoxicity Assay Kit (Promega), as per the manufacturer's instructions. HT-29 cells without the toxin treatment served as the negative control, while the treatment with Triton-X-100 (0.8%) was taken as the positive control with 100% LDH-release.

### 2.3.13 Analysis of the structural models

The structural models of the water-soluble monomeric state and the transmembrane state of protein were generated by using the protein data bank (PDB) ID 1XEZ and 3O44, respectively. The transmembrane heptameric pore structure of VCC was modeled with the OPM server found online (http://opm.phar.umich.edu/server.php) (215). *S. aureus* α-hemolysin and perfringolysin O structural models were generated by using the PDB entry 7AHL and 1PFO, respectively. Structural models were visualized with PyMOL [DeLano WL, The PyMOL Molecular Graphics System (2002) found online (http://pymol.org)].

## 2.4 Results and discussion

### 2.4.1 Characterization of the VCC variants harboring alterations/mutations in the membrane-proximal loop region that might be critical for the membrane interaction

Analysis of the transmembrane oligomer structure of VCC highlights two distinct structural regions which might make intimate associations with the target membrane lipid bilayer: (i) rim region that lie on the surface of the membrane, and responsible for direct contacts with the phospholipid head-groups, and (ii) a transmembrane 'stem-region' that insert into the membrane lipid bilayer. The transmembrane 'stem-region' is composed of fourteen-strand β-barrel generated from the involvement of two β-strands from each of the toxin protomers. In its water-soluble monomeric form, these β-strands are arranged in a structure known as 'pre-stem', packed within the core cytolysin domain. The removal of the 'pre-stem' region from the toxin does not block membrane interaction and traps the toxin in its abortive pre-pore oligomeric state (194). This observation confirms that the association of the 'stem region' with the membrane does not play any critical role in the initial stage of the membrane interaction step. The 'rim-region' of VCC oligomeric structure is composed by the three loop sequences ($^{236}$TTL$^{238}$, $^{359}$DALW$^{362}$, and $^{420}$YYVVGA$^{425}$), contributed by each of the toxin protomers. These three loops are positioned at the bottom tip of the cytolysin domain. However, no report is available to confirm any involvement of these regions in the membrane interaction step of the toxin.

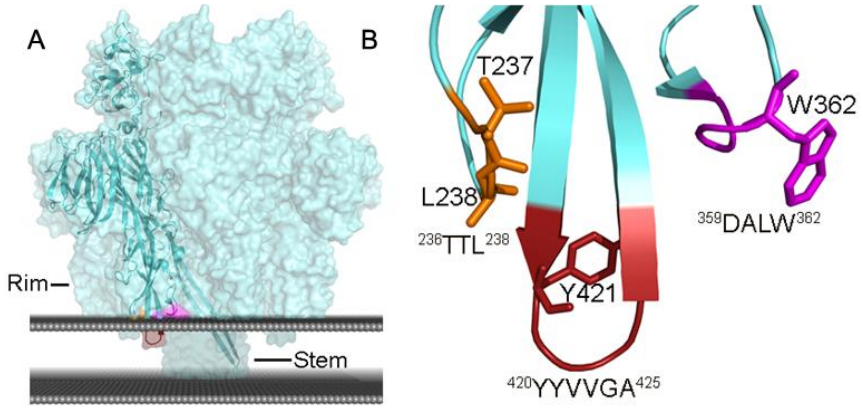


**Figure 2.1: (A) Structural model of the transmembrane oligomeric form of VCC (B) Zoomed view of the three membrane-proximal loop sequences of the VCC. (A**) Molecular Structure model of the transmembrane

oligomeric form of VCC. Membrane-interacting loop sequences are highlighted (orange, $^{236}$TTL$^{238}$; magenta, $^{359}$DALW$^{362}$; red, $^{420}$YYVVGA$^{425}$). (**B)** Zoomed view of the three membrane-interacting loop sequences.

In the present study, we have elucidated the roles of the three loop sequences, $^{236}$TTL$^{238}$, $^{359}$DALW$^{362}$, and $^{420}$YYVVGA$^{425}$ present in VCC structure, for the membrane interaction and oligomeric pore-formation mechanism of the VCC (Figure 2.1 A).

The three loop sequences, $^{236}$TTL$^{238}$, $^{359}$DALW$^{362}$, and $^{420}$YYVVGA$^{425}$, present in the membrane-proximal rim region of the transmembrane heptameric pore structure of the toxin, were changed with the flexible linker repeat: the $^{236}$TTL$^{238}$ was changed with GGA, $^{359}$DALW$^{362}$ was changed with GGAG, and $^{420}$YYVVGA$^{425}$ was changed with GGAGGA (Figure 2.1 B). The corresponding VCC mutants were named as Loop$^{236\text{-}238}$, Loop$^{359\text{-}362}$, and Loop$^{420\text{-}425}$, respectively. To further explore the functional importance of these loop sequences, one of the hydrophobic and/or aromatic residues from each loop was subjected to point mutation with alanine (T237A, L238A, W362A, and Y421A mutants). Furthermore, W362 was also changed with either tyrosine or phenylalanine (W362Y and W362F).

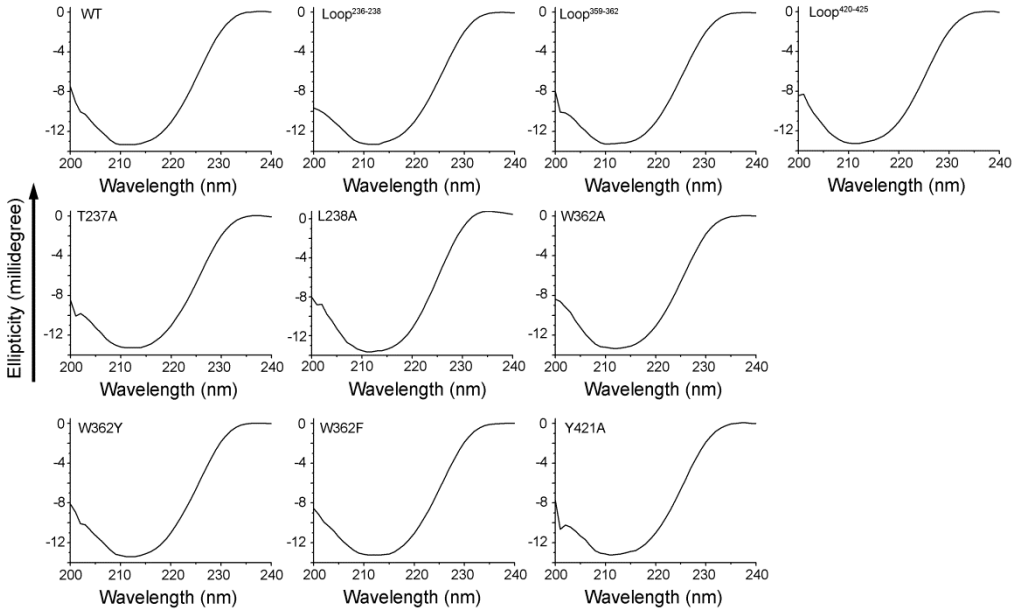


**Figure 2.2: Far-UV CD spectra of the VCC variants.** Analysis of the far-UV circular dichroism (CD) profile of the VCC variants confirmed the structural integrity of the proteins.

VCC mutants harboring the changed loop sequences were recombinantly overexpressed, purified and were examined for their structural integrity by recording the far-UV CD and intrinsic tryptophan fluorescence emission spectra (216).

All the VCC mutants showed almost similar far-UV CD and tryptophan fluorescence emission spectra profile as observed with the wild type VCC toxin, indicating that the mutations in the specific loop regions did not change the secondary and tertiary structural organization of the mutants (Figure 2.2 and Figure 2.3).

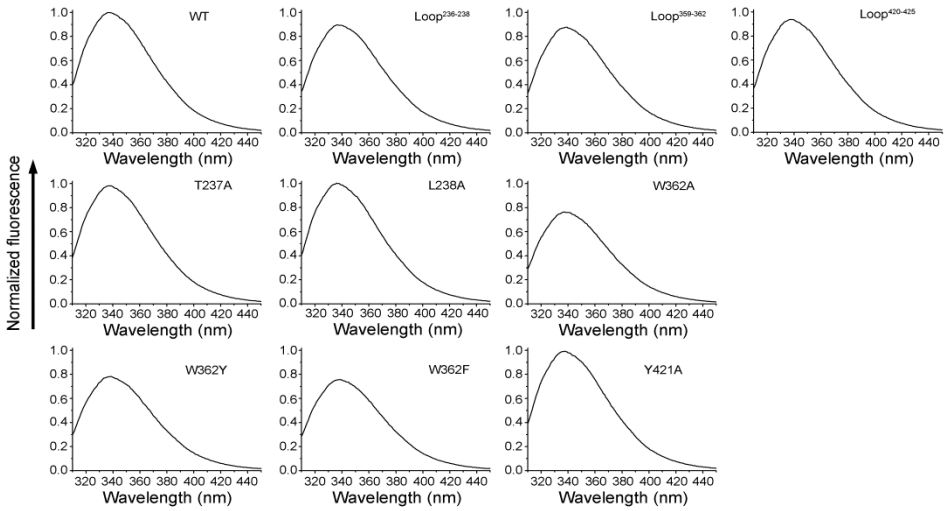


**Figure 2.3: Intrinsic tryptophan fluorescence spectra of the VCC variants.** Analysis of the intrinsic tryptophan fluorescence emission spectra of the VCC variants confirmed folding and structural integrity of the proteins.

### 2.4.2 Alterations in the loop sequence affect functional pore-formation

VCC generates oligomeric transmembrane β-barrel pores in the membrane lipid bilayer of the human erythrocytes, hence leading to the colloid-osmotic lysis of the cells. Membrane-permeabilization ability of the VCC mutants towards the human erythrocyte membranes was examined by the hemolytic activity assay, where the cells were incubated with toxins (100 nM) over a period of 1 hour. Under the similar condition, wild-type VCC (WT) triggered complete lysis of the human erythrocytes. Out of the three loop mutants, Loop$^{359\text{-}362}$ showed marginal ~10% hemolytic activity, whereas Loop$^{236\text{-}238}$ and Loop$^{420\text{-}425}$ were unable to show any noticeable hemolytic activity (Figure 2.4). Among the point mutants, T237A induced ~45% hemolysis while alanine substitution of L238A, W362A and Y421A resulted in complete loss of

activity. W362F showed marginal ~20% hemolysis, whereas W362Y was devoid of any detectable activity.

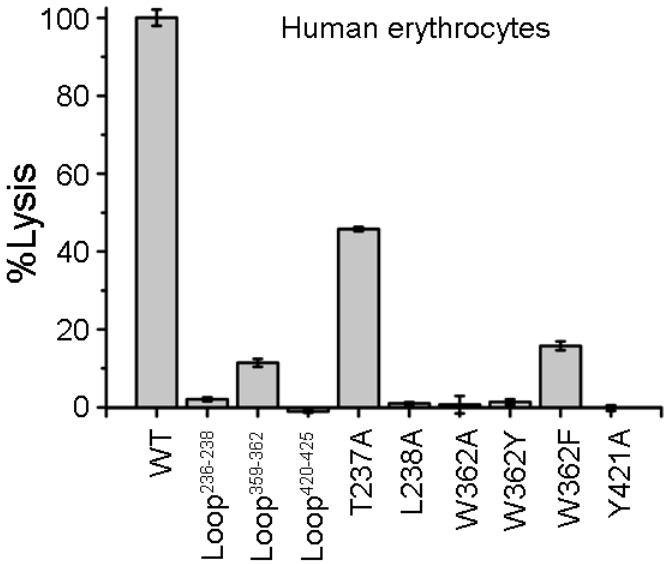


**Figure 2.4: Hemolytic activity of the VCC loop variants against the human erythrocytes.** The pore-forming activity of the VCC variants against the human erythrocytes. Data presented here are the average ± standard deviation of three independent experiments.

VCC mutants were also examined for their pore-forming ability against the Asolectin-cholesterol liposomes, by observing the release of entrapped calcein from within the Asolectin-cholesterol liposome vesicles with treatment with 1 μM proteins for 30 min. Under the similar experimental condition, wild type VCC induced nearly 80% calcein release. Consistent with the hemolytic activity data against human erythrocytes, T237A trigger almost 45% calcein release. Loop$^{359\text{-}362}$ displayed ~25% calcein release while ~18% activity was observed for the mutants Loop$^{420\text{-}425}$ and W362F. For the rest of the mutants, marginal ~5% calcein release activity was recorded. Overall, our experimental results suggested that the mutation in the loop sequences, $^{236}$TTL$^{238}$, $^{359}$DALW$^{362}$, and $^{420}$YYVVGA$^{425}$, severely affected the pore-forming activity of toxin against the human erythrocytes and the membrane lipid bilayer of Asolectin-cholesterol liposomes vesicles (Figure 2.5). Also, the single point mutations within the loop regions drastically abrogated the membrane permeabilization ability of the toxin; only T237A mutant displayed significantly less affected pore-forming activity.

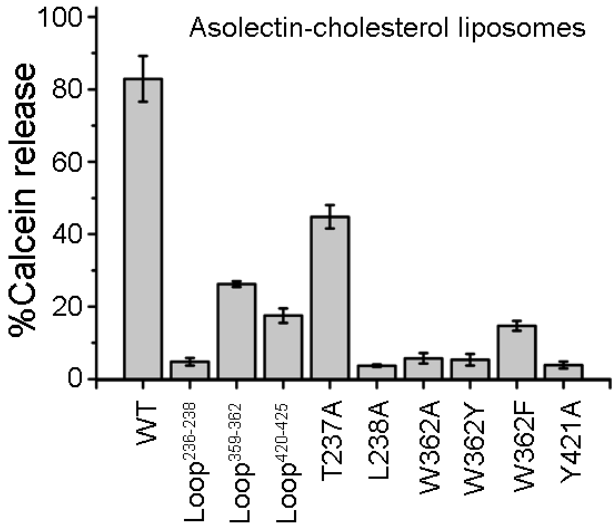


**Figure 2.5: Calcein-release assay to monitor membrane pore-forming activity of the VCC loop variants.** Membrane permeabilization ability of the VCC variants/mutants against the Asolectin-cholesterol liposomes, as observed by the calcein-release assay. Data presented here are the average ± standard deviation of three independent experiments.

### 2.4.3 Alterations in the loop sequences abrogate the membrane interactions of the toxin without inhibiting its lectin activity

#### 2.4.3.1 Interaction with the human erythrocytes

VCC toxins with mutation in the loop region were examined for their efficacy to interact with the membrane of human erythrocytes. A flow cytometry-based experiment was employed to probe the interaction with the human erythrocytes by VCC mutants (75 nM) at a low-temperature condition of 4 $^{o}$C.

The low-temperature condition has been shown to inhibit the pore formation-mediated lysis of the human erythrocytes, without affecting the cell-interacting efficacy of the VCC protein. Also, the low-temperature condition is suggested to reduce the hydrophobicity-driven non-specific binding of the toxin with the target cell membranes, and therefore probably allowing detection of specific mode of interaction of VCC to the membrane of human erythrocytes.

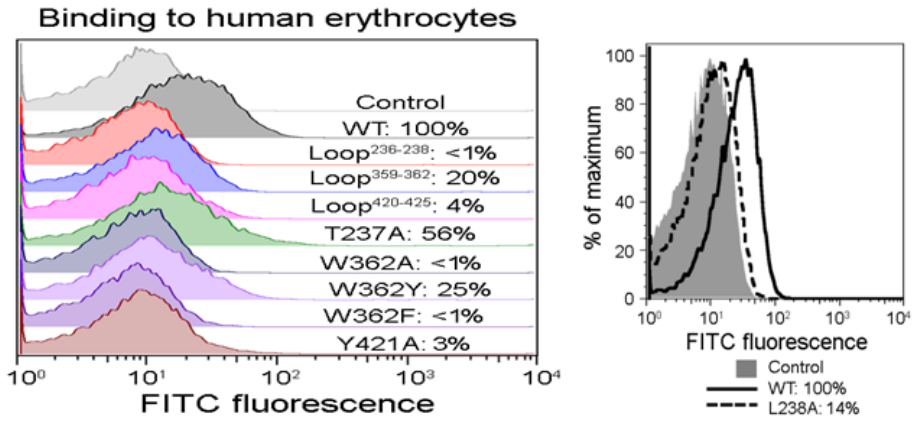


**Figure 2.6: Flow cytometry-based assay to monitor binding of VCC variants to human erythrocytes.** Interaction of the VCC variants (75 nM) to human erythrocytes membrane was monotored by the flow cytometry-based experiment.

The experimental results displayed a severely abrogated human erythrocyte interacting profile for all the VCC loop mutants as compared to that result obtained with the wild-type VCC. The T237A mutant exhibited ~56% of the wild-type VCC interaction, whereas for all the other variants interaction was in the range of nearly 25% or less with compared to the wild-type interacting activity (Figure 2.6).

### 2.4.3.2 Lectin activity of the VCC variants

Wild-type recombinant VCC displayed a prominent lectin-like activity towards β1-galactosyl-terminated complex glycoconjugates, which is employed by its C-terminal β-Prism lectin-like domain. The carbohydrate binding activity of the toxin has been demonstrated to play a significant governing role in the membrane association process of the VCC toxin (217) (presented in the later part of the present thesis work). We, therefore, examined the possibility whether the inhibition of the erythrocytes interaction of the VCC variants was caused due to an abortive lectin activity of the VCC variants (Figure 2.7).

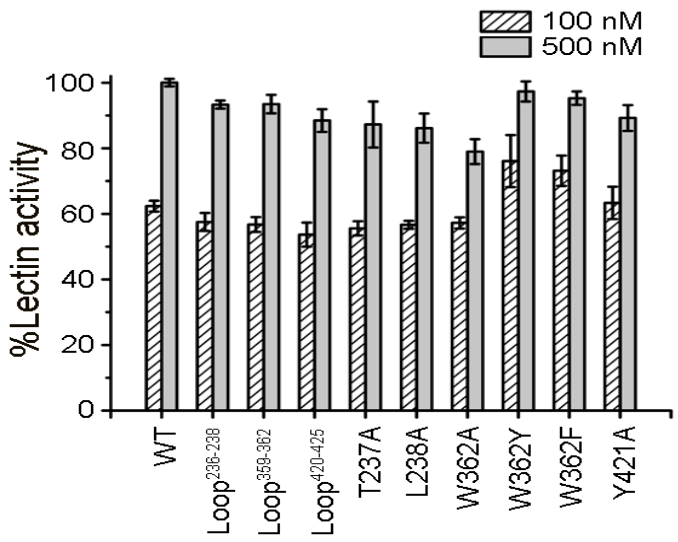


**Figure 2.7: ELISA-based assay to determine binding of VCC variants with immobilized asialofetuin.** Lectin property of the VCC variants (with two different protein concentrations of 100 and 500 nM) was monitored by examining binding to the glycoprotein asialofetuin using the ELISA-based experiment. Data presented here are the average ± standard deviation of three independent experiments.

Notably, all the VCC mutants with altered loop sequences displayed wild type-like lectin efficacy. This data indicated that the changed loop structures of $^{236}$TTL$^{238}$, $^{359}$DALW$^{362}$, and $^{420}$YYVVGA$^{425}$ did not block the lectin activity of VCC variants with the glycoprotein.

### 2.4.3.3 Association with Asolectin-cholesterol liposomes

We probed the interacting ability of the VCC loop mutants with the lipid bilayer of the Asolectin-cholesterol liposomes by employing a surface plasmon resonance (SPR)-based experiment. Each of the VCC mutants (with three different concentrations; 250, 500 and 1000 nM) was injected over the liposome layer at a particular flow rate, and at the end of the injection blank buffer was passed, to obtain an end point response signal showing the degree of irreversible associated toxin with the liposome membranes.

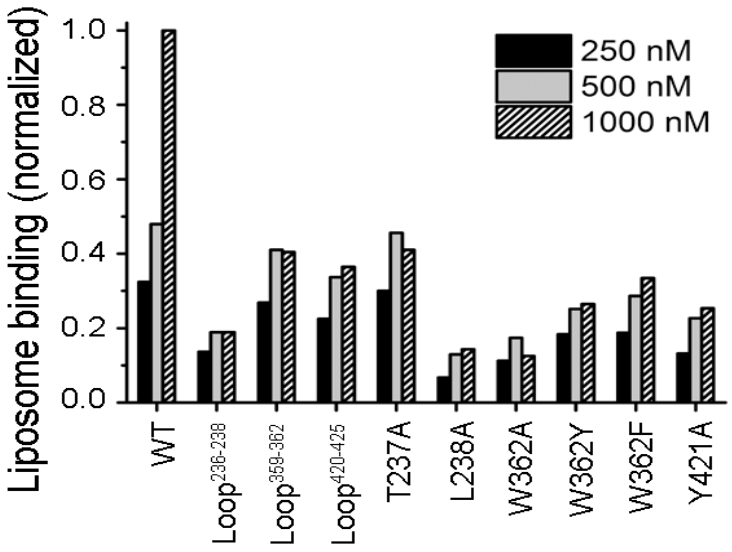


**Figure 2.8: Binding of the VCC variants to the membrane lipid bilayer of the Asolectin-cholesterol liposomes was examined by employing the SPR-based assay.** Association of the VCC variants to the membrane lipid bilayer of the Asolectin-cholesterol liposomes was monitored by employing the SPR-based experiment. Concentrations of protein used for the SPR assay were 250, 500, and 1000 nM.

All the VCC loop variants displayed significant inhibition of association to the Asolectin-cholesterol liposomes as compared to the wild-type toxin, indicating that the mutations of the loop sequences in $^{236}$TTL$^{238}$, $^{359}$DALW$^{362}$, and $^{420}$YYVVGA$^{425}$ (both in case of replacement and point mutations) severely affected interaction of the VCC mutants to the lipid components of the Asolectin-cholesterol liposome vesicles (Figure 2.8 and Figure 2.10).

**2.4.3.4 Association with Asolectin liposomes**

Many previous studies reported that the membrane lipid component of the target cell membrane play a significant role in the pore-forming ability of the toxin. Cholesterol has been shown to play an important role(s) in the membrane pore-forming ability of the toxin (119,207,209,213). We tested whether the loop sequences $^{236}$TTL$^{238}$, $^{359}$DALW$^{362}$, and $^{420}$YYVVGA$^{425}$ in VCC toxin played any significant role in terms of more specific interaction with cholesterol present in the target host cell membrane. For this, we examine the interaction of the VCC mutants with the Asolectin liposomes in the absence of cholesterol, by employing the SPR-based experiment. Consistent with the previous observation, interaction of wild-type VCC toxin to the Asolectin liposomes was drastically less as compared to the Asolectin-cholesterol liposomes (Figure 2.9

and Figure 2.11). However, interacting ability of the VCC variants with the Asolectin liposomes were less than the wild type VCC toxin.

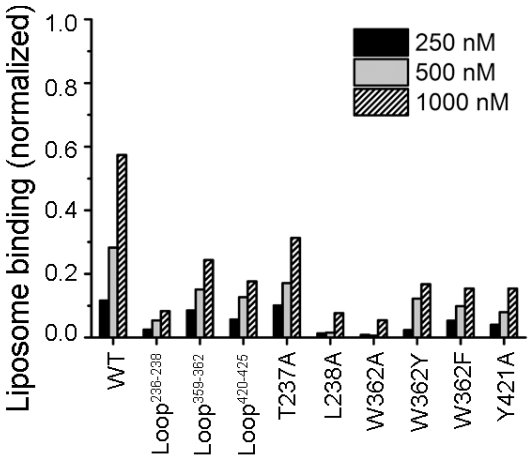


**Figure 2.9: Binding of the VCC variants to the membrane lipid bilayer of the Asolectin liposomes was examined by employing the SPR-based assay.** Association of the VCC variants to the membrane lipid bilayer of the Asolectin liposomes was monitored by using the SPR-based assay. Concentrations of protein used for the SPR assay were 250, 500, and 1000 nM.

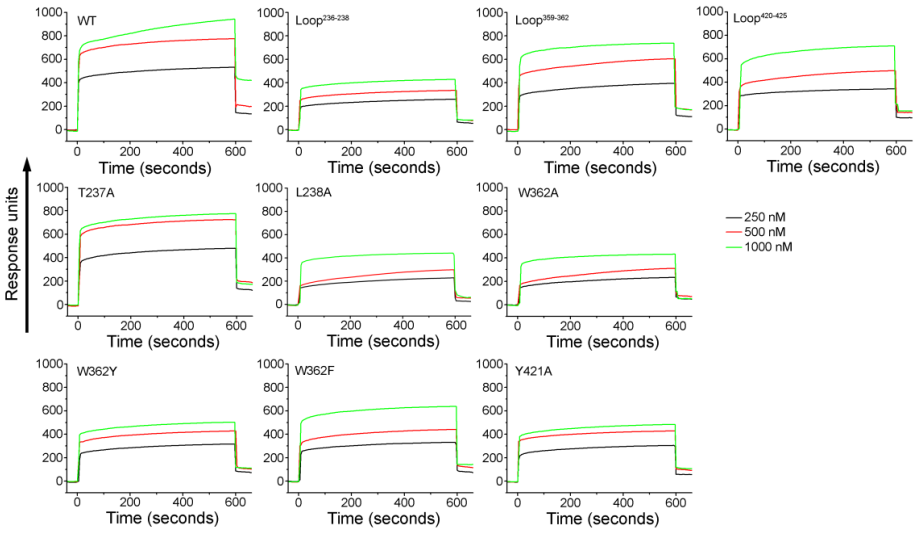


**Figure 2.10: SPR sensogram profile is showing binding of the VCC variants to the Asolectin-cholesterol liposomes.**

These experimental results indicated that the mutation of the loop sequences in VCC inhibited the interacting ability of the VCC toxin to the membrane lipids in general, and not that specifically towards the cholesterol present in the membrane. If the loop sequences were particularly identified by the cholesterol present in the membrane, then the VCC variants would have displayed the similar extent of interaction with the Asolectin liposomes, as compared to the wild-type toxin.

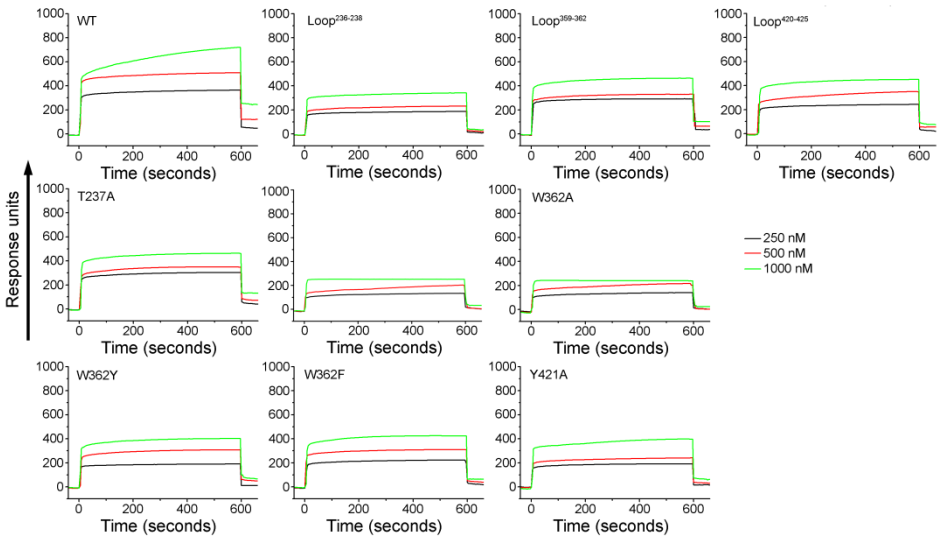


**Figure 2.11: SPR sensogram profile is showing binding of the VCC variants to the Asolectin liposomes.**

### 2.4.4 VCC variants retain hydrophobicity-driven membrane interaction

#### 2.4.4.1 Amphipathicity-driven partitioning to the Asolectin-cholesterol liposomes

Wild-type VCC toxin exhibits high degree of global amphipathicity in terms of its ability to partition into the detergent-rich phase of Triton X-114. Such quality is observed with the membrane proteins, and is not commonly reported in case of typical water-soluble proteins. This high global amphipathicity of the VCC toxin has been suggested as the driving forces allowing its spontaneous partitioning to the amphipathic environment of the lipid bilayer. VCC mutants containing the altered loop region displayed partitioning into the detergent-rich phase of Triton X-114, similar to that of the wild type VCC, indicating that the VCC variants having alterations/mutations in the loop region did not show any change in their global amphipathicity (Figure 2.12).

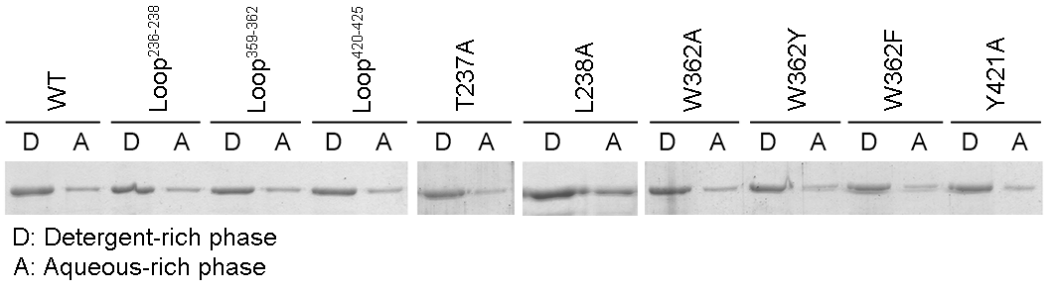


**Figure 2.12: Partitioning of the VCC loop variants into the detergent-rich phase of Triton X-114**

We performed a pull-down-based experiment to examine whether the VCC variants could associate with the Asolectin-cholesterol liposomes. Certainly, all the VCC mutants displayed prominent association with the Asolectin-cholesterol liposome vesicles, presumably due to their high global amphipathicity (Figure 2.13).

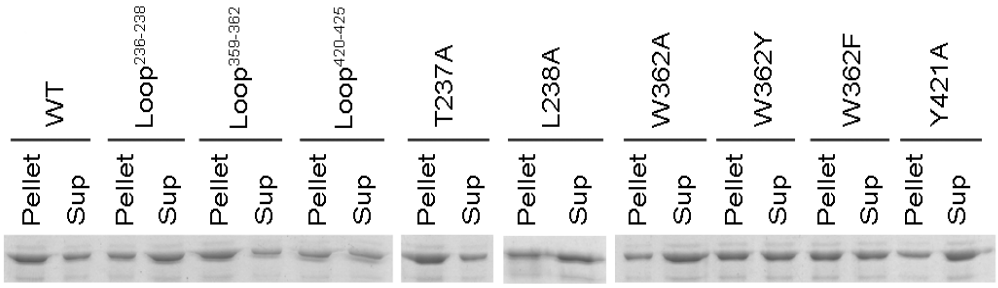


**Figure 2.13: Pull-down assay to monitor association of the VCC variants with the Asolectin-cholesterol liposomes.** Binding of the VCC variants with the Asolectin-cholesterol liposomes as examined by the pull-down experiment.

### 2.4.4.2 Intimate association with the lipid head-group of the Asolectin-cholesterol liposomes

We monitored whether the VCC variants could mediate interaction with the lipid head-groups of the liposomes while associating with the Asolectin-cholesterol liposomes. To observe the intimacy of the membrane-bound VCC protein with the lipid head-groups of the membrane, we examined FRET from the tryptophan residue(s) in VCC toxin to the Dansyl-PE incorporated in the Asolectin-cholesterol liposomes. Because of its close proximity to the membrane surface, W362 (out of the 11 tryptophan amino acid residues in wild-type VCC toxin) has been anticipated to make the most of the FRET contributions to the Dansyl fluorophore covalently bound with the head-group of PE in the liposomes (Figure 2.14). Based on such proposition, a significant increase in tryptophan-to-dansyl FRET signal upon incubation of wild-type VCC with

the Dansyl-PE-containing liposomes would suggest proximity and an intimate association of W362 with the membrane lipid head-groups.

Intimate interaction of the VCC variants with the lipid head-groups of the Asolectin-cholesterol liposome was examined by monitoring the FRET signal from the tryptophan residues in protein to Dansyl-PE in the liposome membranes.

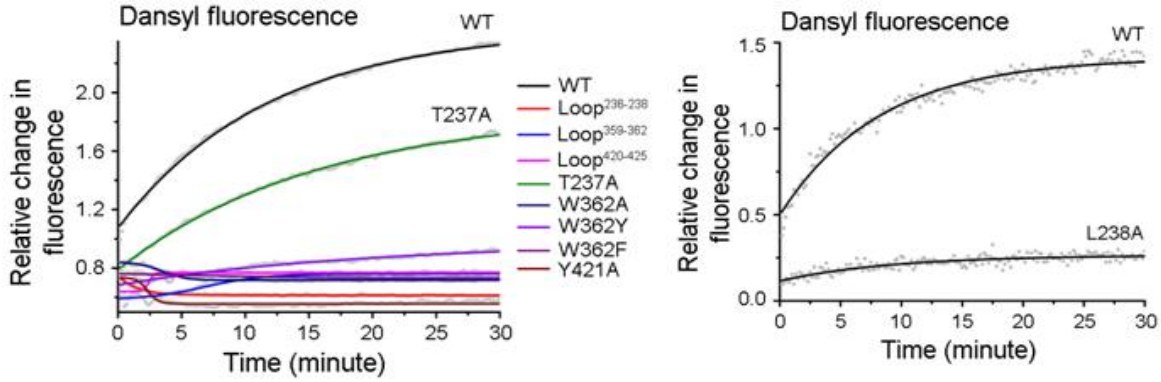


**Figure 2.14: Intimate interaction of VCC with the lipid head-groups of the Asolectin-cholesterol liposomes probed by the FRET signal from the tryptophan residues in protein to Dansyl-PE in the liposome membranes.**

Consistent with the previous observation, wild type VCC showed a significant time-dependent increase in the tryptophan-to-dansyl FRET signal upon incubation with the Dansyl-PE-labelled Asolectin-cholesterol liposomes. Interestingly, relative fluorescence of different constructs at time zero varies due to the different ability of the VCC variants to make intimate interaction with liposomes and also the quantity of dansyl labeled in liposome affected the FRET efficiency. All the VCC variants that were lacking W362 (Loop$^{359\text{-}362}$, W362A, W362Y, and W362F) failed to induce any such FRET signal. Notably, all the other loop mutants, with the presence of W362, were also shown severely abrogated tryptophan-to-Dansyl FRET. The mutant T237A displayed a marginal increase in the time-dependent FRET signal, albeit significantly less as compared to the wild-type toxin. Overall, these experimental data suggested that the mutation of the loop sequences $^{236}$TTL$^{238}$, $^{359}$DALW$^{362}$, and $^{420}$YYVVGA$^{425}$ severely compromised the interaction of VCC with the lipid head-groups in the Asolectin-cholesterol liposomes.

### 2.4.4.3 Membrane oligomerization and the membrane insertion in the membrane lipid bilayer of the Asolectin-cholesterol liposomes

VCC mutants could not make an intimate interaction with the membrane lipid component of the Asolectin-cholesterol liposomes. However, VCC mutants displayed a significant association with the Asolectin-cholesterol liposomes, probably through the amphipathicity-driven non-specific partitioning into the liposome membranes (218). That interaction was appeared to be abortive in the nature, as the VCC variants could not induce any permeabilization of the membrane lipid bilayer of the Asolectin-cholesterol liposomes. Therefore we examined whether these VCC mutants could generate functional transmembrane oligomeric pore structure in the absence of any specific intimate interaction towards the membrane lipid components of the Asolectin-cholesterol liposomes (Figure 2.15). For this, we examined the ability of the VCC variants to generate any oligomeric assembly (SDS-labile pre-pore oligomers and SDS-stable oligomers) in the Asolectin-cholesterol liposomes.


**Figure 2.15: Monitor the formation of the SDS-stable oligomer by VCC variants in the presence of Asolectin-cholesterol liposomes.**

Wild-type VCC toxin generated SDS-stable and also SDS-labile oligomers. The experimental data indicated that the loop mutant T237A also displayed SDS-labile and SDS-stable oligomer generation in the membrane lipid bilayer of liposomes (Figure 2.16). The loop mutants Loop359-362 showed moderate oligomerization generation efficacy, in terms of the noticeable level of SDS-labile oligomer generation and hugely reduced the level of SDS-stable oligomer generation.

All the other VCC mutants could not generate any SDS-stable and SDS-labile oligomer in the membrane lipid bilayer of the Asolectin-cholesterol liposomes.

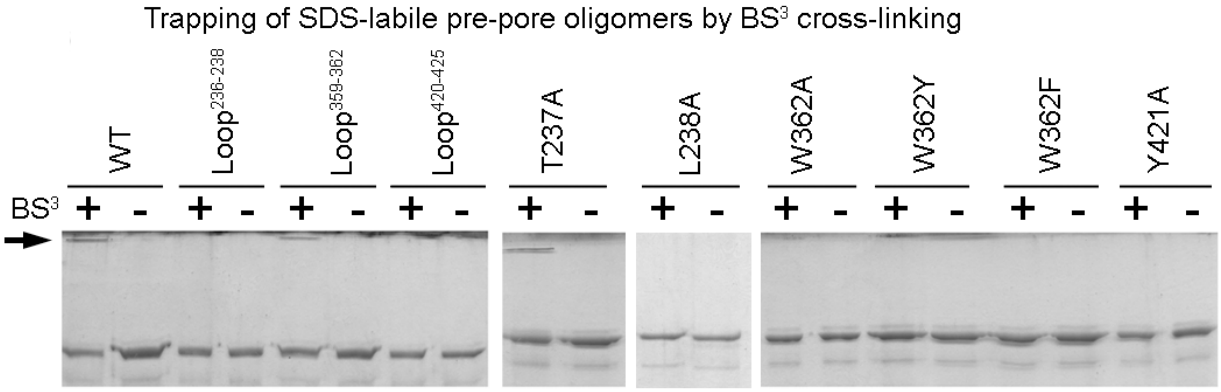


**Figure 2.16: Monitor the generation of the SDS-labile pre-pore oligomer by using $BS^3$ cross-linking in the Asolectin-cholesterol liposomes.**

VCC loop mutants were also examined for their efficacy to insert the pore-forming 'stem-loop' into the membrane. The pore-forming 'stem-loop' harbors a tryptophan residue (W318). FRET from W318 to DPH incorporated in the liposomes has been confirmed as a significant indicator to examine the membrane insertion step (219). Consistent with the previous reports, wild type VCC displayed a significant increase in the tryptophan-to-DPH FRET signal with the Asolectin-cholesterol liposomes (Figure 2.17). The loop point mutant T237A also exhibited a moderate rise in the FRET signal, however significantly low level as compared to the wild-type VCC. No other loop variants displayed any such FRET signal, indicating the blocking of the membrane insertion step of the toxin.

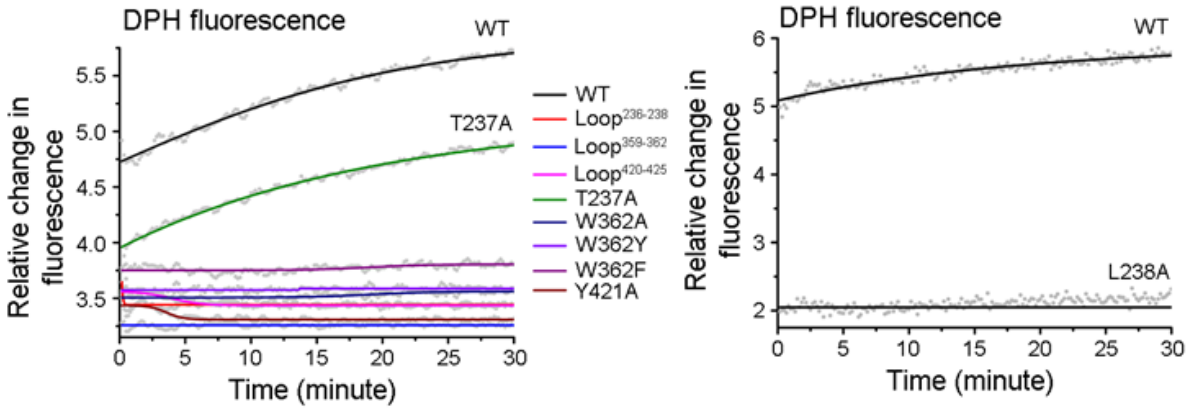


**Figure 2.17: Monitoring membrane insertion of the pore-forming stem loop of VCC by using tryptophan-to-DPH FRET signal.**

Overall, these results indicated that the mutations in the loop region in $^{236}$TTL$^{238}$, $^{359}$DALW$^{362}$, and $^{420}$YYVVGA$^{425}$ severely affected the oligomerization and membrane insertion step of the membrane-bound VCC toxin, probably by abrogating the intimate mode of interaction of toxin with the target cell membrane lipid components.

### 2.4.5 Alterations in the VCC loops $^{236}$TTL$^{238}$, $^{359}$DALW$^{362}$, and $^{420}$YYVVGA$^{425}$ compromise binding and cytotoxicity in HT-29 human colorectal adenocarcinoma cells

VCC mutants displayed significant inhibition in the functional membrane pore-forming ability, and also abrogation in the functional membrane interaction efficacy against the human erythrocytes and the membrane lipid bilayer of the Asolectin-cholesterol liposomes. To examine their functionalities further, the loop mutants were probed for their binding and cytotoxic ability towards the human colorectal adenocarcinoma cells HT-29.

Binding of the VCC mutants was probed by the flow cytometry-based experiment at 25 $^{o}$C. As compared to the human erythrocytes, the nucleated eukaryotic cells are more resistant against the lysis triggered by pore-formation. Hence, VCC association to the HT-29 cells could be probed at room temperature. Under this experimental condition, we could observe the combined effects of the amphipathicity-driven membrane interaction, specific interaction with the lipid component of the target cell membrane and carbohydrate-dependent membrane association with the glycolipids or glycoprotein receptor molecule present in the cell surface (Figure 2.18).

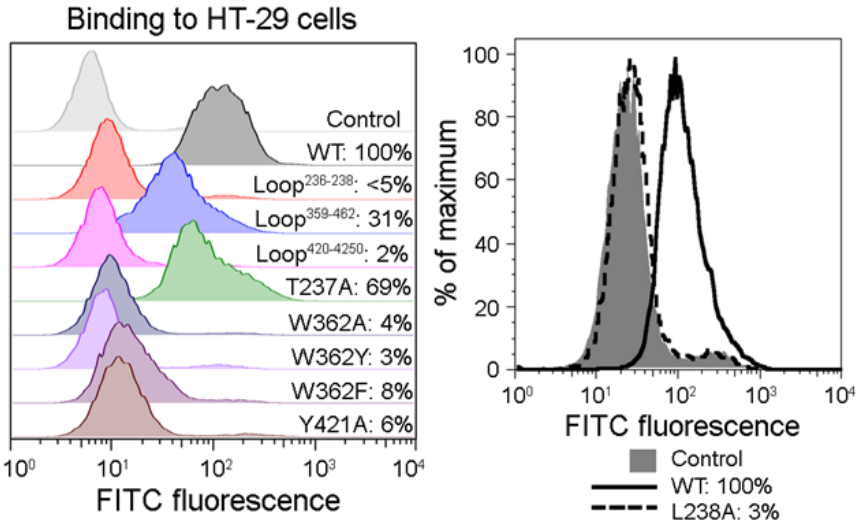


**Figure 2.18: Interaction of the VCC variants with HT-29 cells was monitored by the flow cytometry-based assay.**

Our data suggest that T237A mutant displayed ~70% of the wild-type VCC interaction, whereas Loop359-362 showed ~30% of wild-type interacting ability. All other mutant showed less than 10% of the binding activity (Figure 2.18). These results were consistent with the binding data obtained from the human erythrocytes and membrane lipid bilayer of the Asolectin-cholesterol liposomes. Therefore, the data obtained from our study suggested that the mutation of the loop regions $^{236}$TTL$^{238}$, $^{359}$DALW$^{362}$, and $^{420}$YYVVGA$^{425}$ in VCC toxin abrogated its efficient association to HT-29 cells and also confirmed the specific role of the loop sequences in the membrane interacting mechanism of the VCC toxin.

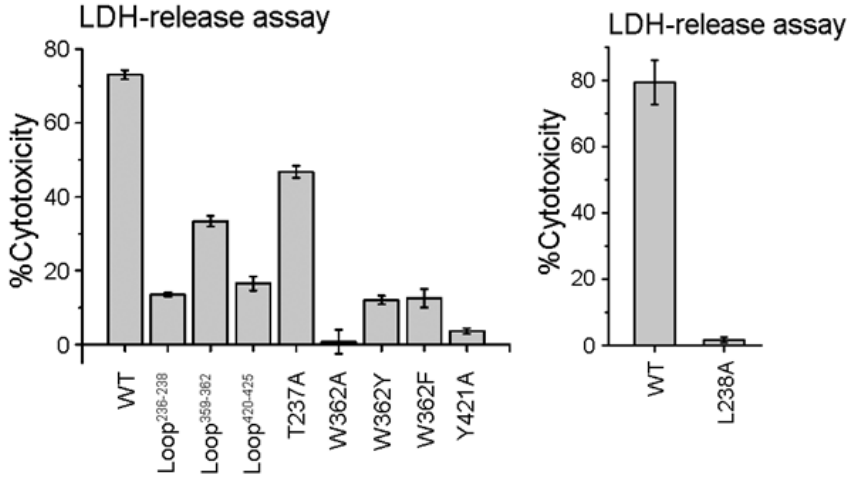


**Figure 2.19: LDH-release assay to examine cytotoxic activities of the VCC variants against the HT-29 cells.** Cytotoxic activities of the VCC variants against the HT-29 cells were probed by the LDH-release assay. Data presented here are the average ± standard deviation of three independent experiments.

VCC variants were examined for the cytotoxicity against the HT-29 cells, by employing the LDH-release experiment. The data obtained from our study suggested that the wild-type VCC displayed ~72% cytotoxicity, while the mutant T237A, and Loop$^{359-362}$ induced ~48% and 32% cytotoxicity, respectively. Other VCC variants could trigger less than 20% cytotoxicity against the HT-29 cells (Figure 2.18). These data confirmed the role of the specific loop sequences for the functional membrane association and cytotoxic activity of the toxin.

**2.5 Conclusion**

The present study provided the insight that the mutation of the membrane interacting loop sequences, $^{236}$TTL$^{238}$, $^{359}$DALW$^{362}$, and $^{420}$YYVVGA$^{425}$, in the VCC toxin molecule abrogated its association with the target cell membrane and inhibited the membrane permeabilization

potency of the toxin. The mutation in the loop sequences could not alter amphipathicity-driven membrane interaction of the toxin; however, such interaction was non-functional in nature and did not allow the intimate interaction of VCC with the membrane lipid head-groups. Previous studies also reported similar loop architecture in the rim domain of other members of the β-PFTs family for example *S. aureus* α-hemolysin and staphylococcal LukF.

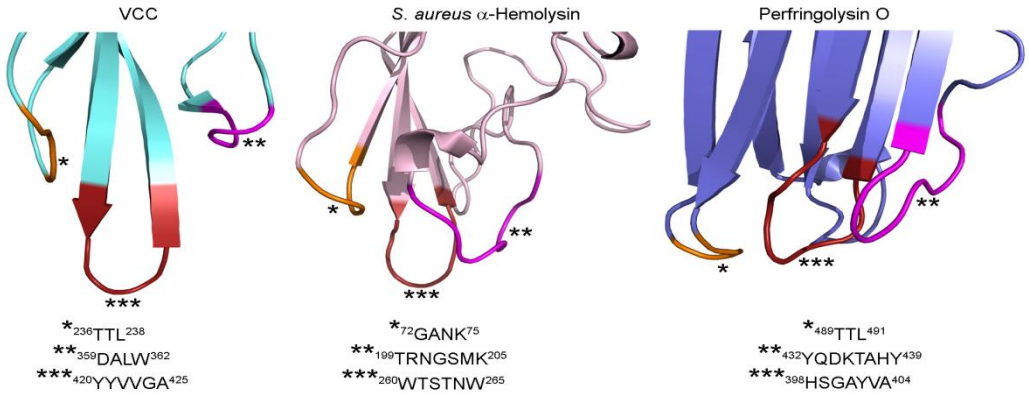


**Figure 2.20: Schematic representation of structural models highlights the location of the loop sequences.** Comparison of the membrane-proximal loop sequences in VCC, with those of *S. aureus* α-hemolysin and cholesterol-dependent cytolysin perfringolysin O.

The high-resolution molecular structures also reveal the similar homologous loops of *S. aureus* α-hemolysin and staphylococcal LukF, interacting with the phospholipids present in the membrane lipid bilayer of the target cells (107,220,221). A similar mode of membrane interaction has been documented in the case of perfringolysin O, streptolysin O, and pneumolysin. The prominent members of the subclass of cholesterol-dependent cytolysin in the β-PFT family also exhibit the presence of the similar, prominent loop structures (namely, the L1-L3 loop) in their membrane interacting domains (207,222-224) (Figure 2.20). Notably, these L1-L3 loops in the CDCs have been reported to be the important structural architectures playing the critical role in the cholesterol-dependent membrane interaction. Particularly, the conserved 'Thr-Leu' pair positioned within the L1 loop region of the CDCs has been identified as the key element for the recognition and binding to the membrane cholesterol (206). More interestingly, this 'Thr-Leu' pair is a presence in the rim domain of the VCC toxin as a part of the $^{236}$TTL$^{238}$ loop region. The results obtained from our study suggested that the replacement of the $^{236}$TTL$^{238}$

loop in protein with GGA sequence appeared to inhibit the interaction with the phospholipids of the membrane in general, and not specifically with the cholesterol present in the membrane of the target cells. Single point mutation of T237A abrogated the membrane interaction only to a marginal extent, as compared to the more severe effects observed in the case of the other VCC variants within the loop sequences.

A previous report on VCC has shown that the single point mutation of A425V in the VCC loop sequence $^{420}$YYVVGA$^{425}$ abrogates the cholesterol-dependent membrane association of the toxin (212). It has been hypothesized that the introduction of a highly hydrophobic side chain of valine residue at Ala425 location might have affected the ability of VCC to bind with the membrane cholesterol (212).

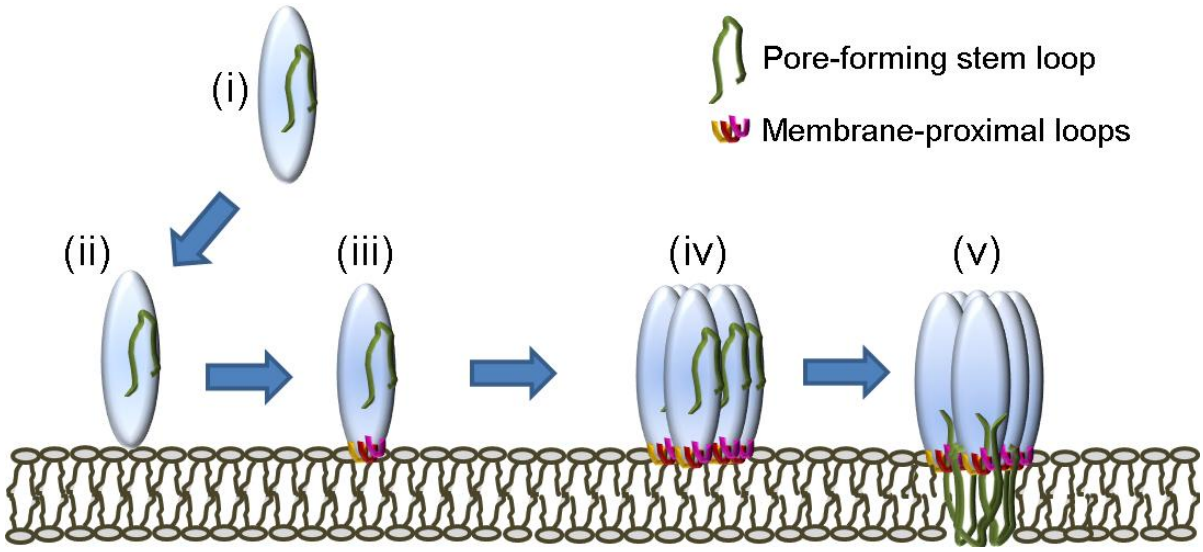


**Figure 2.21: Schematic representation of membrane-proximal loop sequences in VCC mediate crucial interaction with the target membrane lipid component.** (i) Water-soluble monomeric form of VCC. (ii) Amphipathicity-driven non-specific membrane association of the toxin. (iii) Intimate interactions of the membrane-proximal loop sequences with the membrane lipid components. (iv) Pre-pore oligomer formation. (v) Formation of the oligomeric transmembrane β-barrel pore. Alterations of the loop sequences affect the step iii of the process. In the absence of the step iii, subsequent events of the membrane pore-formation mechanism cannot be executed.

Overall, the present study demonstrated that the three loop sequences present in VCC, $^{236}$TTL$^{238}$, $^{359}$DALW$^{362}$, and $^{420}$YYVVGA$^{425}$, constitute a potent lipid-binding scaffold within the VCC toxin. These three distinct loop sequences, $^{236}$TTL$^{238}$, $^{359}$DALW$^{362}$, and $^{420}$YYVVGA$^{425}$ of VCC, are not only critical for the membrane interaction efficacy of VCC, but also for regulating the

functional membrane oligomerization toward an efficient pore-formation mechanism. A previous study has reported multiple mode of the membrane interaction mechanism of VCC, including the non-specific membrane association, specific lipid-dependent interaction, and the β-prism domain's lectin activity-mediated binding towards the cell surface glycan receptor(s) (180) However, how all these multiple modes of interaction are working together to regulate the functional pore-formation mechanism of the toxin has remained unclear. Based on the results obtained from our study, we propose a sequence of these membrane interactions events toward the functional pore-formation by VCC (Figure 2.21). We propose that an amphipathicity-driven partitioning of VCC allows it to non-specifically associate with the membrane in the absence of any specific recognition of the membrane components. However, a specific association with the lipids is critical for the the subsequent pore-formation process by the toxin.

Lectin-activity of VCC further facilitates oligomeric pore-formation in the membrane. It appears to play as a regulatory switch towards the structural reorganizations of the β-Prism domain, in the absence of which membrane oligomerization is sterically prohibited. Our study suggests that the lectin-activity-dependent association of the toxin with the membrane glycan receptor(s) would be allowed only if the primary lipid-dependent association via VCC loops is functional. In the absence of this lipid-dependent interaction, membrane binding, pore-formation and cytotoxicity are severely affected. In summary, this study provides novel insights regarding the structural basis of membrane association mechanism of the VCC toxin.

# Chapter 3

## Implication of the C-terminal β-prism lectin domain on the pore-formation mechanism of VCC

### 3.1 Abstract

VCC exhibits potent carbohydrate-binding ability in terms of interacting with the glycosylated proteins and lipids. Apart from the central core cytolysin domain, VCC also contains two extra C-terminal domains: namely a β-Prism lectin-like domain and a β-trefoil lectin-like domain that are structurally similar to many carbohydrate-binding proteins. However, the specific role of these lectin-like domains for the carbohydrate-binding property of VCC still remains unclear. To have a better understanding of the lectin-like property of VCC, a structure-function relationship approach was employed. For the first time through our study we have shown that the β-Prism domain of VCC acts as a structural scaffold responsible for the lectin-like activity of the toxin towards the β1-galactosyl-terminated glycoproteins or glycolipids. Our study has also shown that the β-Prism domain-mediated carbohydrate-binding activity of the toxin plays a critical role for the efficient interaction of VCC with the target cells, thus establishing the physiological significance of the β-Prism domain of the toxin. Our study further suggests that the carbohydrate-binding ability of the β-Prism domain also facilitates oligomerization propensities of the membrane-bound VCC molecules. Based on our observation, we propose a novel regulatory mechanism in case of the membrane pore-formation process employed by VCC, which is mediated by the C-terminal β-Prism domain's lectin activity.

### 3.2 Introduction

VCC is secreted as a water-soluble monomeric inactive form, which after removal of the N-terminal Pro-domain converts into the active form. Upon binding to its target host cell membranes, the active form of the toxin generates transmembrane heptameric β-barrel channels thus leading to the colloid-osmotic lysis of the cells. In this part of the present thesis work, we have characterized the physiological implication of the β-Prism domain of VCC. The results obtained from our study suggest that the presence of the β-Prism domain-mediated lectin activity is critical for an efficient binding of the toxin towards the target host cells membrane. In our

study, we have demonstrated that the β-Prism domain-mediated lectin activity also regulates the membrane oligomeric pore-formation mechanism of the membrane-bound toxin (217).

'How proteins interact with a target cell membrane' is a fundamental question of protein-membrane-interaction. Toxins apply different approaches for the initial recognition of the target host cell membrane. Exploring the basis of membrane association is crucial for understanding the mechanism of the mode of action of secreted bacterial toxin. Glycoprotein and glycolipid present on the surface of a cell membrane acts as a receptor for many bacterial toxins, e.g. B subunit of cholera toxin binds to the $GM_1$ ganglioside, aerolysin from *Aeromonas hydrophilia* binds to the N-linked sugars on glycosyl phosphatidyl inositol-conjugated proteins and *Streptococcus mitis* lectinolysin binds to Lewis y and b glycans. In many proteins, a specific glycan-binding domain with lectin-like fold mediates their interaction with the glycan molecule of the target cell membrane (184).

The crystal structure of the water-soluble monomeric form of VCC revealed that the toxin molecule harbors one central cytolysin domain that displays a comprehensive structural resemblance to those found in other archetypical members of the β-PFTs family, including Staphylococcal LukF toxin and *Staphylococcus aureus* α-hemolysin (99,174,220,225). VCC molecule possesses two additional C-terminal domains exhibiting the structural features of the carbohydrate-binding proteins. The first domain known as the β-Trefoil lectin-like domain consists of a β-Trefoil fold. A similar structural fold is also found in the human mannose receptor and plant toxin ricin (199). The second domain known as the β-Prism lectin-like domain consist of β-Prism fold, found in many plants lectins such as *Artocarpus integrifolia*, *Griffithsia sp* griffithsin, jacalin and the *Maclura pomifera* agglutinin (174,200,201,226). In addition to these, the β-Prism fold is also reported in the *Bacillus thuringiensis* δ-endotoxin, which generates the ion channels in the gut membrane of target insect larvae (52,227).

The presence of a lectin-like domain in VCC structure is consistent with the earlier observation exhibiting the lectin-like property of the toxin, more specifically toward the β1-galactosyl-terminated glycoconjugates (180). However, the specific contribution of the β-trefoil domain and the β-Prism domain toward the carbohydrate-binding property of the toxin has not been explored in detail before.

In this part of the thesis, we have investigated the importance of the β-Prism domain in the pore-formation mechanism of the VCC toxin. We have explored the role of the β-Prism domain in the context of the carbohydrate-binding activity of the toxin. We have shown that the presence of β-Prism domain in the VCC toxin is critically needed for the carbohydrate-binding activity of VCC towards β1-galactosyl-terminated complex glycoconjugates. In the absence of β-Prism domain, the VCC toxin was unable to display any such lectin activity, while the β-Prism domain in isolation displays a significant interaction with the glycoconjugates containing terminal β1-galactosyl groups.

We have also identified the crucial amino acid residues within the β-Prism domain of VCC, which contribute towards the carbohydrate-binding property. Furthermore, toward exploring the physiological implication of the lectin-like activity of VCC, we have shown that the β-Prism domain-mediated lectin activity of the toxin plays a crucial role in the interaction of VCC towards the target cell membranes. The specific blocking of the β-Prism domain-mediated lectin activity is found to have a detrimental effect on the membrane association propensity of the toxin.

We have also proved that the β-Prism domain-mediated carbohydrate-binding activity plays a crucial role in regulating the oligomerization process of VCC. On the basis of our finding, we hypothesize that the β-Prism domain-mediated carbohydrate binding propensity may act as a critical triggering mechanism that allows the formation of a transmembrane oligomeric assembly on the target host cell membrane. This study provides a novel insight into the crucial role of the β-Prism domain in the carbohydrate-binding activity of VCC toxin.

## 3.3 Materials and methods

### 3.3.1 Recombinant VCC variants

All the recombinant VCC variants were generated by PCR-based strategy. Nucleotide sequences of all the construct were confirmed by DNA sequencing. The wild-type and mutant forms of VCC were purified by the same procedure as described previously in chapter 2. The purity of the proteins were analyzed by sodium dodecyl sulfate-polyacrylamide gel electrophoresis (SDS-PAGE) and Coomassie staining. The protein concentrations were determined by monitoring the absorbance at 280 nm on the basis of the theoretically calculated extinction coefficients values

obtained from the analysis of the corresponding amino acid composition of the protein constructs.

### 3.3.2 Intrinsic tryptophan fluorescence emission measurements

Intrinsic tryptophan fluorescence emission spectra of the wild-type and the mutant VCC variants were recorded on a Fluoromax-4 spectrofluorometer (Horiba Scientific, Edison, NJ) equipped with a Peltier-based temperature controller. The protein samples were excited at 290 nm and tryptophan fluorescence emission spectra were recorded between 310-400 nm. The slit widths were set at 2.5 nm and 5 nm for excitation and emission, respectively. The concentration of VCC variants for this experiment was 250-300 nM. An integration time of 10 seconds was used. All fluorescence spectra were corrected with respect to the only buffer spectra.

### 3.3.3 Far-UV circular dichroism measurements

Far-UV circular dichroism spectra were monitored on a Chirascan spectropolarimeter (Applied Photo-physics, Leatherhead, Surrey, UK) with a Peltier-based temperature controlled sample chamber in a quartz cuvette of 5 mm pathlength. The final concentration of VCC variants in each experiment was in the range of 0.5-1 μM. Each CD spectrum was corrected for the baseline via subtraction with the respective buffer blank.

### 3.3.4 Assay of hemolytic activity against human erythrocytes

The pore-forming activity of the wild-type and the VCC mutant variants were examined against the human erythrocytes [suspended in PBS (20 mM sodium phosphate buffer containing 150 mM NaCl, pH 7.4) corresponding to $OD_{650}$ of ~0.9] by monitoring the decrease in the turbidity of the human erythrocytes suspension at 650 nm upon incubation with the VCC variants at 25 $^{o}$C. The concentration of protein incubated with human erythrocytes for the hemolytic assay was 100 nM in a reaction volume of 1 ml.

### 3.3.5 Rabbit anti-VCC serum

Polyclonal anti-VCC antiserum was generated using the Custom made Polyclonal Antibody Service marketed by GeNei/Merck, Bangalore India (228). The polyclonal anti-VCC antiserum was raised in rabbit using the purified form of recombinant VCC protein as an antigen.

### 3.3.6 Enzyme-linked immunosorbent assay (ELISA)

Binding of the VCC variants towards the immobilized asialofetuin (Sigma-Aldrich) were examined following an ELISA-based procedure as described previously. Briefly, 100 μl of asialofetuin with a concentration of 10 μg/ml in PBS 20 mM sodium phosphate buffer containing

150 mM NaCl (pH 7.4) was added into each well of 96-well flat-bottom microtiter plates (Nunc), and plates were kept at 4 $^{o}$C for overnight incubation. After the incubation, the plate was washed three times with PBS containing 0.05% Tween 20(TPBS). For reducing the non-specific binding, blocking was done by using 200 µl of 3% nonfat dry milk powder prepared in PBS with 1hr incubation. After three times washing with TPBS, VCC variants were treated for two hour at 25 $^{o}$C. Subsequently after the washing, wells were treated with 100 µl of rabbit anti-VCC antiserum (1:5000 dilution (v/v) for the full length and β-Prism domain truncated VCC variant; 1:50 (v/v) dilution for the isolated β-Prism domain and mutants of β-Prism domain protein) for 90 minute at 25 $^{o}$C and then washed three times with TPBS, and afterwards incubated with 100 µl of horseradish peroxidase-conjugated goat anti-rabbit IgG antibody with a dilution of 1:10000 v/v for 1 h at 25 °C. Interaction of VCC variants with the asialofetuin were monitored by the color development by addition of o-phenylenediamine (10 mg/ml) in 100 mM sodium citrate buffer (pH 4.5) containing $H_2O_2$ (2 µl/ml of 30% (v/v) $H_2O_2$), reactions were terminated with 2 N $H_2SO_4$, absorbance were recorded at 490 nm by using a microplate absorbance reader (iMark, Bio-Rad).

### 3.3.7 Isothermal titration calorimetry (ITC)

Interaction of the isolated β-Prism domain and its mutants with the asialofetuin was examined by an ITC-based experiment using an iTC200 instrument (MicroCal/GE Healthcare, Piscataway, NJ) (229). All protein samples were prepared in buffer containing 10 mM Tris-HCl (pH 8.0) and extensively dialyzed against the same buffer. All the protein reagents and buffer were freshly prepared and degassed under the vacuum condition. The concentration of β-Prism domain variants was measured by the recording the absorbance at 280 nm as mentioned previously. The concentration of the asialofetuin was determined by the monitoring the absorbance at 280 nm (on the basis of the extinction coefficient of 0.45 for 1 mg/ml asialofetuin with a molecular mass of 48 kDa). For monitoring the interaction with asialofetuin in each ITC experiment, the sample cell (cell volume of 200 µl) was filled with the β-Prism domain variants (47.7 µM), and the reference cell with similar cell volume was filled with the buffer containing Tris-HCl (pH 8.0).

In the titration reaction β-Prism domain protein was titrated against the asialofetuin (330 μM) as the following procedure: The titration started with the first 0.5 μl injection, followed by 19 injections of 2 μl each was applied with a time interval of 3 minutes between the two injections. The titrations were performed at 25 $^{o}$C with a constant stirring at 1000 rpm. The interaction isotherm profile was generated excluding the first data point. The final resulting data were fitted to one-site binding model using Origin 7 software. The interaction values of ΔH (binding enthalpy in kcal/mol), $K_a$ (association constant), and n (number of binding sites per molecule) were kept as adjustable parameters. The dissociation constant ($K_d$) was obtained from $1/K_a$. The experiment were performed with c values ($=K_a.M_t(0)$; Mt(0) being the initial concentration of the macromolecule in the sample cell) in the range $1<c<500$.

### 3.3.8 Flow cytometry based-assay

The binding of full-length VCC and the β-Prism truncated variant of the VCC with the human erythrocytes was monitored by using a flow cytometry-based procedure as described previously in Chapter 2. Briefly, human erythrocytes ($1x10^6$ cells) were treated with various concentration of the VCC variants for 30 minute at 4 $^{o}$C in PBS (20 mM sodium phosphate buffer containing 150 mM NaCl (pH 7.4) in a reaction volume of 100 μl. The cells were centrifuged at 500 x g, washed twice with ice-cold PBS and resuspended in 50 μl PBS containing rabbit anti-VCC antiserum (1:100 v/v dilution) and 0.1% w/v bovine serum albumin (BSA), and incubated for 30 minute at 4 $^{o}$C. After washing twice, the pellet fraction were resuspended in 50 μl ice-cold PBS containing fluorescein isothiocyanate (FITC)-conjugated goat anti-rabbit IgG (1:100 v/v) dilution and 0.1% w/v BSA: Sigma-Aldrich), incubated for 30 minutes at 4 $^{o}$C, washed twice, and resuspended on 500 μl PBS. The cells were analyzed by using FACSCalibur (BD) Biosciences, San Jose, CA, USA) flow cytometer. FITC fluorescence was monitored at an excitation wavelength of 488 nm, with an emission wavelength of 530 nm in the FL1 channel. The geometric mean fluorescence (GMF) values were calculated using FlowJo software (www.flowjo.com). The binding data were calculated using the equation: $\%Binding = [(GMF_{test}-GMF_{control})/(GMF_{maximum}- GMF_{control})] X 100$.

Where, $GMF_{control}$ = GMF for the cells that were not treated with VCC variants, but incubated in presence of anti-VCC and anti-rabbit-FITC; $GMF_{maximum}$ = GMF for the cells treated with the highest concentration of WT-VCC used in the assay (75 nM), followed by incubation with anti-VCC and anti-rabbit-FITC.

### 3.3.9 Binding of VCC to human erythrocytes membrane

The human erythrocytes cells were resuspended in PBS to a final concentration of $OD_{650}$=0.8. The cells were treated with the different concentration of the VCC variants in a reaction volume of 100 µl for 1 hour at 25 $^{o}$C. The reaction mixture was subjected to ultracentrifugation at 105,000 X g for 30 minutes at 4 $^{o}$C. The pellet fraction were washed twice with PBS and resuspended in 50 µl of SDS-PAGE sample buffer (50 mM Tris/HCl, pH 6.8, containing 2% w/v SDS, 2 mM β-mercaptoethanol, 4% v/v glycerol, 0.01% w/v bromophenol blue) (228). The resuspended pellet fractions were divided into two equal parts. One part was kept at room temperature, whereas the other part was boiled for 10 minutes and afterward separated on an SDS-PAGE. After the separation, the VCC variants were transferred onto a polyvinylidene difluoride (PVDF) membrane (BioRad) using a complete wet transfer assembly (BioRad, Hercules, CA, USA) for 90 minutes at 90 volts. The membrane was blocked for with 3% non-fat milk powder (Santa Cruz Biotechnology, Santa Cruz, CA, USA) in PBS containing Tween-20 (Himedia) (TPBS) for overnight at 4 $^{o}$C. After washing with TPBS three times, the blot was treated with rabbit anti-VCC antiserum (1:5000 v/v) for 1 hour at room temperature. After the washing three times with TPBS, the blot was treated with horseradish peroxidase (HRP)-conjugated goat anti-rabbit IgG (Sigma-Aldrich) (1:1000 v/v) for 1 hour at room temperature and washed three times with TPBS. The blot was developed using an ECL Western blotting detection kit (GE Healthcare Life Sciences), and the images were acquired using the ImageQuant LAS 4010 (GE Healthcare Life Sciences).

### 3.3.10 Structural models

The structural coordinates of VCC were obtained from the Protein Data Bank (PDB) (PDB entry 1XEZ for the water-soluble monomeric structure of VCC; PDB entry 3O44 for the oligomeric assembly of VCC) (174,230). Superimposition of structural coordinates was achieved using the software program COOT (231). The structural model of VCC were visualized using PyMOL (DeLano, W.L.(2002). The PyMOL Molecular Graphics System found online (www.pymole.org).

## 3.4 Results and discussion

### 3.4.1 Generation of VCC variant with a truncation of the β-Prism domain

Structural analysis of the VCC molecule reveals that the carboxy-terminal region of the protein encompassing the amino acid residue Gln-584 to Asn-716 constitutes a β-Prism lectin-like

domain. In this part of the study, we generated the truncated mutant of VCC lacking the β-Prism domain (VCC-Δβ-Prism; having the deletion in the region Gln-584 to Asn-716 of the wild-type VCC protein) (Figure 3.1).

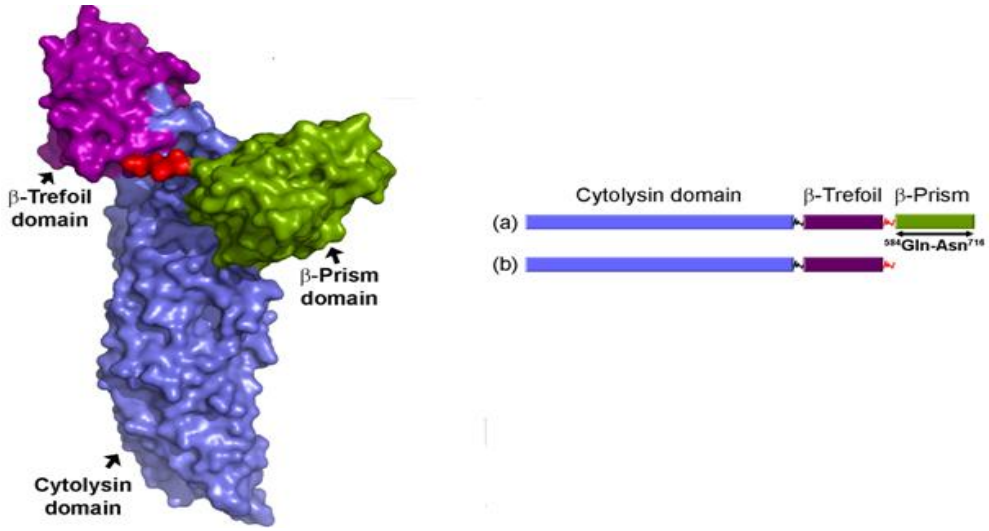


**Figure 3.1: Structural model of the VCC protomer shows its domain organization and schematic representation of the wild-type VCC and the VCC-Δβ-Prism construct**. The molecular structure model of VCC displays its domain organization. The cytolysin (blue), β-Trefoil (magenta) and the β-Prism (green) domains are indicated. The loop region that connects the β-Prism domain lectin to the β-Trefoil domain lectin domain is shown in red. The structural model of the VCC molecule was generated using the PDB ID1XEZ. The schematic of the wild type VCC (a) and the VCC-Δβ-Prism construct (b) are presented.

### 3.4.2 Membrane-permeabilization activity of the β-Prism domain-truncated variant of VCC

The truncated variant of VCC (VCC-Δβ-Prism), exhibited less than 10% of the hemolytic activity as displayed by the wild-type VCC against human erythrocytes, at the concentration 100 nM. Previous studies have also reported that in the absence of β-Prism domain hemolytic activity of the VCC toxin is drastically affected (222,228,232) (Figure 3.2). However, those studies reported noticeable hemolytic activity against rabbit erythrocytes, and rabbit erythrocytes are well known to display significantly increased susceptibility towards VCC-induced hemolysis as compared to the human erythrocytes. Therefore, the obtained differences in the hemolytic activity of the β-Prism domain-truncated variant, as reported in the previous studies and in the

present study could be due to the differences in the susceptibility of the rabbit and human erythrocyte toward the VCC-mediated pore-formation ability.

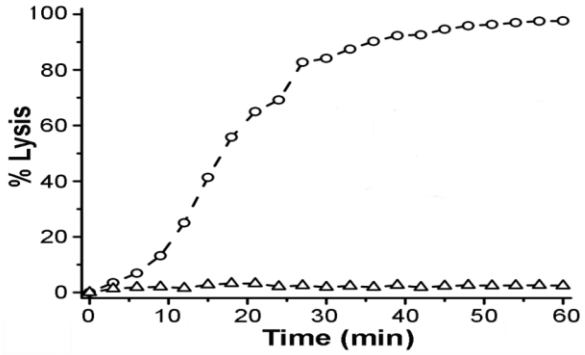


**Figure 3.2: Hemolytic activity of wild-type VCC and VCC-Δβ-Prism variant against human erythrocytes.** The pore-forming activity of wild type VCC and VCC-Δβ-Prism variant against human erythrocytes. Lytic activities of wild type VCC (○) and VCC-Δβ-Prism (Δ) were probed at protein concentration of 100 nM.

### 3.4.3 The structural integrity of the β-Prism domain-truncated VCC variant

The β–Prism domain truncated variant of VCC has shown overall similar intrinsic tryptophan fluorescence emission spectra profile (wild-type VCC harbor 11 tryptophan residue distributed overall in the protein structure; two of the tryptophan residue present in the β-Prism domain of the VCC), when compare to the full length wild-type VCC protein, suggesting that the tertiary structure of the protein is not affected in the absence of the β-Prism domain (232) (Figure 3.3).

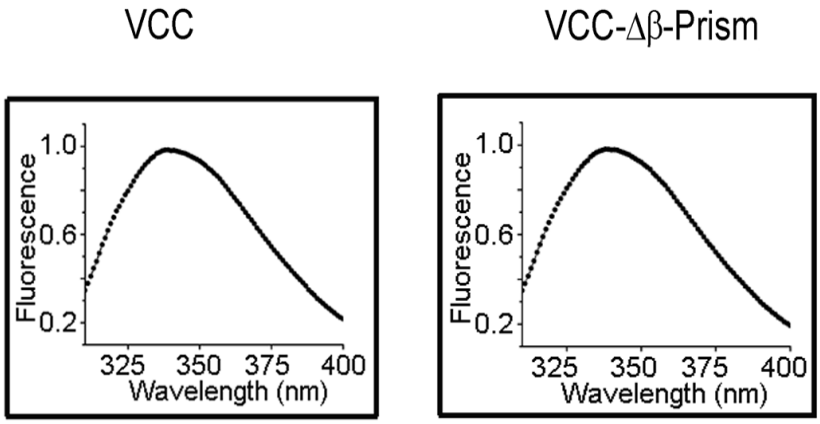


**Figure 3.3: Intrinsic tryptophan fluorescence spectra of the VCC variants.** Analysis of the intrinsic tryptophan fluorescence emission spectra (full-length VCC harbors 11 tryptophan residues distributed overall the protein structure; two of these are positioned within the β-Prism domain) of the VCC-Δβ-Prism variant confirmed folding and structural integrity of the β-Prism-deleted protein.

The β-Prism-truncated variant also displayed similar far-UV circular dichroism (CD), suggesting that the secondary structural profile of the protein is not affected significantly by this deletion (Figure 3.4).

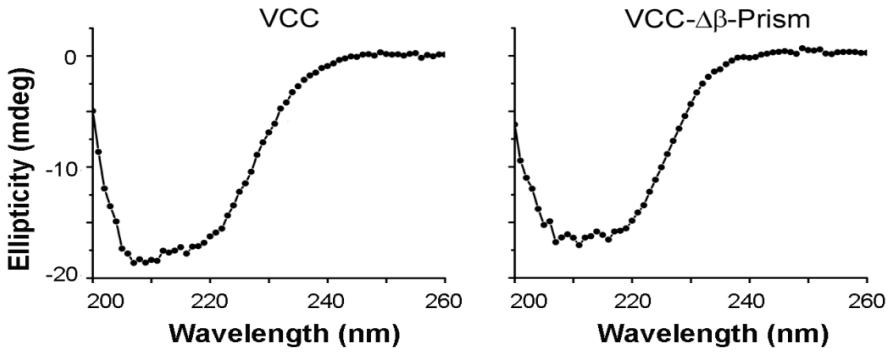


**Figure 3.4: Far-UV CD spectra of the wild-type VCC and the VCC-Δβ-Prism construct.** Analysis of the far-UV circular dichroism (CD) profile of the VCC-Δβ-Prism variant confirmed the structural integrity of the β-Prism-deleted protein.

Altogether, these data suggested that the deletion of the β-Prism domain did not affect the structural integrity and the folding property of the truncated VCC variant.

### 3.4.4 Membrane oligomerization of the β-Prism truncated variant

Membrane oligomerization of VCC is recognized as a crucial step towards the generation of transmembrane oligomeric pore structure. In the mode of action of VCC, the protein first interacts with the target cell membrane that leads to the generation of transient, SDS-labile, pre-pore assembly, followed by their conversion into the SDS-stable transmembrane heptameric pore structures. Therefore, to explore the basis of abortive pore-formation caused by the truncated variant of VCC, we analyzed the oligomerization ability of the toxin in the membrane lipid bilayer of human erythrocytes cells. As reported previously, membrane-bound WT VCC could form SDS-stable oligomeric pore assembly in the lipid bilayer of human erythrocytes. Notably, that the VCC-Δβ-Prism variant, despite having the significant reduction in the pore-forming ability of the toxin, could form a SDS-stable oligomeric assembly in the membrane lipid bilayer of the erythrocytes cells (Figure 3.5).

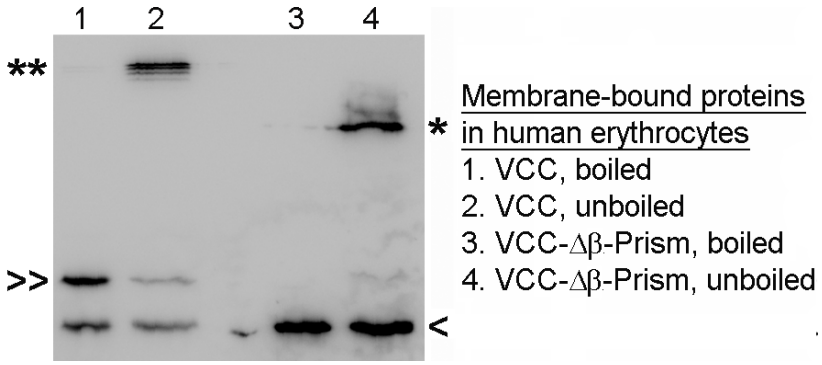


**Figure 3.5: Oligomerization propensities of the wild-type VCC and VCC-Δβ-Prism variant in the membrane lipid bilayer of the human erythrocytes.** Unboiled samples allowed detection of any SDS-stable oligomeric assembly. SDS-stable oligomers of wild type VCC (**) and VCC-Δβ-Prism (*) are marked. Monomer bands of wild type VCC (>>) and VCC-Δβ-Prism variant (>) are also indicated. Data shown here are the representatives of at least three independent experiments.

### 3.4.5 Removal of the β-prism domain abrogates the lectin-like property of VCC against the β-1-galactosyl-terminated complex glycoconjugate

VCC has been shown to display interaction with β-1-galactosyl-terminated complex glycoconjugates, suggesting that VCC possesses a potent lectin-like property. However, it has remained unclear that which of the two lectin-like domains, the β-Trefoil domain and the β-Prism domain of VCC, is responsible for the carbohydrate-binding property of the toxin. To examine the potential role of the β-Prism domain in the lectin-like property of VCC, we employed an ELISA-based experiment to examine the interaction ability of the VCC-Δβ-Prism variant towards the immobilized β-1-galactosyl-terminated glycoprotein asialofetuin (Figure 3.6 A). Previous study has reported that the wild-type VCC protein strongly interacts with the β-1-galactosyl-terminated glycoprotein asialofetuin. Consistent with the previous observation wild-type VCC displayed prominent interaction with the immobilized asialofetuin with a dissociation constant ($K_d$) of 16 nM. In contrast, the β-Prism domain truncated variant of VCC showed no noticeable binding with the immobilized asialofetuin. The result, therefore, suggested that the β-Prism domain of the VCC served as the structural scaffold responsible for the lectin activity of the VCC molecule. This observation also eliminated the contribution of the β-Trefoil domain for the lectin activity of the VCC molecule in terms of its specific interaction with the β1-galactosyl-terminated complex glycoconjugates. However, future study will be required to explore the possibility of any carbohydrate interaction of the β-Trefoil domain of VCC.

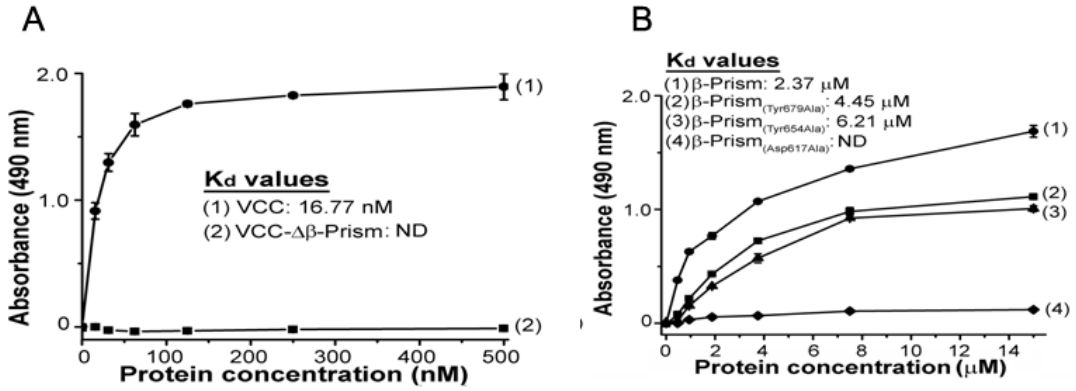


**Figure 3.6: ELISA-based study to determine binding of VCC variants with immobilized asialofetuin. (A)** Interaction of VCC-Δβ-Prism variant to immobilized asialofetuin was compared to that of the wild type VCC protein by employing an ELISA-based experiment. Each data point represents the average of three independent readings. Error bars showed the standard deviations. Data shown here is the representative of at least three independent experiments. Qualitative estimation of $K_d$ value of VCC-asialofetuin binding was obtained by non-linear curve fitting (one site binding model) of the data using GraphPad Prism 4 (GraphPad Software, Inc.). For the VCC-Δβ–Prism variant no detectable binding was obtained, and therefore $K_d$ value was not determined (denoted as ND). **(B)** Binding of wild-type and mutant variants of β-Prism domain protein to immobilized asialofetuin was examined as described above.

### 3.4.6 β-Prism domain of VCC in isolation shows prominent lectin activity toward β-1-galactosyl-terminated glycoconjugates

We also wanted to examine whether the β-Prism domain in isolation could retain its lectin-like activity in terms of specific interaction toward the immobilized asialofetuin. To test this, we generated a histidine-tag containing β-Prism domain VCC variant corresponding to the region spanning from Phe-581 to Asn-716 of the wild type VCC protein. The β-Prism domain protein displayed significant binding with the immobilized asialofetuin, with a dissociation constant $K_d$ in the range of 2 μM as observed by the ELISA-based assay (Figure 3.6 B). This result, therefore, suggested that the β-Prism domain of VCC alone was able to show the lectin-like activity towards the β-1 galactosyl-terminated complex glycoconjugates.

In the ELISA-based experiment, we have observed that the β-Prism domain displayed 100 times weaker affinity towards the β-1-galactosyl-terminated glycoprotein asialofetuin as compared to

the full-length wild-type VCC. It is, therefore, suggested that the other structural scaffold of VCC was essential to enhance the lectin-like activity of VCC.

### 3.4.7 Mapping of the lectin activity site within the β-Prism domain of VCC

Further, we explored the presence the specific binding sites within the β-Prism domain of VCC. The crystal structure of the water-soluble monomeric form of VCC displayed that the carboxy-terminal β-Prism domain of VCC in its solvent-exposed area harbors a potential binding pocket that interacts with the β-octyl glucoside (βOG), a detergent molecule (187). Interestingly, the similar binding pocket has been reported in the other member of the β-Prism lectin family, including jacalin and *Maclura pomifera* agglutinin (MPA). More interestingly, the amino acid residues within this pocket of the β-Prism domain, responsible for generating the side chain interactions with the βOG detergent molecule, are found to be identical with those involved in the carbohydrate-binding property of MPA and jacalin. These amino acid residues are Asp-617, Tyr-654 and Tyr-679 within the β-Prism domain of VCC. On the basis of the structural similarity with the carbohydrate-binding site of MPA and jacalin, we explored the possibility whether the presence of the amino acid triad containing Asp-617, Tyr-654 and Tyr-679 in the β-Prism domain would play any critical role in the lectin activity of VCC (Figure 3.7). For this, we generated three point mutations of Asp-617, Tyr-654 and Tyr-679 within the β-Prism domain of VCC, and examined their ability to bind to the immobilized asialofetuin by employing the ELISA-based assay (Figure 3.6 B). Notably, alteration of Y654A and Y679A caused almost 30% to 40% inhibition in its binding propensity towards the immobilized asialofetuin, whereas D617A mutation resulted in 100% inhibition of its binding propensity towards the immobilized asialofetuin as compared to the wild-type β-Prism domain protein. Therefore these data clearly corroborate the specific role of the three amino acid residues, Asp-617, Tyr-654, and Tyr-679, towards the lectin-like activity of the VCC protein, In particular the Asp-617 amino acid residue play most critical role in the contribution of the lectin activity of the toxin.

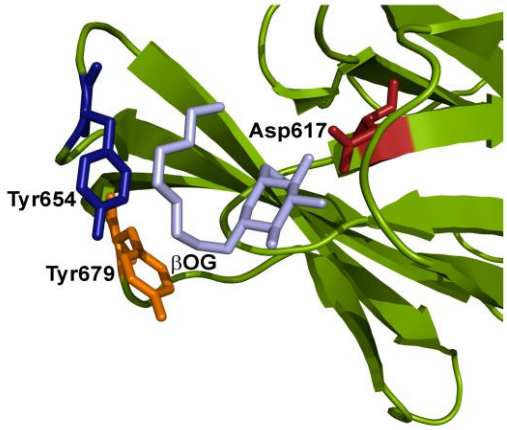


**Figure 3.7: Structural model of the β-Prism domain highlights the three critical amino acid residues for the lectin activity of VCC.** Structural model of the β-Prism domain highlights the three residues (Asp617, Tyr654, and Tyr679) associated with the lectin activity of the VCC toward asialofetuin. The βOG molecule, bound to the β-Prism domain (as observed in the high-resolution crystal structure of VCC), is also indicated in the model.

We also confirmed the interaction ability of the wild-type β-Prism domain protein and D617A mutant of the β-Prism domain protein against the β-1-galactosyl-terminated glycoprotein asialofetuin by employing the ITC-based experiment. Consistent with the results obtained from the ELISA-based assay, the β-Prism domain protein in isolation displayed prominent interaction with the asialofetuin as revealed by the binding isotherm profile. Analysis of the ITC experiment data revealed a $K_d$ value of 4.717 μM for the interaction of β-Prism domain and asialofetuin, that was similar to the estimated $K_d$ value resulted from the ELISA-based assay. The D617A variant of β-Prism domain protein did not display any heat release while being titrated with the asialofetuin, suggesting this particular mutation resulted in complete loss of asialofetuin interaction ability of the β-Prism domain protein (Figure 3.8). Altogether, the results confirmed the specific site within the β-Prism domain of VCC responsible for the β-1-galactosyl-terminated glycoconjugate-specific lectin activity of the VCC toxin.

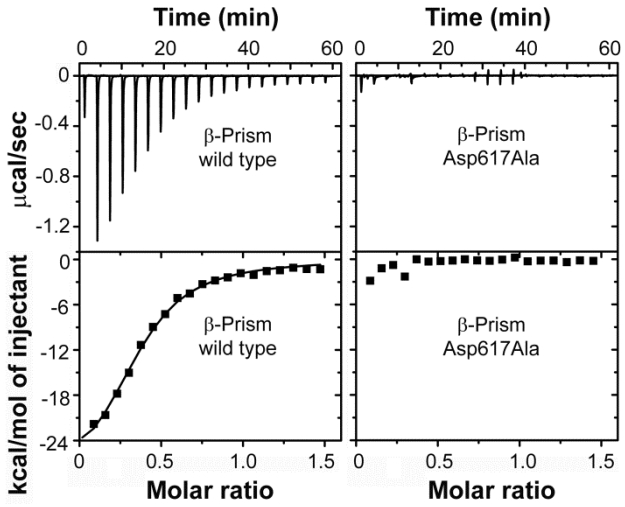


**Figure 3.8: Isothermal titration calorimetry-based study to determine the binding of the β-Prism domain protein to asialofetuin.** Wild-type and Asp617Ala mutant of β-Prism domain protein (47.7 μM) were titrated with asialofetuin (330 μM). Upper panel shows the ITC titration profile and the lower panel shows the interacting isotherm. Following thermodynamic parameters were obtained from the fitting of the experimental data for the wild type β-Prism domain protein: $K_a$=2.12x10$^5$ (± 0.2x10$^5$) M; ΔH=-30.46 (±1.224) kcal/mol. The $K_d$ value for the β-Prism:asialofetuin binding was determined to be 4.717 μM.

### 3.4.8 Implication of the β-Prism domain-mediated lectin activity for the interaction of VCC with human erythrocytes

We also examine the physiological significant of the lectin activity contributed by the β-Prism domain of VCC toxin. In this direction, we investigate the possibility whether such lectin activity of the VCC toxin played any critical role in the membrane interaction process of the toxin, possibly via identification of, as yet unknown, cell surface glycoprotein or glycolipid receptor(s).

#### 3.4.8.1 Removal of the β-Prism domain of the VCC critically compromised binding ability of the toxin towards the human erythrocytes

We examined whether in the absence of β-Prism domain of the VCC, the binding ability of the toxin is affected towards the human erythrocytes. A pull-down based experiment with the human erythrocytes qualitatively suggested that the β-Prism domain truncated variant of VCC could associate with the lipid bilayer of the human erythrocytes when incubated at 25 $^o$C. However, such interaction may not represent the specific mode of the association of the VCC variant with the cell membrane of the human erythrocytes, as VCC is known to display nonspecific hydrophobicity-driven association with the lipid component of the target host cell membrane (218). Therefore, to explore the more specific estimation of the interaction of the VCC variants

with the human erythrocytes, we examined and compared the association of the VCC variants by employing a flow cytometry-based experiment. In this method, we monitored the association ability of the VCC variant with the human erythrocytes at a low temperature of 4 $^{o}$C. It has been shown earlier that at the low temperature, the membrane oligomerization and the pore-forming ability of the toxin affect significantly, but the membrane association propensity of the toxin is not affected in the similar condition (169). Also, the incubation of the VCC toxin in low temperature would decrease the non-specific hydrophobicity-driven interaction of the toxin with the lipid bilayer of the target cells. Therefore, under such condition, association of the protein with the human erythrocytes would be expected to be the result of the more specific association of the VCC variants with the target human erythrocytes cell surface receptor(s). Notably, in the flow-cytometry based experiment β-Prism domain truncated variant of VCC (with a protein concentration in the range of 25-75 nM) displayed significant inhibition of interaction ability toward the human erythrocytes membrane, as compared to the full-length wild-type VCC protein. The β-Prism domain truncated variant of VCC displayed only 15% of the wild-type binding activity in the concentration range of 75 nM (Figure 3.9). The result, therefore, confirmed that the removal of the β-Prism domain of VCC critically compromised the association ability of the VCC toxin towards the human erythrocytes cell membrane.

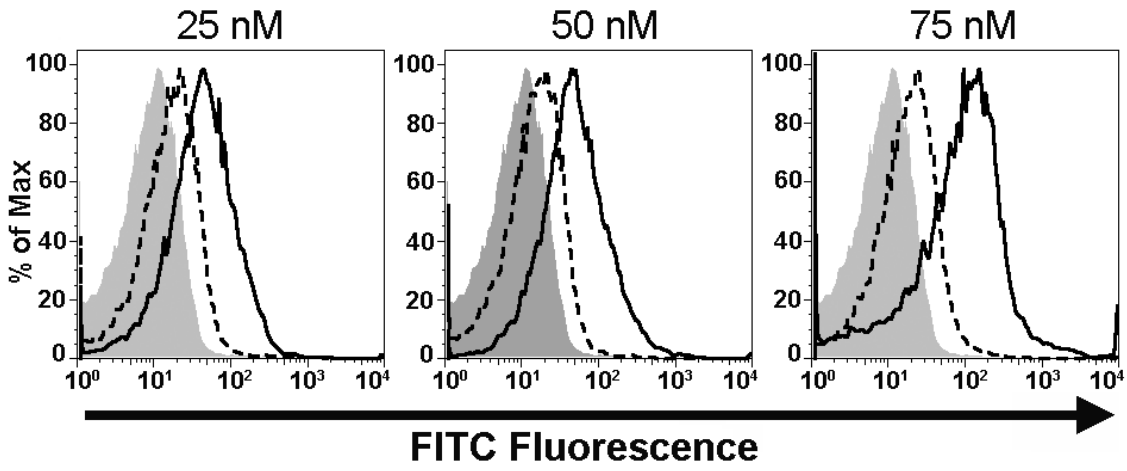


**Figure 3.9: Flow cytometry-based assay to monitor interaction of the full-length VCC and the VCC-Δβ-Prism variants to the human erythrocytes.** Deletion of the β-Prism domain critically compromised interaction of VCC toward human erythrocytes. Association of full-length VCC and the VCC-Δβ-Prism variant to human erythrocytes were monitored by the flow cytometry-based assay. Protein concentrations are shown at the top of each panel. Shaded peak, control; solid line, VCC; dashed line, VCC-Δβ-Prism.

### 3.4.8.2 Pre-incubation of the VCC toxin with β-1-galactosyl-terminated glycoconjugate asialofetuin abrogates interaction of the VCC with the human erythrocytes membrane

Pre-incubation of the wild-type full-length VCC protein in the presence of asialofetuin abolishes the interaction ability of the toxin to the human erythrocytes cell membrane to a significant extent. As the toxin could interact only with the glycan part of the asialofetuin, probably via the β-Prism domain-mediated lectin activity of the toxin, it appeared that the abrogation of the β-Prism domain-mediate lectin activity of the toxin was detrimental for an efficient association of VCC with the human erythrocytes membrane (Figure 3.10 A).

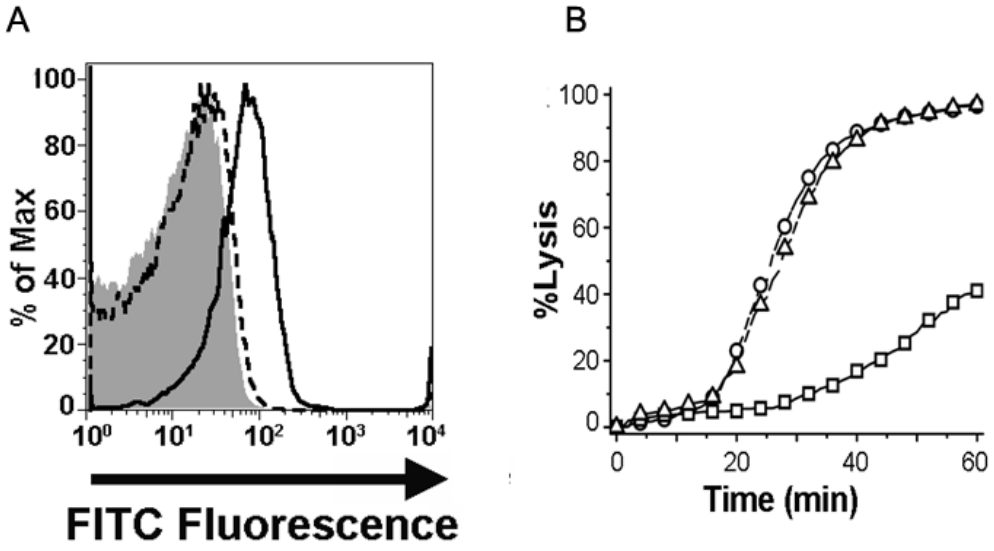


**Figure 3.10: Effect of asialofetuin in the binding and cytotoxic activity of the VCC against human erythrocytes. (A)** Pre-incubation of wild-type VCC with the asialofetuin blocks interaction of the toxin with human erythrocytes. Full-length wild type VCC (75 nM) was pre-incubated with asialofetuin (1 μM) at 25 $^{o}$C for 1 hour. Subsequently, interactions of the protein with human erythrocytes were probed by the flow cytometry-based assay. Shaded peak, control; solid line, VCC; dashed line, VCC pre-treated with asialofetuin. **(B)** Pre-incubation of human erythrocytes with wild type β-Prism domain protein abrogated VCC-induced lysis of the cells. Asp617Ala mutation in the β-Prism domain protein caused a reversal of such inhibitory effect. Human erythrocytes were treated with β-Prism domain variants (100 μM) at 25 $^{o}$C for 1 hour, and subsequently incubated with full-length VCC protein (100 nM) to examine the kinetic of cell lysis. Open circle is VCC-induced lysis of human erythrocytes; open box is VCC-induced lysis of human erythrocytes pre-incubated with wild type β-Prism domain protein; open triangle is VCC-induced lysis of human erythrocytes pre-incubated with β-Prism domain protein containing the Asp617Ala mutation.

### 3.4.8.3 Pre-incubation of the human erythrocytes with the isolated β-Prism domain protein abrogates VCC-induced pore-forming activity

The significance of the β-Prism domain-mediate lectin activity for the binding process of the VCC with the human erythrocytes was further confirmed from the fact that the pre-incubation of the human erythrocytes with wild-type β-Prism domain protein resulted in the significant inhibition of the VCC-induced pore-forming activity. In contrast, the D617A mutation in the β-Prism domain of the VCC reversed such effect (Figure 3.10 B). The result obtained from ELISA-based assay, and ITC-based assay suggested the D617A mutation in the β-Prism domain of the VCC resulted in the complete loss of the lectin activity of the toxin. Therefore, these data altogether established that the β-Prism domain of the VCC played a significant role for a potent targeting of the VCC toward the human erythrocytes cell membrane (228).

### 3.4.9 Effect of the D617A mutation on the pore-forming ability of the toxin

As mention above, the mutation of D617A within the β-Prism domain of the VCC critically abrogated lectin activity of the isolated β-Prism domain protein. Therefore to precisely establish the physiological significance of the carbohydrate-binding property of VCC contributed by the β-Prism domain, we monitored the effect of D617A mutation in the full-length VCC protein.

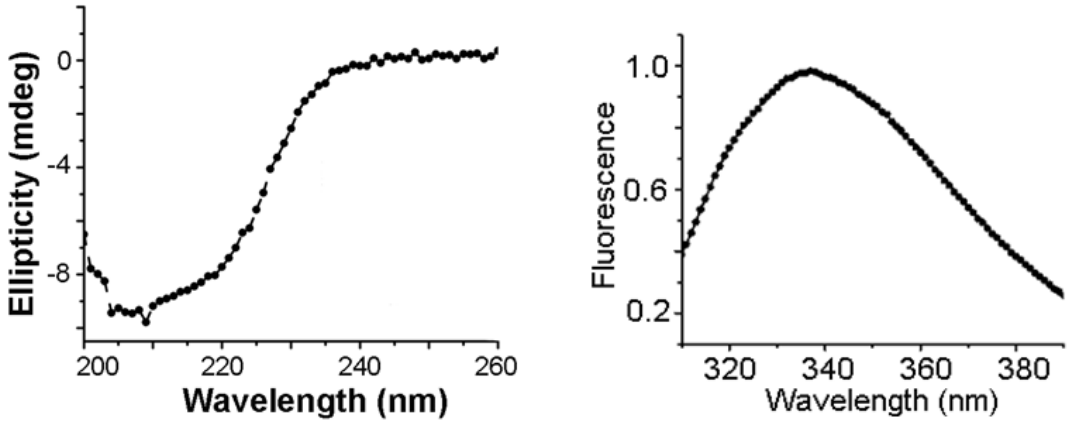


**Figure 3.11: Far-UV CD spectrum and intrinsic tryptophan fluorescence emission profile of the D617A mutant of VCC.**

Mutation of D617A did not affect the structural integrity of the VCC variant as suggested by its intrinsic tryptophan fluorescence emission and far-UV CD spectra profiles (222,228) (Figure 3.11). Notably, VCC protein harboring the D617A mutation displayed severely compromised hemolytic activity against the human erythrocytes.

The Mutant D671A protein exhibited less than 5% of the wild-type hemolytic activity at the protein concentration of 100 nm at 25 $^{o}$C over the period of 1 hr (Figure 3.12 A). Even in the concentration of 1000 nm, the D617A mutant did not display any noticeable hemolytic activity against human erythrocytes. Consistent with our result obtained regarding the isolated β-Prism domain variant of the VCC, D617A mutant also critically abrogates the lectin activity of the full-length VCC protein towards the β-1-galactosyl-terminated glycoprotein asialofetuin (Figure 3.12 B). When we tested the membrane association ability of the D671A mutant toward the human erythrocytes by employing the flow-cytometry based experiment (with a protein concentration in the range of 75 nm) and the result showed drastic inhibition of the membrane interaction ability of the VCC variant. The D617A mutant showed less than 5% of binding with the human erythrocytes of the wild-type VCC (Figure 3.13 A). These data once again confirmed the specific role of the β-Prism domain-mediated lectin activity and its role in the functional association with the erythrocytes cell membrane.

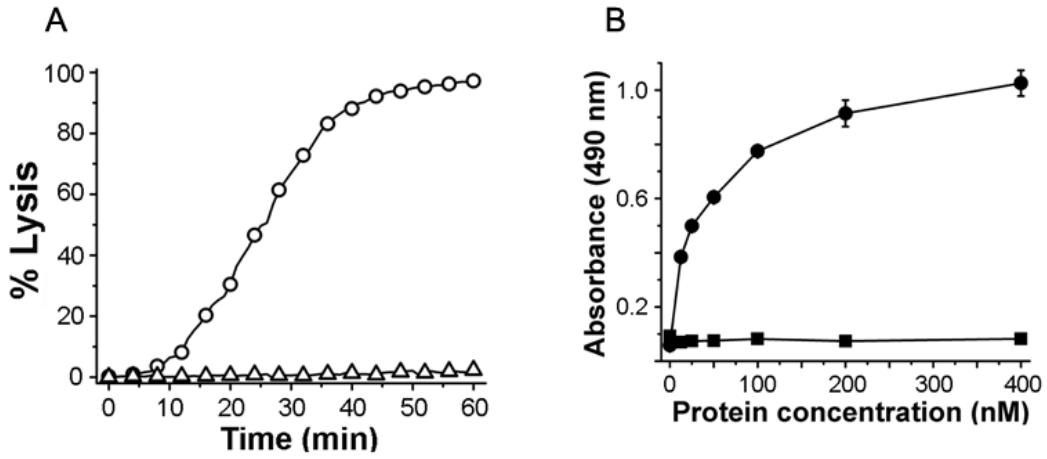


**Figure 3.12: (A) Hemolytic activity of wild-type and D617A-VCC mutant against human erythrocytes (B) ELISA-based study to determine binding of D617A mutant to immobilized asialofetuin with compared to the wild-type protein. (A)** Pore-forming activity of the Asp617Ala-VCC mutant (Δ) against human erythrocytes. Lytic activity of wild type full-length VCC (○) is indicated as a control. **(B)** Interaction of Asp617Ala-VCC mutant protein (■) to immobilized asialofetuin was compared to that of the wild-type VCC protein (●) using an ELISA-based experiment. Each data point showed the average of three independent readings. Error bars showed the standard deviations.

We examined the ability of the D617A mutant to associate with the human erythrocytes using the pull-down based assay done at room temperature. The D617A mutant associated with the human erythrocytes membrane, presumably through the hydrophobicity-driven association with

the human erythrocytes membrane. Interestingly, the D617A mutant protein could not generate any detectable amount of SDS-stable oligomeric assembly in the human erythrocytes membrane while monitored at the concentration of 100 nM (Figure 3.13 B). Even in the concentration of 1000 nM mutant protein could not generate any noticeable SDS-stable oligomeric assembly. These observations was unexpected, since the D617A mutation is present within the β-Prism domain of the VCC, any direct involvement of the Asp-617 residue in the membrane oligomerization would be unexpected as the removal of the whole β-Prism domain of VCC did not affect the ability of the truncated variant to generate SDS-stable oligomeric assembly in the human erythrocytes membrane (228). Therefore, this unexpected observation of the D617A mutation located within the β-Prism domain of the VCC was possibly the reflection of the more complicated regulatory mechanism of the membrane pore-formation process of the toxin.

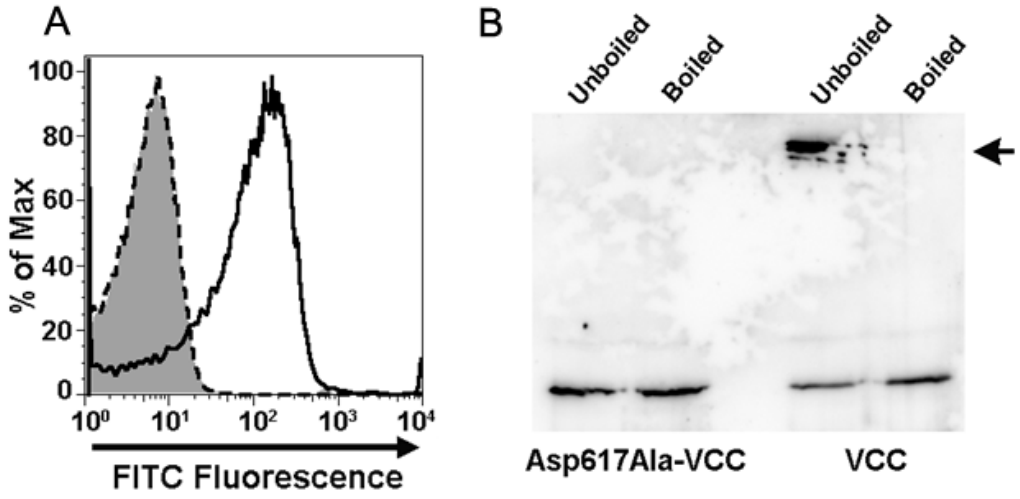


**Figure 3.13: (A) Flow cytometry-based study to monitor interaction of D617A VCC mutant and wild-type VCC (B) Oligomerization efficacy of the bound fraction of WT-VCC and D617A with human erythrocytes.** **(A)** Interaction of Asp617Ala-VCC (dashed line) and the wild type VCC (solid line) to human erythrocytes were monitored by the flow cytometry-based assay with the protein concentration of 75 nM. Shaded peak represents the control sample without any protein treatment. **(B)** Membrane oligomerization ability of the Asp617Ala-VCC mutant in the human erythrocyte membrane. Unboiled samples allowed detection of any SDS-stable oligomeric assembly. SDS-stable oligomer of wild type VCC was indicated with an arrow. Data shown here are the representatives of at least three independent experiments.

Structural analysis of the water-soluble monomeric form of the toxin and the transmembrane oligomeric structure of VCC reveals that the C-terminal β-Prism domain of the VCC undergoes significant structural reorganization with respect to the central core cytolysin domain in the

process of membrane oligomerization of the VCC. It appears that such structural reorganization is essential for the consecutive conformational reorganization of the pre-stem loop towards forming the β-barrel stem region of the transmembrane oligomeric assembly. More importantly, repositioning the β-Prism domain of the VCC is mandatory for the membrane oligomerization of the VCC monomers. Unless the β-Prism domain undergoes such structural reorganization, it will generate steric clashes between the β-Prism domains of the neighboring subunits during the membrane oligomerization process of the toxin. Therefore, to accommodate the protomers in the oligomeric pore assembly, the β-Prism domain from all the contributing monomer must reposition with respect to the central core cytolysin domain (Figure 3.14).

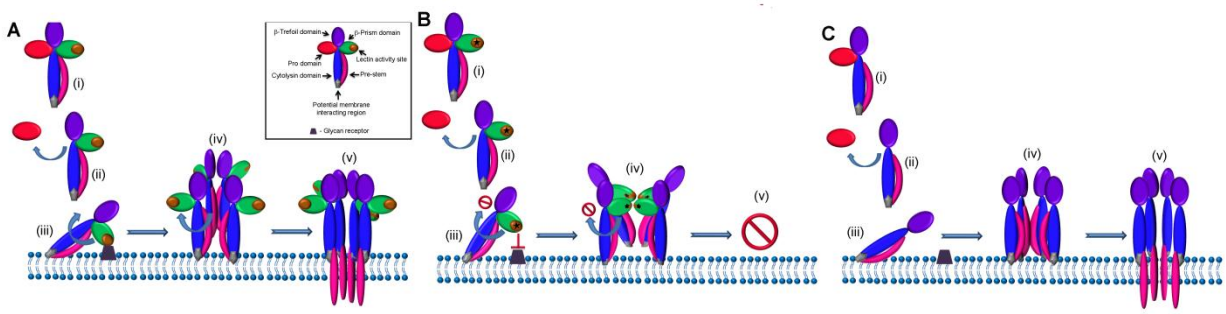


**Figure 3.14: Proposed model showing the role of the β-Prism domain in the lectin activity of VCC. (A)** (i) VCC is secreted by the *Vibrio cholerae* in the form of a inactive Pro-VCC. (ii) With removal of the 'Pro-domain', mature VCC is generated. (iii) VCC associate with the target host cell membrane. (iv-v) Upon association to the target cell membrane, VCC self-assemble to generate the membrane-inserted transmembrane heptameric channel. Membrane oligomerization requires structural reorganization of the β-Prism domain with respect to the VCC structure to allow oligomerization of the VCC protomers. **(B)** Mutation of Asp617Ala within the β-Prism domain blocks the lectin activity and inhibits the membrane oligomerization of VCC. We hypothesize that the blocking of the β-Prism domain-mediated lectin activity, mediated by the Asp617Ala mutation, is possibly arresting the structural reorganization of the β-Prism domain, and thus abrogating the oligomeric assembly the protein in the target membrane. **(C)** Without the β-Prism domain, membrane-associated VCC protomers can self-assemble to generate the transmembrane oligomeric structure, without having any steric clash. The star mark indicated the Asp617Ala mutation.

Based on the data from our study, and based on the available structural data, we hypothesize that the association of the β-Prism domain with the target cell glycoprotein or glycolipid would not only allow the adequate functional targeting of the toxin towards the target cell membrane, but it would also regulate a triggering mechanism for the structural repositioning of the β-Prism

domain of the VCC so as to allow generation of the functional transmembrane oligomeric assembly. Our study suggested that the D617A mutation within the β-Prism domain of the VCC is affecting the membrane interaction ability of the toxin with the target cell surface glycoprotein or glycolipid receptor, probably through blocking of the lectin activity of the VCC. This effect, in turn, would abrogate the structural reorganization of the β-Prism domain of the protein, thus ultimately block the membrane oligomerization process of the VCC toxin. In case of β-Prism domain-truncated variant, the absence of the β-Prism domain would abolish the mentioned steric constraint (s) towards the membrane oligomerization of the truncated variant of VCC. As a result, the membrane oligomerization of the truncated variant of the VCC would not be regulated anymore through the carbohydrate-binding activity of the β-Prism domain of the toxin (Figure 3.15). Consistent with such assumption, the β-Prism truncated variant of the VCC was found to form the oligomeric assembly in the human erythrocyte membrane. It is important to note here, that the oligomer generated by the truncated variant is non-functional.

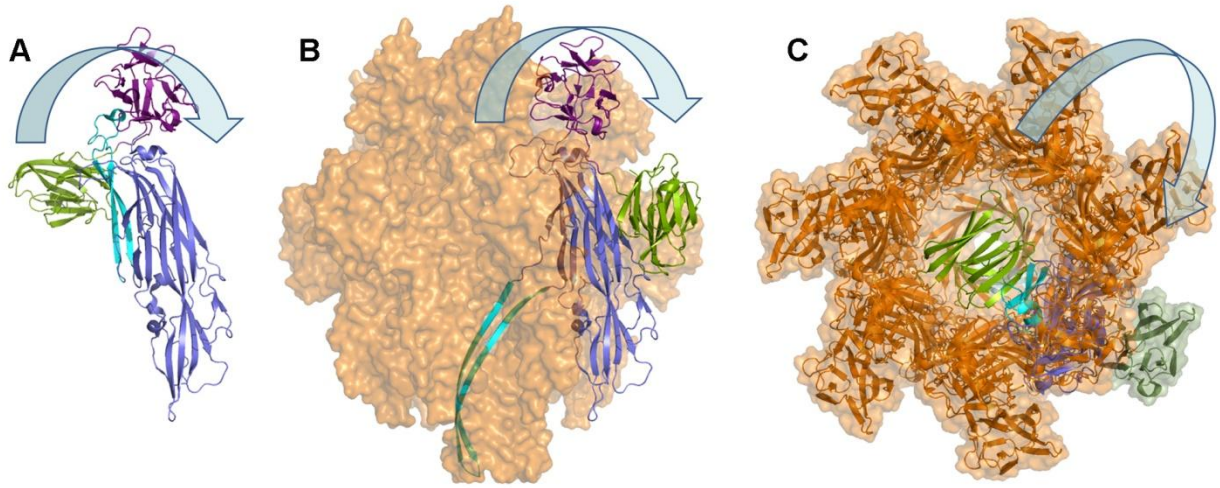


**Figure 3.15: Structural rearrangement of the β-prism domain during membrane oligomerization of VCC. (A)** Structural model of the mature active form of VCC in its water-soluble monomeric state. **(B)** The transmembrane oligomeric assembly of VCC. **(C)** Top view of the transmembrane oligomeric pore assembly of VCC. The β-Prism domain is shown in green. Structural reorganization of the β-Prism domain during membrane oligomerization indicated with the arrow. Without this structural reorientation, β-Prism domain would be located at the central core of the oligomeric pore structure, thereby generating steric clash toward the generation of the transmembrane oligomeric pore assembly. The structural models of the water-soluble monomeric form and the transmembrane oligomeric form of VCC were generated by using the PDB entries 1XEZ and 3O44, respectively.

The regulatory role of the β-Prism domain-mediated lectin activity on the membrane interaction and the membrane oligomerization process of the toxin appear to suggest a novel model of the regulatory mechanism modulating the membrane pore-forming activity of the VCC protein.

**3.5 Conclusion**

Altogether, the data obtained from this study provided a novel molecular mechanism with respect to the role of the β-Prism domain of the VCC in the mode of action of the toxin. From this study, we conclusively established that the β-Prism domain of the VCC acted as the structural scaffold determining the lectin activity of the protein towards the β-1-galactosyl terminated complex glycoconjugates. We also identified the critical amino acid residue(s) responsible for the lectin activity of VCC. Our data suggested that the β-Prism domain of VCC employed a canonical structural mechanism, which is also involved in determining the lectin activity of the members of the β-Prism lectin family. Toward the direction of probing the physiological importance of the β-Prism domain-mediated lectin activity of VCC, we established a crucial involvement of the β-Prism domain in determining the binding propensity of VCC towards the target host cell membrane, presumably through the interaction with the glycolipid or glycoprotein receptor(s) present in the surface of the target host cell membrane. Also, our results suggested that the β-Prism domain-mediate lectin activity may act to regulate the membrane oligomerization process of the membrane-bound VCC protein. From this part of study, we concluded that the β-Prism domain of the VCC acted to determine the critical regulatory role(s) in terms of modulating the different steps of the membrane pore-formation mechanism of VCC. Since the β-Prism domain is not commonly present in any other member of the β-PFTs family, it would be more interesting in future to explore how the VCC structure-function relationship has evolved to harbor a regulatory structural module within the proteins of the β-PFT family.

# Chapter 4

## Trapping of VCC in the membrane-bound monomeric state abrogates oligomerization, membrane insertion and functional pore-formation

### 4.1 Abstract

VCC follows the similar scheme of pore-formation as followed by archetypical β-barrel pore-forming toxins. In the mode of action of the toxin, VCC is first secreted as the water-soluble monomers that interact with the target host cell membranes, and then assemble into the intermediate transient pre-pore oligomers, and finally convert into the functional transmembrane heptameric β-barrel pore. However, there exists an important void area regarding the understanding of the molecular mechanism of the pore-formation mechanism carried out by VCC. Specifically, the membrane oligomerization and membrane insertion steps of the process have not been elucidated in detail. In this part of the study, we have identified the key amino acid residues in VCC which play a critical role to initiate membrane oligomerization of VCC. The alterations of such amino acid residues trap VCC in its membrane-associated monomeric state, and block the subsequent oligomerization, membrane insertion, and functional pore-formation steps of the toxin. The results obtained from this study suggested that the membrane insertion of the stem-loop of the toxin critically depended on the membrane oligomerization process, and it could not be initiated in the membrane-bound monomeric form of the toxin. Overall, our study dissected the membrane interaction from the following oligomerization and membrane insertion steps of the toxin, and thus, revealed the exact sequence of the events in the functional pore-formation process employed by VCC.

### 4.2 Introduction

The generation of the transmembrane oligomeric pore structure comprises membrane insertion of the pore-forming stem region from each of the toxin protomer (174,233). However, it has not been examined experimentally, in particular in the case of VCC, whether the membrane insertion of the stem region could occur in the membrane-associated monomeric state before the pre-pore oligomer generation, or whether the pre-pore oligomer generation precedes the membrane insertion of the stem region of VCC. Even in the case of generalized β-PFT membrane pore-formation mechanisms, such sequence of pore-formation events has not been established conclusively.

Previous studies have explored the mechanism of membrane oligomerization process of the β-PFT family members, including VCC. It is suggested that the associations of the β-PFT monomers with the membrane of the target host cells act as the triggering mechanism to initiate the subsequent steps leading towards oligomerization, membrane insertion, and functional transmembrane pore formation (128,234). Analysis of VCC transmembrane oligomer structure highlights extensive inter-protomer interactions between the neighboring subunits (174). The most critical interactions are observed between the residues within the membrane-inserting loop region. Notably, trapping of the stem region in its pre-stem configuration has been shown to block functional transmembrane oligomeric structure without affecting pre-pore oligomer generation (235). It has also been demonstrated that, even in the absence of the stem region, a truncated variant of VCC can generate the pre-pore oligomer structure on the membrane (194). These observations clearly suggest that the inter-protomer interactions of the stem region are critically participated in the formation of functional transmembrane pore without playing any important role in initiating the oligomerization event of the membrane-associated VCC molecules. Therefore, it appears that the additional associations that are not part of the pore-forming stem loop might be playing critical role(s) in triggering membrane oligomerization of the toxin.

In this study, to explore the details of the molecular mechanism of the membrane oligomerization process of VCC, we have identified the key residues in VCC structure that are crucial to trigger oligomerization of the membrane-associated molecules. Mutations of such key residues abrogates the membrane oligomerization step, traps the toxin in its membrane-associated monomeric state, and does not allow membrane insertion of the pore-forming stem-loop from the monomers. Our study, for the first time, dissects the membrane interaction step from the subsequent membrane oligomerization and insertion step of VCC, This study also establishes that the membrane insertion critically requires oligomerization of the membrane-associated VCC.

## 4.3 Materials and methods

### 4.3.1 Purification of recombinant VCC variants

The recombinant variants of VCC harboring single point mutation of D241A, W318A, R330A, or F581A were generated by PCR-based strategy as described previously in chapter 2. Nucleotide sequences of all constructs were confirmed by DNA sequencing. VCC variants were

purified following the same procedure as described for the wild-type toxin in chapter 2. The homogeneity of the VCC variants was analyzed by SDS-PAGE and Coomassie staining.

### 4.3.2 Intrinsic tryptophan fluorescence and far-UV CD

Intrinsic tryptophan fluorescence spectra were recorded using Fluoromax-4 spectrofluorometer (Horiba Scientific, Edison, NJ) upon excitation at 290 nm. The slit widths were set at 2.5 nm and 5 nm for excitation and emission, respectively. The concentration of VCC variants for this experiment was 250-300 nM in Tris-HCl buffer (pH 8.0).

A Chirascan spectropolarimeter (Applied Photo-physics, Leatherhead, Surrey, UK) was used to monitor far-UV CD spectra of VCC variants. The final concentration of proteins in each experiment was in the range of 400- 800 nM.

### 4.3.3 Hemolytic activity assay

The hemolytic activity of the VCC variants were determined against the human erythrocytes as described previously in chapter 2. The kinetics of hemolysis was monitored by recording the decrease in the turbidity of the human erythrocytes suspension in PBS at 650 nm upon incubation with the VCC variants at 25 $^{o}$C.

### 4.3.4 Flow cytometry-based assay

The binding of VCC variants with the human erythrocytes was monitored by using a flow cytometry-based assay as described previously in the chapter 2. Briefly, human erythrocytes ($1x10^6$ cells) were incubated with 75 nM concentration of VCC variants for 30 minutes at 4 $^{o}$C in PBS. The cells were washed and incubated with rabbit anti-VCC antiserum, followed by treatment with FITC-conjugated goat-rabbit antibody. The cells were analyzed by using FACSCalibur (BD Biosciences), flow cytometer.

### 4.3.5 Calcein release assay

The membrane permeabilization activity of VCC variants against the membrane lipid bilayer of the Asolectin-cholesterol liposomes was determined by monitoring the release of trapped calcein dye from within the liposome vesicles, as described earlier in chapter 2. VCC variants concentration was adjusted to 1 μM while the liposomes concentration was 25 μg/ml. The calcein fluorescence was recorded at 520 nm on a Perkin-Elmer LS 55 spectrofluorimeter at room temperature, upon excitation at 488 nm, using the excitation and emission slit width of 2.5 and 5 nm, respectively.

### 4.3.6 Pull-down assay to monitor association of VCC variants with liposomes

The interaction of VCC variants with the Asolectin-cholesterol liposomes was probed by a pull-down-based experiment as described previously in Chapter 2. Briefly, VCC variants (1 μM) were treated with the Asolectin-cholesterol liposomes (6.5 μg) in a 100 μl reaction volume at room temperature for 30 minutes. The reaction mixture was subjected to ultracentrifugation at 105,000 x g for 30 minutes at 4 $^{o}$C. After collecting the supernatant fraction, pellet fraction was washed twice with PBS and then resuspended in 100 μl of PBS. For detecting the free and liposome-bound VCC proteins, an equal volume of the sample from the supernatant and pellet fraction were examined by SDS-PAGE/Coomassie staining after boiling the sample in the presence of SDS-PAGE loading buffer.

### 4.3.7 SDS-stable oligomer formation by membrane-bound VCC variants

For detection of SDS-stable oligomer formation in human erythrocytes membrane, VCC variants (100 nm) were incubated with human erythrocytes suspension ($OD_{650}$ was adjusted to 0.9) in a reaction volume of 100 μl in PBS for 1 hour at 25 $^{o}$C and subjected to ultracentrifugation at 105,000 x g. Pellet fractions were washed with the PBS and were dissolved in 50 μl SDS-PAGE loading buffer and divided into two equal parts. One part was incubated at room temperature, whereas the other half was boiled for 10 minutes and subsequently analyzed by immunoblotting. The sample without boiling would allow the detection of the SDS-stable oligomer of VCC variants while the boiled sample allowed detection of membrane-associated fractions of VCC variants.

For detection of the SDS-stable oligomers in the Asolectin-cholesterol liposomes, VCC variants (1μM) were incubated with Asolectin-cholesterol liposomes (6.5 μg) in a 100 μl reaction. Liposome-associated VCC variants were pelleted by ultracentrifugation at 105,000 x g at 4 $^{o}$C for 30 minutes. Pellet fractions were washed with the PBS, dissolved in 50 μl SDS-PAGE sample buffers, and divided into two equal aliquots. One aliquot was kept in room temperature while the other aliquot was boiled. Samples were probed by SDS-PAGE/Coomassie staining.

### 4.3.8 FRET assay

FRET from the tryptophan residue to DPH embedded in the Asolectin-cholesterol liposomes was monitored as described previously in chapter 2. VCC variants (1μM) were incubated with the DPH embedded liposomes (50 μg/ml) at 25 $^{o}$C. Tryptophan-to-DPH FRET signal was recorded at 470 nm upon excitation at 290 nm.

### 4.3.9 Detection of SDS-labile oligomer by $BS^3$ cross-linking

For the detection of the SDS-labile pre-pore oligomeric assembly generated by VCC mutants in the presence of Asolectin-cholesterol liposomes, covalent cross-linking of the pre-pore oligomeric species was performed using $BS^3$ [bis(sulfosuccinimidyl) suberate, Thermo Pierce], following the method described earlier in Chapter 2.

### 4.3.10 Surface plasmon resonance measurements

The interaction of VCC variants with the Asolectin-cholesterol liposomes was probed by surface plasmon resonance (SPR)-based experiment on a Biacore 3000 platform (GE Healthcare Life Sciences) at 25 $^{o}$C using L1 sensor chip as described earlier in chapter 2.

### 4.3.11 Amino acid sequence alignment

Amino acid sequences were obtained from the NCBI server (http://www.ncbi.nlm.nih.gov/protein). The amino acid sequence alignment was prepared by employing ClustalW within the Biology Workbench server (236,237). The sequence alignment was rendered with the ESPript server (238).

### 4.3.12 Visualization of the structural models

The coordinates of VCC molecular structure (PDB ID 1XEZ and 3O44) were obtained from the Protein Data Bank. The structural model of the transmembrane oligomeric form of VCC was generated by using the orientations of toxins in the membrane database server (215).

## 4.4 Results and discussion

### 4.4.1 Characterization of the recombinant VCC variants

Analysis of the inter-protomer interfaces of VCC oligomer structure shows the presence of an aspartate residue at location 214 (Asp-214), an arginine at location 330 (Arg-330), and a phenylalanine residue at location 581 (Phe-581). These residues, Asp214, Arg330, and Phe581, are found to be highly conserved in the related cytolysin/hemolysin proteins of *Vibrionaceae* bacteria (174,239,240) (Figure 4.1).

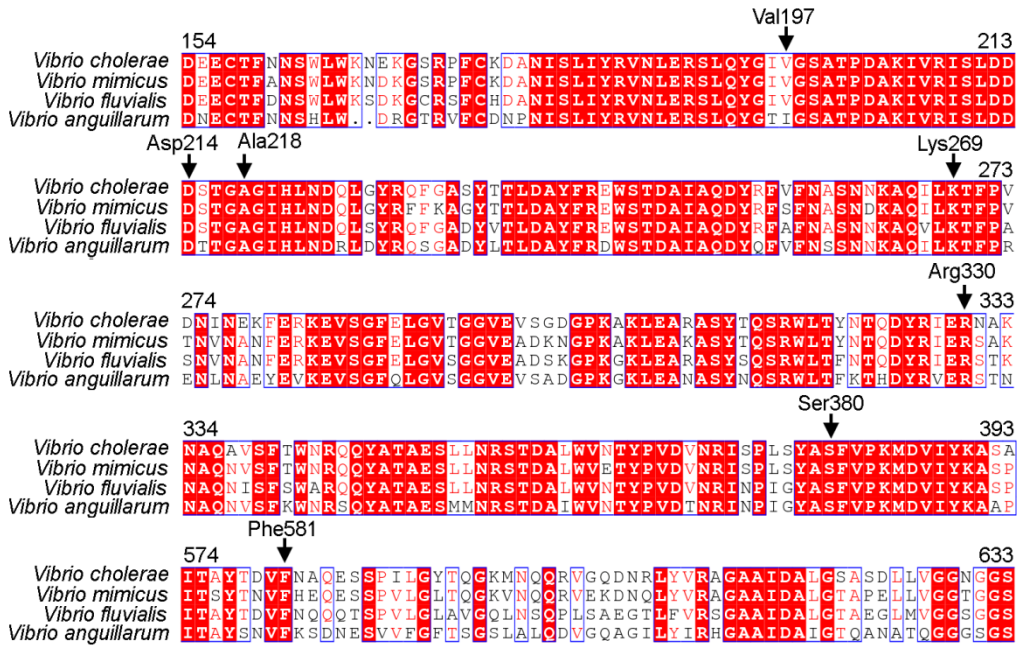


**Figure 4.1: Amino acid sequence alignment of VCC and its related cytolysins from *Vibrio* species.** Positions of the conserved residues, Asp-214, Arg-330 and Phe-581, in VCC are shown. Other conserved residues, Lys-269 (making contact with Asp-214), Ser-380 and Ala-218 (making contact with Arg-330), and Val-197 (making contact with Phe-581) at the protomer-protomer interface of VCC oligomer, are also indicated.

Asp-214 is located within a unique loop structure in the cytolysin domain of VCC. It appears to be involved in a salt bridge interaction with a Lys-269 amino acid residue located in the neighboring protomer within the VCC oligomer structure. The Arg-330 residue is located within the first β strand next to the membrane inserting stem-loop. In VCC oligomer structure, Arg-330 is participated in the hydrogen bond interactions with the side chain of conserved residues, Ser-380, and the main chain carbonyl group of the other conserved residue, Ala-218, from the neighboring protomer. The Phe-581 residue is positioned at the carboxy-terminal boundary of the β-Trefoil domain of VCC, and it appears to involve in the van der Waals interaction with a conserved residue, Val-197, within the cradle loop of the neighboring protomer (174) (Figure 4.2 A). To probe the role of these three conserved residues, Asp-214, Arg-330, and Phe-581, in regulating the membrane oligomerization mechanism of VCC, we generated three recombinant variants of VCC harboring the single point mutation of D214A (D214A-VCC), R330A (R330A-VCC), and F581A (F581A-VCC) (219) (Figure 4.2 B).

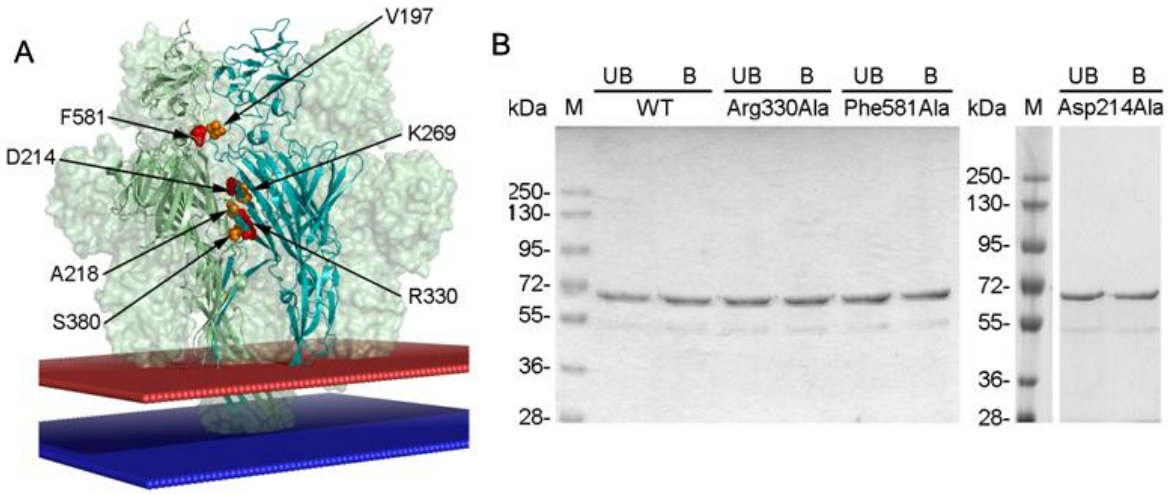


**Figure 4.2: (A) Transmembrane oligomeric structural model of VCC showing the position of the conserved residues at the interface of the protomers (B) Purified form of the wild-type and mutant VCC variants examined by SDS-PAGE/Coomassie.** Proteins were treated in the presence of SDS-PAGE sample buffer with (marked as B) or without boiling (marked as UB). Protein standards are shown in lane M.

All three VCC variants displayed similar intrinsic tryptophan fluorescence and far-UV CD spectra profile with the wild-type toxin (Figure 4.3). Similar intrinsic tryptophan fluorescence emission spectra of the wild-type and its three variants suggested a similar environment for all tryptophan residues within the structure of VCC variants, indicated overall similar global tertiary structures of D241A-VCC, R330A-VCC, and F581A-VCC with compared to the wild-type toxin (174). Additionally, similar far-UV CD profile of the three VCC variants and wild-type protein also suggested their similar secondary structural organization.

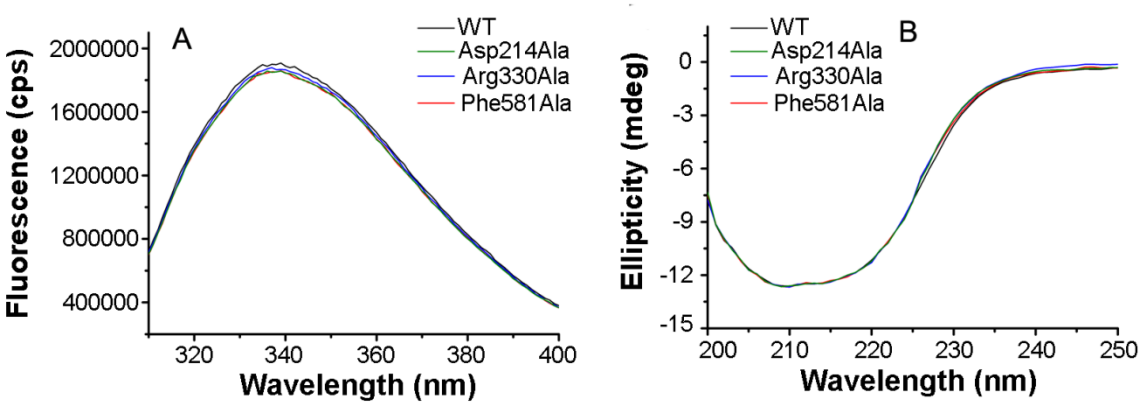


**Figure 4.3: (A) Intrinsic tryptophan fluorescence emission spectra of the VCC variants. (B) Far-UV CD spectra of the VCC variants.**

Altogether, these data suggest that the mutations of D214A, R330A, and F581A in VCC did not change the overall secondary and the tertiary structural arrangements of the VCC variants.

### 4.4.2 VCC mutants display abrogated pore-forming activity in the membrane lipid bilayer of human erythrocytes and synthetic lipid vesicles

VCC generates transmembrane β-barrel pores in the membrane lipid bilayers of the human erythrocytes membrane, thereby leading to the colloid osmotic lysis of the cells. VCC-induced lysis of the human erythrocytes is considered to be the quantitative measure of the membrane permeabilization ability of VCC. Therefore, the functional membrane pore-forming activity of the D214A-VCC, R330A-VCC, and F581A-VCC were examined by assaying their ability to induce membrane-damaging cytolytic activity against human erythrocytes. We examined the lysis of human erythrocytes upon incubation with VCC variants over a period of 1 hr at 25 $^{o}$C. We observed that, F581A-VCC displayed only 30% of the wild-type lytic activity, while R330A-VCC could not show any detectable hemolytic activity (< 5% lytic activity) at a concentration of 100 nM. D214A-VCC displayed almost 55% of hemolytic activity under similar conditions (Figure 4.4). When examined over an extended period of up to 6 hours, F581A-VCC showed 60% of the wild-type activity while the R330A-VCC variant was still lacking any lytic activity against human erythrocytes. Notably, D214A-VCC started showing wild type-like activity at extended time period of 3-4 hours.

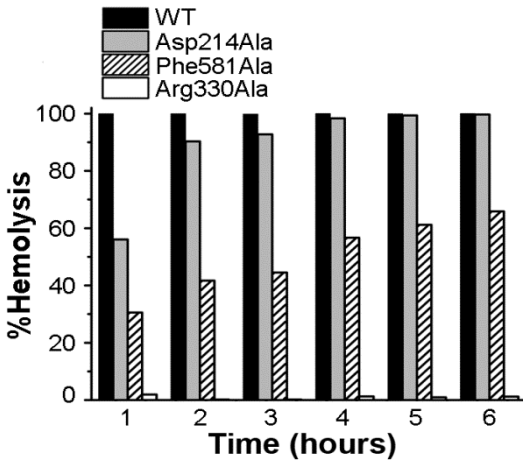


**Figure 4.4: Hemolytic activity of wild-type VCC and VCC variants against human erythrocytes.** Pore-forming activity of the VCC variants probed by monitoring the hemolytic activity of the proteins (100 nM) against human erythrocytes.

We examined whether the reduced activities were due to the abrogated ability of the VCC variants to interact with the erythrocytes cells. For this, we investigated the interaction of VCC

variants with human erythrocytes by using a flow cytometry-based assay. Results obtained from this assay suggested that all three VCC variants D214A-VCC, R330A-VCC and F581A-VCC, associated with the human erythrocytes with the similar efficiency compared with that of the wild-type VCC toxin (Figure 4.5). These results, therefore, suggested that the mutations of D214A, R330A, and F581A in VCC could block the pore-forming ability of the toxin in human erythrocytes without affecting their efficacy to interact with the cell membranes. The effect of the R330A mutation on the membrane permeabilization ability appeared to be more severe compared with that of the F581A mutation. The D214A mutation appeared to have a marginal effect on the pore-forming activity.

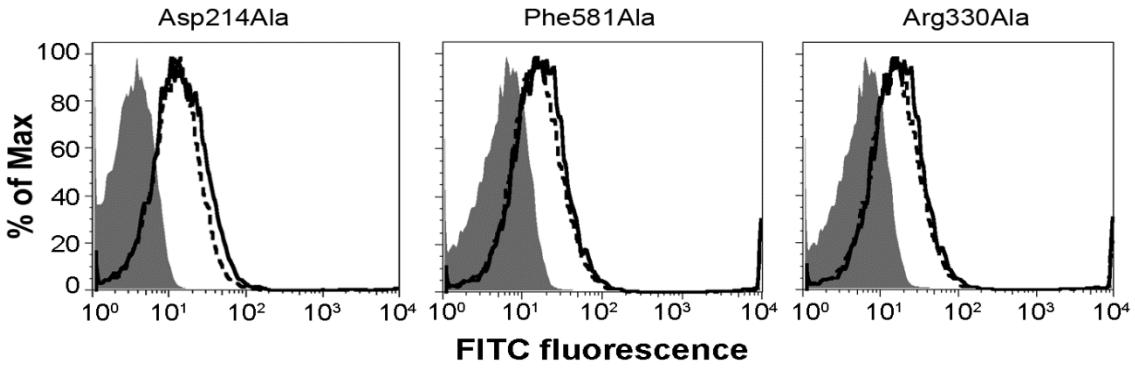


**Figure 4.5: Flow cytometry-based experiment to monitor interaction of VCC variants against human erythrocytes.** Interaction of the VCC variants (75 nM) with human erythrocytes was monitored by the flow cytometry-based assay. Solid line, WT-VCC; dashed line, mutant VCC variants as indicated on top of the panel; shaded curve, control without any protein treatment.

We further examined the pore-forming activity of D214A-VCC, R330A-VCC, and F581A-VCC in the lipid bilayer of the Asolectin-cholesterol liposomes in terms of inducing the release of the encapsulated calcein from within the liposome vesicles. As observed previously in chapter 2, wild-type VCC displayed ~90% of the calcein release activity compared with sodium deoxycholate as a positive control within 30 minutes of the treatment with Asolectin-cholesterol liposomes, In contrast, VCC variants showed severely compromised calcein release from the Asolectin-cholesterol liposome vesicles upon incubation over a period of 30 minutes. Extended incubation of liposomes with D214A-VCC and F581A-VCC resulted in a significant extent of the calcein release. When probed at the 6-hour time point, D214A-VCC and F581A-VCC could trigger ~80% and ~50% of the calcein release from the Asolectin-cholesterol liposomes,

respectively. Notably, the R330A variant could not induce any significant calcein release, even after prolonged incubation of 6 hours (Figure 4.6).

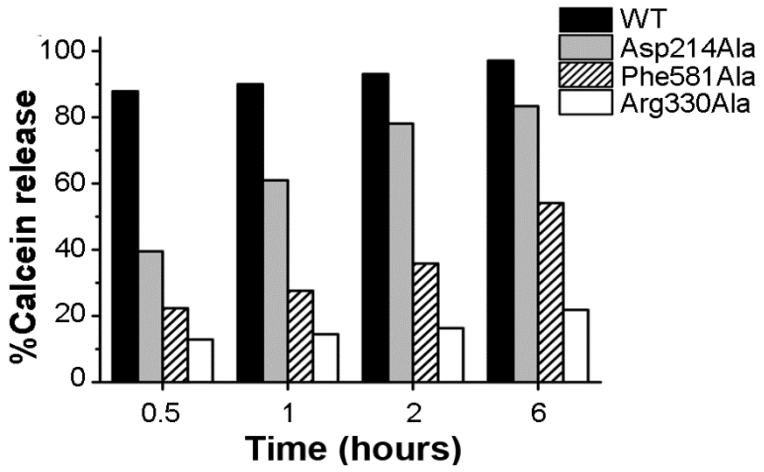


**Figure 4.6: Membrane permeabilization ability of the VCC variants in the presence of synthetic liposomes.** Pore-forming activity of the VCC variants (1 μM), as determined by monitoring the calcein release from the Asolectin-cholesterol liposomes.

Consistent with our data regarding the human erythrocytes, all three VCC variants showed wild-type-like interaction with the membrane lipid bilayer of the Asolectin-cholesterol liposome vesicles. A pulldown-based assay showed that the D214A, R330A, and F581A variants of VCC could interact efficiently with the Asolectin-cholesterol liposomes, as observed with the wild-type VCC toxin (Figure 4.7).

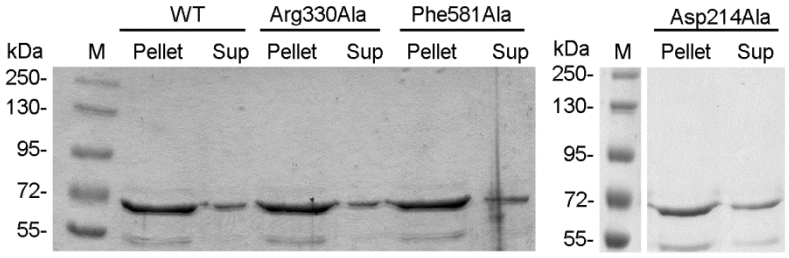


**Figure 4.7: Pull-down based assay to monitor association of the VCC variants to the Asolectin-cholesterol liposomes.** Pellet fractions containing liposome-associated proteins and the supernatant fraction containing unbound proteins were analyzed by SDS-PAGE/Coomassie staining.

We also used a quantitative SPR-based experiment to examine the association of the VCC variants with the Asolectin-cholesterol membrane lipid bilayer. The steady-state interacting sensograms displayed that the D214A-VCC, R330A-VCC, and F581A-VCC toxins retained the

wild-type-like binding ability with the Asolectin-cholesterol liposomes (Figure 4.8 A). Analysis of the end point response units (as resulted from the stable phase of the respective sensograms after completion of the protein injection) also revealed a similar irreversible membrane interaction for the VCC variants and wild-type protein (Figure 4.8 B).

Altogether, these data suggest that the single point mutations of the D214A, R330A, and F581A in VCC abrogated the membrane pore-formation ability of the protein without significantly affecting the membrane association ability of the toxin. Our results also suggest that, although the D214A and F581A mutations affected the membrane pore-forming ability to a marginal extent; the mutation of R330A had drastic, deleteroius effect on the process of membrane pore-formation by VCC.

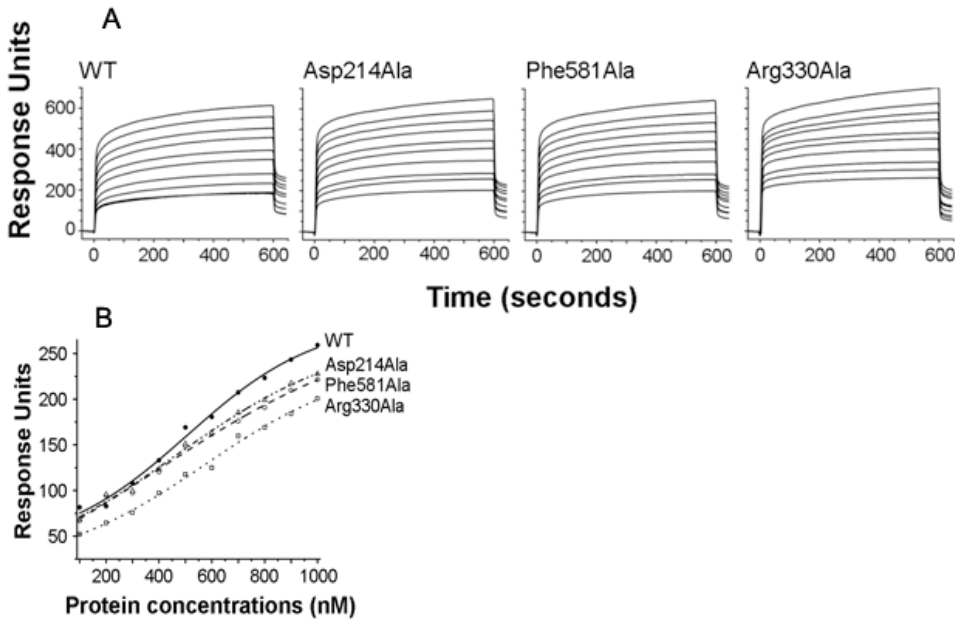


**Figure 4.8: SPR-based assay to determine binding of VCC variants to the membrane lipid bilayer of Asolectin-cholesterol liposomes. (A)** Overlay of the interacting sensograms shows steady-state binding of the VCC variants. **(B)** Analysis of the end point response units displays a concentration-dependent increase in irreversible association of the VCC variants toward the Asolectin-cholesterol membrane lipid bilayer.

### 4.4.3 VCC variants displayed critically compromized membrane oligomerization ability

Oligomerization of VCC in the membrane lipid bilayer is considered to be a key event toward formation of the transmembrane pore structure. Consistent with the generalized β-PFT mode of action, association of VCC with the target membrane leads to the generation of the SDS-labile, pre-pore oligomeric intermediates, followed by their conversion into robust, SDS-stable transmembrane oligomeric pore assembly. Hence, to explore the mechanistic basis of the

abortive membrane pore-formation process caused by the D214A, R330A, and F581A mutations in VCC, we analyzed the membrane oligomerization ability of D214A-VCC, R330A-VCC, and F581A-VCC in the lipid bilayer of the human erythrocytes membrane and the Asolectin-cholesterol liposomes system. For this, we examined the ability of the membrane-associated VCC variants to form SDS-stable oligomeric structure, a property commonly recognized as the signature of the members of archetypical β-PFT family, including VCC. As reported previously, wild-type VCC could generate the SDS-stable oligomeric assembly in the membrane lipid bilayer of the human erythrocytes. In comparison, F518A-VCC was found to shown a reduced ability to form SDS-stable oligomeric assembly in the lipid bilayer of the human erythrocytes. F581A-VCC also displayed a limited ability to generate SDS-stable oligomer when incubated with the lipid bilayer of Asolectin-cholesterol liposomes compared with the wild-type toxin (Figure 4.9). F581A-VCC showed a marginal extent of the membrane oligomerization in the membrane lipid bilayer of the human erythrocytes and Asolectin-cholesterol liposomes that corresponded to the moderate extent of the membrane pore-forming ability, the membrane oligomerization efficacy of D214A-VCC was found to be only marginally decreased compared with that of the wild-type VCC toxin (Figure 4.10).

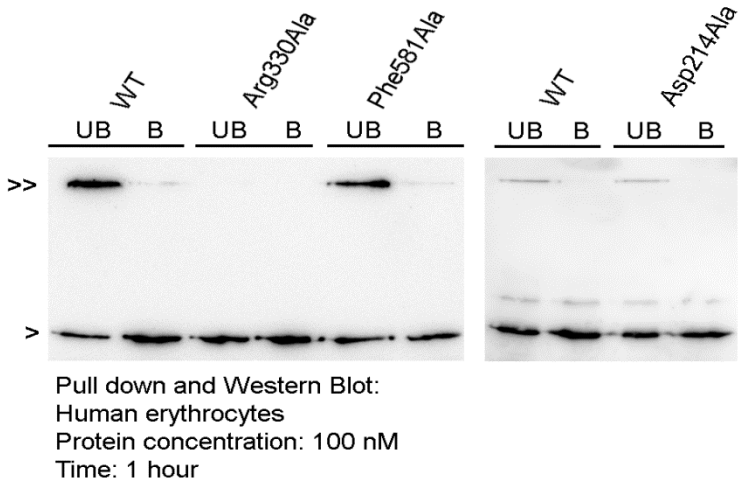


**Figure 4.9: Western blot analysis to monitor SDS-stable oligomerization of VCC variants in the presence of human erythrocytes membranes.** Erythrocyte membrane-associated proteins were pelleted by ultracentrifugation and were examined by immunoblotting. Samples incubated with SDS-PAGE sample dye without boiling (UB) allowed probing of the SDS-stable oligomers.

Notably, R330A-VCC did not generate any noticeable extent of SDS-stable oligomeric assemblies in the membrane lipid bilayer of the Asolectin-cholesterol liposomes and human erythrocytes. Even after extended incubation of 6 hours of interaction with the Asolectin-

cholesterol liposomes, the membrane-associated fraction of the R330A-VCC failed to form a SDS-stable oligomeric species (Figure 4.11). We also explored whether the R330A-VCC mutant of VCC could generate any SDS-labile pre-pore oligomeric species in the membrane lipid bilayer of Asolectin-cholesterol liposome vesicles.

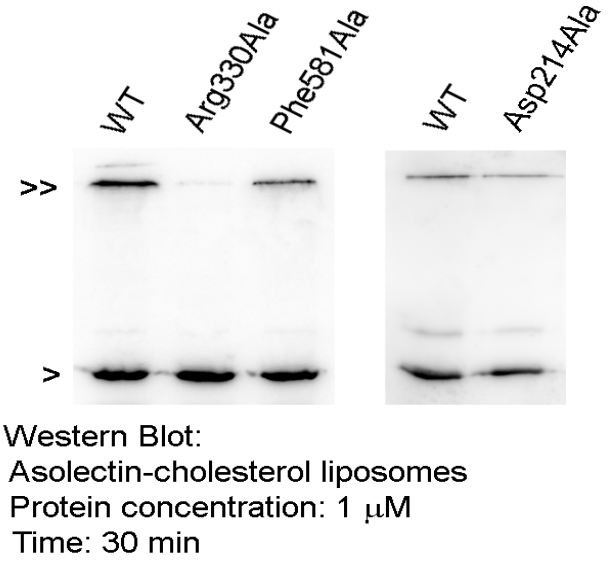


**Figure 4.10: Immunoblot analysis to examine the SDS-stable oligomer generation by the VCC variants in the presence of Asolectin-cholesterol liposomes.** No significant extent of SDS-stable oligomer formation was detected for Arg330Ala-VCC. Asp214Ala-VCC display marginally reduced oligomer formation as compared to WT-VCC. WT-VCC was used as a control in each of the immunoblots.

To arrest any SDS-labile oligomers of the toxin generated in the lipid bilayer of the Asolectin-cholesterol liposomes, we used the cross-linking agent $BS^3$. $BS^3$-mediated, covalent cross-linking could trap the SDS-labile oligomers of wild-type VCC generated in the liposomes within 30 minutes of the association. In contrast, $BS^3$ cross-linking could not trap any such oligomeric structure for R330A-VCC in the presence of Asolectin-cholesterol liposomes under similar condition. These results, therefore, suggested that the alteration of R330A in VCC toxin not only abrogated the SDS-stable oligomeric assembly generation but also critically affected the generation of SDS-labile pre-pore oligomer assembly (Figure 4.12).

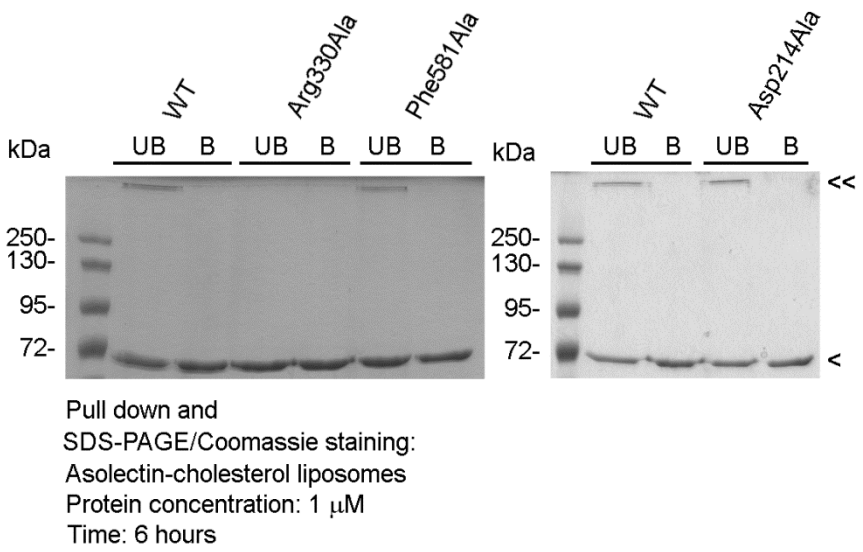


**Figure 4.11: Oligomerization of the membrane-bound fraction of VCC variants in the presence of Asolectin-cholesterol liposomes.** VCC mutants were treated with the liposomes, liposome-bound proteins were pelleted by ultracentrifugation and were analyzed by SDS-PAGE/Coomassie staining. Samples incubated with SDS-PAGE sample buffer without boiling (UB) allowed detection of the SDS-stable oligomers.

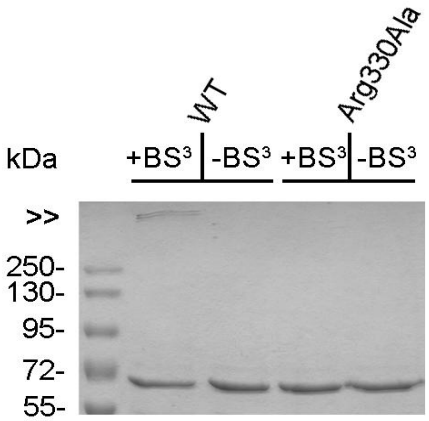


**Figure 4.12: Formation of the SDS-labile pre-pore oligomer by using $BS^3$ cross-linking in the Asolectin-cholesterol liposomes.**

Altogether, our results establish that the alteration of R330A and F581A in VCC critically affected the membrane oligomerization process of the pore-formation process. The D214A mutation affected the membrane oligomerization of VCC only to a marginal extent. Although the F581A mutation imposed only a modest membrane oligomerization defect, the R330A mutation caused severe inhibition of the oligomerization step, thereby trapping the membrane-associated form of the toxin in an abortive monomeric state.

### 4.4.4 The mutation in inter-protomer interfaces in VCC affects membrane insertion step of the toxin

We monitored whether the D214A-VCC, R330A-VCC, and F581A-VCC mutants could insert their pore-forming stem-loop into the membrane lipid bilayer in the absence of the membrane oligomerization. For this, we monitored FRET from the tryptophan residue (Trp-318) positioned within the pore-forming stem-loop of VCC to the DHP fluorescence embedded within the hydrophobic core of the membrane lipid bilayer, as described earlier in chapter 2.

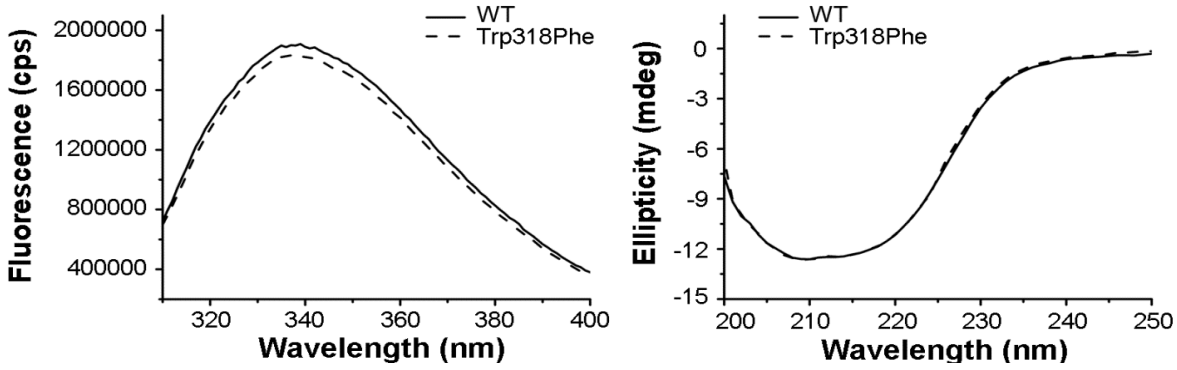


**Figure 4.13: Far-UV CD spectra and intrinsic tryptophan fluorescence emission profile of the W318A mutant of VCC with compared to wild-type VCC.**

A time-dependent increaseed tryptophan-to-DPH FRET signal, upon treatment of VCC mutants in the presence of the DPH-labeled Asolectin-cholesterol liposomes, would show the membrane insertion of the pore-forming stem-loop. As reported previously that a truncated mutant of VCC lacking the stem-loop could not show any detectable tryptophan-to-DPH FRET in the presence of the DPH-labeled Asolectin-cholesterol liposomes compared with that observed with the wild-type VCC toxin (194). To further confirm the specific role of Trp-318 in mediating such a FRET process, we generated a W318F mutant of VCC (W318F-VCC). W318F-VCC displayed almost overlapping intrinsic tryptophan fluorescence emission and far-UV CD spectra profile compared with that of the wild-type VCC protein, indicating no structural defect in the variant (Figure 4.13). Notably, W318F-VCC displayed potent membrane-pore forming activity against human erythrocytes and Asolectin-cholesterol liposomes, indicating that the mutation of W318F did not trigger any defect in the protein in terms of the oligomeric membrane pore-forming activity (Figure 4.14).

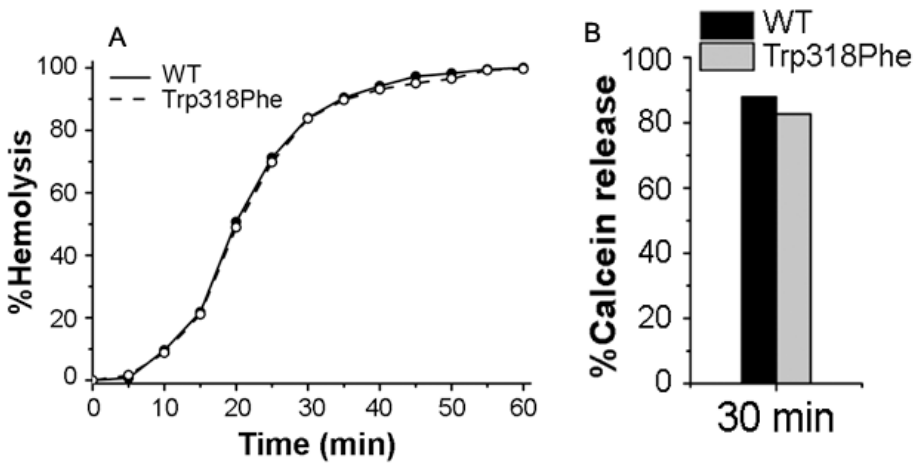


**Figure 4.14: Monitor efficacy of membrane permeabilization of WT-VCC and W318A by using hemolytic activity and calcein release assay.** Trp318Phe-VCC displayed similar extent of pore-forming activity (A), and liposome permeabilization as compared to that of WT-VCC (B).

On the basis of our proposition, however, the mutation of Trp-to-Phe at position 318 within the membrane pore-forming stem-loop would be expected to block the tryptophan-to-DPH FRET signal. Indeed, in our experiment, we found that W318F-VCC did not display any time-dependent increase in the tryptophan-to-DPH FRET when treated in the presence of the DPH-labeled Asolectin-cholesterol liposomes (Figure 4.15).

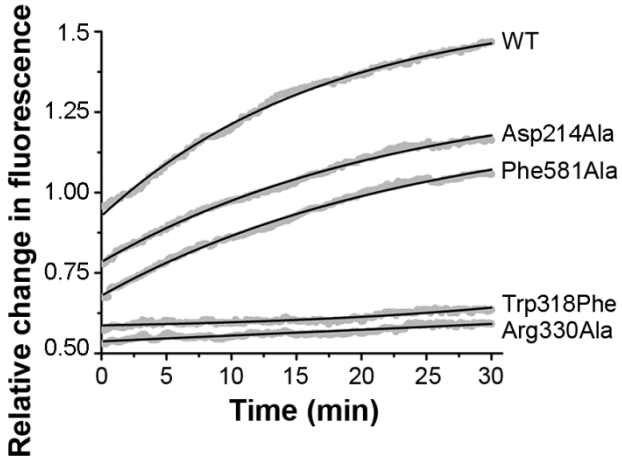


**Figure 4.15: DPH FRET based assay to monitor membrane insertion of the pore-forming loop of the VCC.**

Consistent with this notion, D214A-VCC and F581A-VCC displayed a considerably decreased tryptophan-to-DPH FRET signal compared with that of wild-type VCC, indicating that the alterations of D214A and F581A not only decreased the efficacy of the membrane oligomerization but also affected the membrane insertion step of the toxin to a marginal extent.

Interestingly, no prominent time-dependent increase in the tryptophan-to-DPH FRET was observed for the R330A-VCC variant.

These data, therefore, suggest that the R330A mutation could not only abrogate membrane oligomerization of VCC but also arrest the membrane insertion of the pore-forming stem region of the toxin from the membrane-associated monomeric protein molecules.

**4.5 Conclusion**

The generalized mechanism of membrane pore-formation by β-PFTs involves three different steps: membrane interaction, oligomerization, and membrane insertion of the pore-forming stem loop to generate the transmembrane β-barrel pore. However, the crucial associations that regulate the formation of the oligomeric assembly on the membrane surface have not been explored previously in mechanistic detail. Also, it has not been confirmed before whether the membrane insertion event of VCC precedes pre-pore generation or whether it occurs only upon generation of the pre-pore intermediate. It has also not been examined before, for VCC, whether the membrane interaction, oligomerization, and membrane insertion events are discrete events or whether they proceed altogether in a concerted manner.

In this study, we examined the role of the conserved Asp-214, Arg-330, and Phe-581 residue in regulating the membrane oligomerization mechanism of VCC. Our study demonstrated that the single point mutation of D214A, R330A, and F581A abrogated the membrane oligomerization ability of VCC without affecting the membrane interacting property of the toxin. Although the mutations of D214A and F581A appeared to have marginal affects, the R330A mutation exerted a severe block on the process. Our experimental data suggested that the alteration of R330A in VCC not only abrogated oligomerization of the membrane-associated toxins, but it also arrested the membrane insertion of the pore-forming stem-loop from the membrane-bound toxin monomers. Our study for the first time highlights the key residue(s) in VCC, the mutation of which abrogates oligomerization of the membrane-associated protein monomers without even allowing the generation of the pre-pore oligomeric assembly. This study also enriches our knowledge regarding the membrane oligomerization of the β-PFT family members in general. In summary, this study explored the important interactions and some critical key residues implicated in the oligomerization process of VCC. Blockade of these interactions traps the toxin in its membrane-associated monomeric form and blocks the membrane insertion event towards the formation of the functional transmembrane oligomeric β-barrel pore assembly by the toxin.

# Chapter 5

## Physicochemical constraints of elevated pH abrogate efficient membrane interaction and trap an abortive membrane-bound oligomeric intermediate of VCC

### 5.1 Abstract

The membrane pore-formation mechanism by VCC follows the overall scheme of the archetypical β-barrel pore-forming toxins, in which the water-soluble monomeric form first interacts with the target cell membranes, then assembles into the transient pre-pore oligomeric intermediate, and finally converts into the transmembrane β-barrel pore. The membrane pore-formation process of the toxin is regulated by multiple complex mechanisms that are only partly understood. In this study, we have explored the role(s) of the physicochemical constraints, specifically imposed by the elevated pH conditions, on the pore-formation mechanism of VCC. Elevated pH compromises efficient interaction of VCC with the target membranes, and blocks its pore-formation activity. Under the elevated pH conditions, membrane-associated toxin is trapped in the form of non-functional oligomeric species that fail to generate the functional heptameric pores. Such a non-functional oligomeric species appears to represent a distinct, more advanced intermediate state than the pre-pore state. This study provides the novel insights regarding the implication of the physicochemical constraints for regulating the membrane interaction and the functional pore-formation by VCC.

### 5.2 Introduction

Interaction of the toxin to its target cell membranes represents one of the most critical steps towards the membrane pore-formation mechanism. It has been suggested that the global amphipathicity of the protein may act as the possible driving force towards triggering the initial binding of VCC with the membrane lipid bilayer (218). However, more specific interactions of VCC with the membrane-associated receptor (s) or receptor-like molecule(s) have already been reported in previous studies (180,218). For example, VCC harbors a specific carbohydrate-binding site within its structure that could be implicated for its interaction with the cell-surface glycan receptors (222,228). The association of the toxin with the membrane, followed by the membrane pore-formation processes of the toxin can be mimicked in the membrane lipid bilayer of the liposomes that contain cholesterol (205,212). It, therefore, appears that the membrane binding and pore-formation mechanism of VCC do not strictly require any non-lipid

component(s) present in the membranes. However, multiple aspects of the membrane binding of VCC still remain unknown. For example, the physicochemical constraint(s) that regulate the efficacy of VCC-membrane binding and subsequent membrane pore-formation events have been elucidated only to a limited extent.

Here, we have studied the effect of the physicochemical constraint(s), imposed by the elevated pH conditions (in the range of pH 7 to pH 10), on the membrane interaction and pore-formation process of VCC. When examined at elevated pH conditions, which did not significantly affect the structural integrity of the toxin, VCC displayed drastically compromised membrane pore-forming ability. Elevated pH conditions also affected the efficient membrane binding of VCC towards target cell membranes. Nevertheless, elevated pH conditions did not affect global amphipathicity of VCC, and it allowed detectable extent of membrane association and oligomerization of the toxin. However, under such elevated pH conditions, a membrane-associated oligomeric fraction of the toxin remained trapped in the form of non-functional oligomeric state that failed to execute efficient membrane insertion and functional pore-formation. Such oligomeric state of VCC represented an intermediate assembly that appeared to be more advanced than the pre-pore intermediate state of the toxin.

## 5.3 Materials and methods

### 5.3.1 Purification of the recombinant VCC

The water-soluble monomeric form of the mature toxin was produced as described previously in Chapter 2. Briefly, the inactive precursor form of the toxin (Pro-VCC) with an N-terminal hexahistidine-tag was over-expressed in *Escherichia coli* Origami B cells (Novagen), and was purified from cell lysates of bacteria by employing Ni-affinity chromatography followed by anion-exchange chromatography. The functional form of the toxin was generated by limited proteolysis by using trypsin, subsequently with a second round of anion-exchange chromatography. Homogeneity of the protein was examined by SDS-PAGE and Coomassie staining (Figure 5.1).

### 5.3.2 Intrinsic tryptophan fluorescence and far-UV circular dichroism (CD)

Intrinsic tryptophan fluorescence spectra of VCC (400 nM) were recorded by using Fluromax-4 (Horiba Scientific, Edison, NJ) spectrofluorimeter, upon excitation at 290, with the slit widths of 2.5 and 5 nm for excitation and emission, respectively.

Far-UV CD spectra of VCC (400 nM) were recorded by using a Chirascan spectropolarimeter (Applied Photophysics, Leatherhead, Surrey, UK) with 5 mm path length quartz cuvette.

### 5.3.3 Analytical ultracentrifugation

Beckman Coulter ProteomeLab XL-I analytical ultracentrifuge equipped with an An-50 Ti 8-hole rotor was used to perform sedimentation velocity analytical ultracentrifugation experiments. 380 µl sample of VCC (absorbance at 280 nm = ~0.6 corresponding to 5.76 µM VCC) in 10 mM Tris-HCl buffer, containing 150 mM NaCl, adjusted to the specific pH, and 400 µl reference buffer were taken in the channels of two-channel centerpiece (Epon charcoal-filled) with 12 mm path length, and were spun at 20 $^{o}$C at 42,000 rpm. Absorbance scans (300 scans for each sample) were collected using the continuous scan mode without any time delay between the scans. The Sedfit program was used for the data analysis in the continuous c(S) distribution model. The sednterp server available online (http://sednterp.unh.edu/) was used for the calculation of the partial specific volume (0.724868 ml/gm), buffer density (1.0047 gm/ml), and viscosity (0.01018 P) values.

### 5.3.4 Hemolytic activity assay of VCC against human erythrocytes

Hemolytic activity of VCC was examined against the human erythrocytes as described earlier in Chapter 2. Briefly, lysis of human erythrocytes was monitored by measuring the decrease in the turbidity (OD at 650 nm) of the human erythrocytes suspension (in 10 mM Tris-HCl buffer containing 150 mM NaCl, regulate with specific pH in the range of 7-10).

### 5.3.5 Calcien release assay

The membrane permeabilization efficacy of VCC in the lipid bilayer of the Asolectin-cholesterol liposomes was monitored by release of the entrapped calcein dye from within the liposome vesicles as described in Chapter 2. The fluorescence of calcein dye was recorded at 520 nm on a Perkin-Elmer LS 55 spectrofluorimeter at 25$^{o}$C, upon the excitation at 488 nm by using excitation and emission slit widths of 2.5 and 5 nm, respectively.

### 5.3.6 Flow cytometry

Interaction of the toxin towards the human erythrocytes was examined by employing a flow cytometry-based experiment, following the methods as described previously. Briefly, the human erythrocytes (with cells number $10^{6}$) were treated with VCC toxin (75 nM) at 4 $^{o}$C for 30 minute in a reaction volume of 100 µl in 10 mM Tris-HCl buffer in the presence of 150 mM NaCl, adjusted with a specific pH range of 7-10. Following the protein incubation, the human

erythrocytes cells were treated with rabbit anti-VCC antiserum, followed by treatment with FITC-conjugated goat anti-rabbit antibody. The FITC fluorescence of human erythrocytes cells was recorded on an FACSCalibur (BD Biosciences) flow cytometry.

### 5.3.7 Surface plasmon resonance

The interaction of VCC with the lipid bilayer of the Asolectin-cholesterol liposomes was examined by using the SPR-based experiment on a Biacore 3000 instrument (GE Healthcare Life Sciences), as described earlier in Chapter 2. Briefly, the L1 sensor chip was prepared with the buffer with the specific pH in the range of 7-10. The L-1 sensor chip was coated by injecting the Asolectin-cholesterol liposomes suspension for a 10 min with a flow rate of 1μl/min, washed with one injection of 20 mM NaOH with a flow rate of 100 μl/min for 12 seconds. Liposome-binding efficacy of the L-1 chip was similar for all the pH conditioned examined. To block the non-specific interaction, one injection of 0.1 mg/ml BSA was used at a flow rate of 10 μl/min for 5 minutes. For the association of VCC with the lipid bilayer of the Asolectin-cholesterol liposomes in different pH conditions, proteins was injected for 600 seconds with the flow rate of 5 μl/min (to get a complete binding sensogram), followed by injecting the corresponding buffer for additional 42 seconds, to achieve the endpoint binding data. Ten different concentrations (100-1000 μM) of VCC toxin were used.

### 5.3.8 Protein amphipathicity determination by Triton X-114 partitioning

The amphipathicity of VCC was estimated by monitoring its partitioning into the detergent-rich phase of Triton X-114 as described in chapter 2. TritonX-114 is a non-ionic detergent that generates a single phase with water-based buffer at a low temperature of 4 $^{o}$C, and separates into water-rich phase and detergent-rich phase at or above the 22 $^{o}$C. VCC proteins (100 μg/ml) were mixed with 2% (volume/volume) Triton X-114 in 10 mM Tris-HCl buffer containing 150 mM NaCl, adjusted with the specific pH in the range of 7-10, in a reaction volume of 500 μl at 4 $^{o}$C. When temperature of the reaction mixture increased to 25 $^{o}$C, the two different phase of the reaction mixture separated into each other, aliquots of 100 μl were collected from each phases, proteins were precipitated by using the 9-volume ice-cold acetone. The acetone precipitated samples obtained from the reaction setup were analyzed by SDS-PAGE and Coomassie staining.

### 5.3.9 Pull-down assay

The binding of the toxin with the lipid bilayer of the Asolectin-cholesterol liposomes was monitored by employing the pull-down based experiment. Briefly, protein (1 μM) was treated

with 6.5 μg of Asolectin-cholesterol liposomes suspension in a 100 μl reaction volume at 25 $^{o}$C for 30 min, after completion of the incubation, reaction mixture was subjected to ultracentrifugation at 105,000 × g for 30 min at 4 $^{o}$C, pellet fraction was washed with the respective buffer, mix with 50 μl SDS-PAGE sample buffer. The pellet fractions were divided into two equal parts. One part was incubated at room temperature, whereas the other half was boiled for 10 minutes and was analyzed by SDS-PAGE/Coomassie staining.

For probing the interaction of VCC with the membrane of the human erythrocytes, VCC protein (100 nM) was treated with human erythrocytes ($OD_{650}$ of ~0.9) in a reaction volume of 100 μl (with 10 mM Tris-HCl buffer containing 150 mM NaCl, adjusted to specific pH) for 1 hour at 25 $^{o}$C. After the incubation, the reaction mixture was subjected to ultracentrifugation at 105,000 × g for 30 min at 4 $^{o}$C. The pellet fraction was washed with the respective buffer, and mixed with 50 μl SDS-PAGE loading dye and divided into two equal aliquots. One-half was incubated at room temperature while the other half was boiled for 10 minutes. The samples were analyzed by SDS-PAGE followed by immunoblotting.

### 5.3.10 FRET assay

Fluorescence resonance energy transfer (FRET) from the tryptophan residue (Trp318) located in the stem region of the toxin to DPH (Diphenylhexatriene) embedded in the Asolectin-cholesterol liposomes was monitored to detect the membrane insertion step of VCC. The DPH embedded Asolectin-cholesterol liposomes were prepared as described previously in chapter 2. The tryptophan-to-DPH FRET signal was probed on a Perkin-Elmer LS 55 spectrofluorimeter by recording the intensity of fluorescence at 470 nm upon excitation at 290 nm, with excitation and emission slit widths of 2.5 nm and 5 nm, respectively.

### 5.3.11 Analysis of the structure models

The structural coordinate of VCC toxin was prepared in PDBSET within the CCP4 suite by using the Protein Data Bank (PDB) ID 1XEZ (241). For visualizing the surface electrostatics on protein at a particular pH state, corresponding PQR files were generated from the PDB file using the PDB2PQR server available online (http://nbcr-222.ucsd.edu/pdb2pqr_1.8/), and further processed by employing the APBS plugin within PyMOL [DeLano, W. L. (2002) The PyMOL Molecular Graphics System, found online (http://www.pymol.org)].

## 5.4 Results and discussion

### 5.4.1 Structural integrity of VCC at elevated pH conditions

Analysis of the VCC structural model suggested that the protein molecular surface appeared to become more populated with negative electrostatics with the increase in pH from 7 to 10 (Figure 5.1). Such observation was consistent with the de-protonation of the protein surface moieties under the high pH conditions. Next, we wanted to explore the possibility whether the high pH conditions abrogated the pore-forming activity of VCC by compromising the structural integrity of the toxin, through alterations of the change distribution on the protein surface.

Towards elucidating the effect of elevated pH on the structure-functional mechanism of VCC, we examined the structural integrity of the toxin at different high pH conditions in the range of 7-10. We first probed any alteration in the secondary structural rearrangements of the toxin under such pH conditions by using far-UV CD spectroscopy. Protein in the pH range of 7-10 showed similar far-UV CD spectra profile, indicating that the exposure to elevated pH up to 10 did not trigger any change in the secondary structural organization of the protein (Figure 5.2 A).

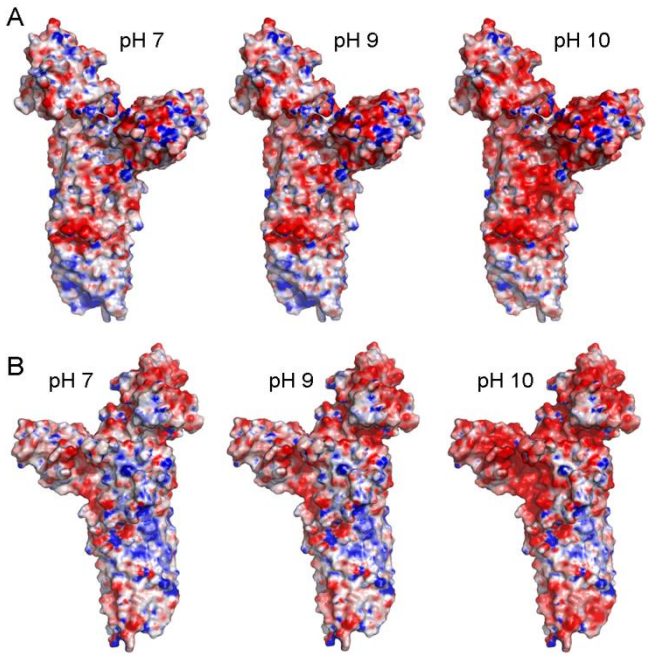


**Figure 5.1: Distribution of surface electrostatics on VCC at specific pH conditions of 7, 9, 10, as calculated from the analysis of the protein structural model.**

Similarly, overlapping intrinsic tryptophan fluorescence emission spectra profile of VCC was observed at different pH conditions in the range of 7-10, indicating that the exposure to an

elevated pH up to 10 did not affect the overall tertiary structural organization of the protein (Figure 5.2 B).

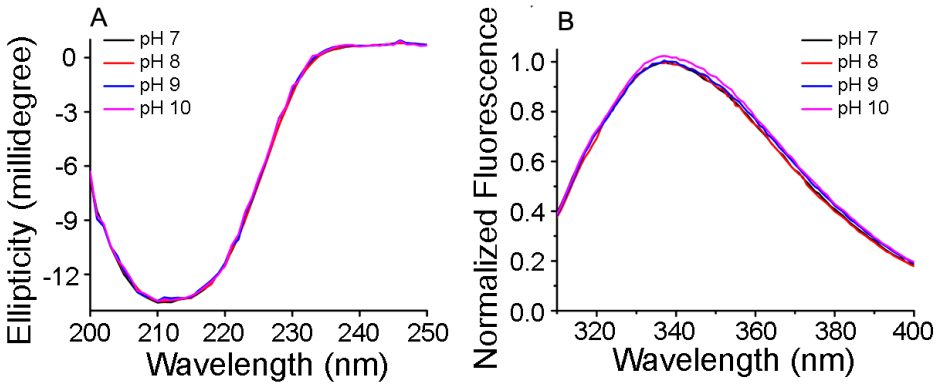


**Figure 5.2: (A) Far-UV CD spectra of VCC at the pH conditions of 7, 8, 9, and 10. (B) Intrinsic tryptophan fluorescence emission spectra of VCC at the pH conditions of 7, 8, 9, and 10.**

We also monitored any alteration in the solution assembly state of the VCC at different elevated pH condition by using sedimentation velocity analytical ultracentrifugation (AUC)-based study. Analysis of the data obtained from the sedimentation velocity AUC of VCC at pH 7 and pH 10 displayed overlapping distribution of sedimentation coefficients, with the peaks at around 4.17 Svedberg units that corresponded to the water-soluble monomeric state of the VCC (Figure 5.3).

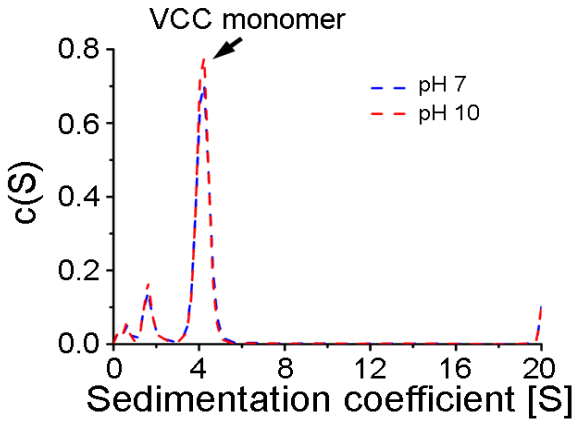


**Figure 5.3: Sedimentation velocity analytical ultracentrifugation profile of VCC at the pH conditions of 7 and 10.** A plot of sedimentation coefficient distribution, c(S), against the sedimentation coefficient, [S], in Svedberg unit.

This result, therefore, indicated that even at the elevated pH conditions of 10, VCC remained in its monomeric form in solution, thus eliminating the possibility of any premature oligomerization or aggregation of the toxin in solution. Overall, these data suggested that under the high pH

conditions examined in our study, VCC lost the membrane-damaging pore-forming activity, without affecting its overall structural organization.

### 5.4.2 Membrane pore-forming activity of VCC is abrogated at elevated pH conditions

We examined the membrane permeabilization efficacy of the toxin under the elevated pH conditions in the range of pH 7 to pH 10 to explore the implication of physicochemical constraint(s) regulating the pore-forming activity of the toxin.

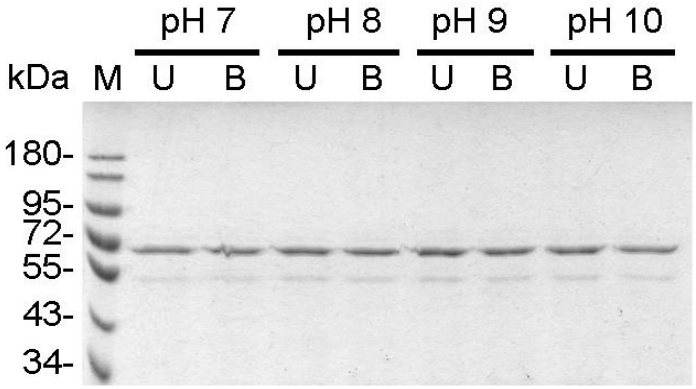


**Figure 5.4: SDS-PAGE and Coomassie staining profile of VCC at different pH conditions.** Samples were treated with the SDS-PAGE loading buffer with (lanes marked as B) or without boiling (lanes marked as U).

We first examined the membrane pore-forming activity of the toxin against the human erythrocytes. As shown in Figure 5.5 (A) with increase in the pH condition of the experiment, pore-forming activity of VCC against the human erythrocytes decreased progressively. At pH 8, with a protein concentration of 100 nM, VCC toxin displayed almost 80% hemolytic activity, whereas only ~20% of lytic activity was observed in case of pH 9, when examined over a period of 1 hour of incubation. No detectable pore-forming activity was observed at pH 10, under the same condition. When examined over an extended period up to 4 hours, VCC toxin at pH 8 showed ~100% hemolytic activity while at pH 9 obtained almost 90% of the lytic activity. More importantly, under the condition of pH 10, VCC did not display any significant membrane pore-forming activity against the human erythrocytes (Figure 5.5 B).

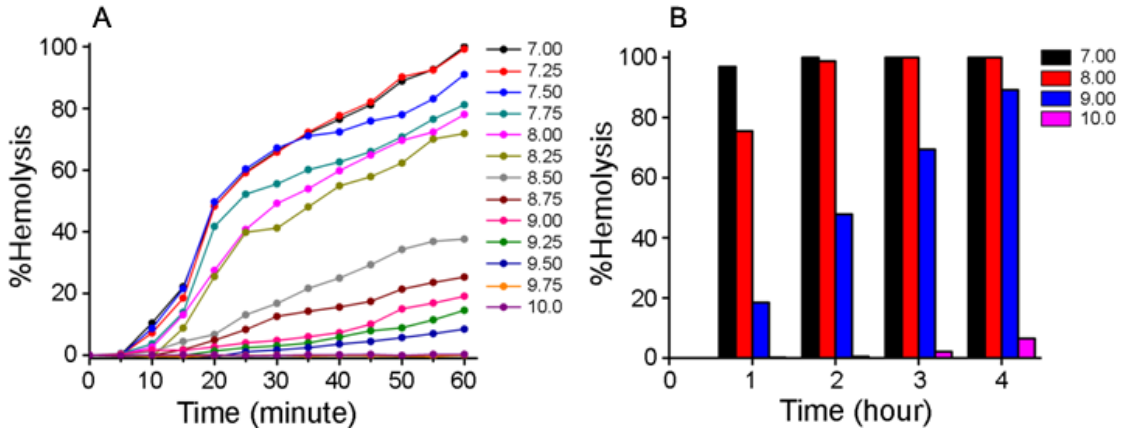


**Figure 5.5: (A) Hemolytic activity of VCC against human erythrocytes (B) Pore-forming hemolytic activity of VCC against human erythrocytes over an extended incubation period.**

Similar results were obtained, when membrane permeabilization activity of the toxin was probed against the synthetic membrane lipid bilayer of the Asolectin-cholesterol liposomes by using the calcein-release assay. When examined over 30 minutes of incubation period, VCC (1 μM) at pH 7 displayed ~85% of the calcein release, whereas at pH 8 it displayed ~75% calcein release. At pH 9, VCC induced less than 25% of calcein release from the Asolectin-cholesterol liposomes. Drastically reduced calcein release (~15%) was observed under the pH 10 (Figure 5.6). These results, therefore, suggested that at an elevated pH condition of 10, membrane pore-forming activity was drastically abrogated.

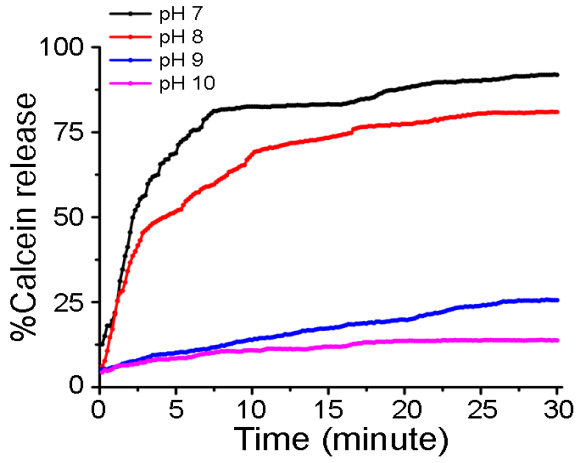


**Figure 5.6: Membrane permeabilization ability of VCC in the Asolectin-cholesterol liposome membranes as examined by the calcein release assay, under specific pH conditions.**

### 5.4.3 Elevated pH conditions abrogate the membrane interaction of VCC with the target cell membranes

We probed the membrane interaction of the toxin (100 nM) to human erythrocytes at pH conditions in the range of 7 to 10 by using the flow cytometry-based experiment. In this experiment, interactions of VCC to erythrocytes were examined at a lower temperature of 4 $^{o}$C that abrogated the functional oligomeric pore-formation of the protein, and subsequent lysis of the target cells. Also, the hydrophobicity-driven non-specific interaction of the toxin believed to be marginal under the low temperature. Thus, in this experimental condition, any association of the toxin would reflect specific binding of the toxin with the human erythrocytes membrane components. The results obtained from this experiment suggest that the interaction of VCC towards the human erythrocytes decreased with increase in pH, above the physiological condition of pH 7. Notably, the interaction of VCC toxin was found to be significantly affected at pH 9, whereas at pH 10 the effect was found to be more severe (Figure 5.7).

We also probed the association of VCC towards the membrane lipid bilayer of the Asolectin-cholesterol liposomes by using the SPR-based experiment under the different pH conditions in the range of 7-10. In this experiment, VCC (in the concentration range of 100-1000 nM) in solution was allowed to flow over the membrane lipid bilayer of the Asolectin-cholesterol liposomes, coated onto a SPR sensor-chip (Figure 5.8).

Interaction of VCC to the lipid bilayer was examined in real time by recording the changes in the sensogram response unit up to 600 seconds, while the protein solution was being injected. The endpoint sensogram response unit was recorded to measure the extent of irreversibly-associated protein on the liposome membrane at the end of protein injection by washing with the respective buffer with additional 42 seconds.

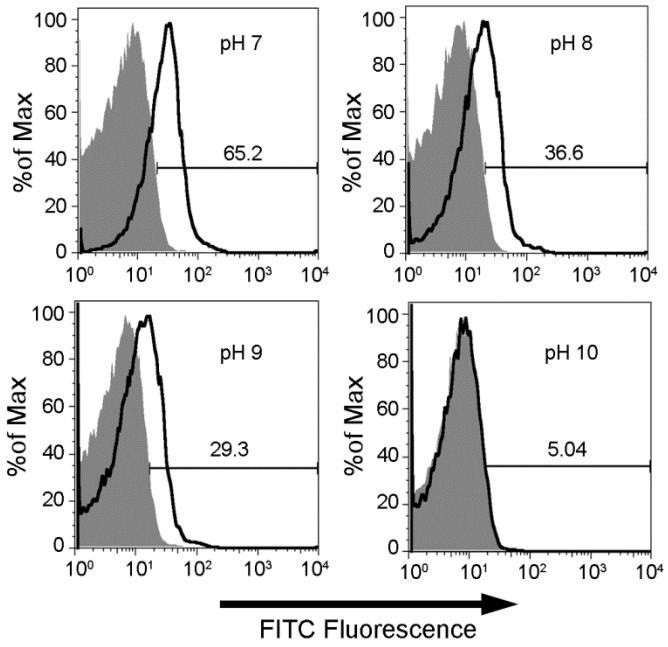


**Figure 5.7: Interaction of VCC with human erythrocytes as determined by the flow cytometry-based assay.** Shaded curves, control at the corresponding elevated pH condition; solid lines, binding of VCC at the corresponding elevated pH condition.

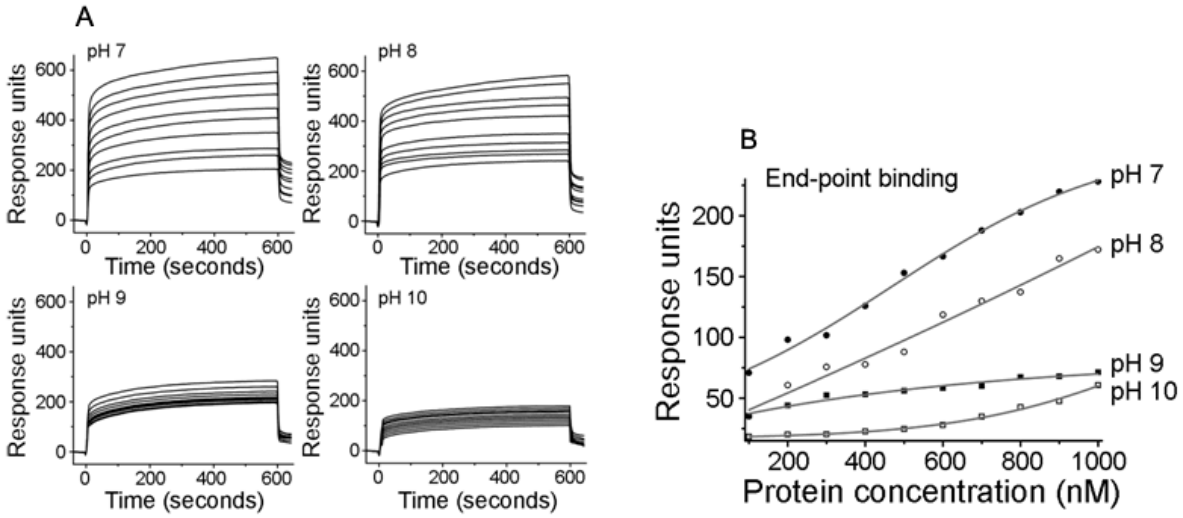


**Figure 5.8: Association of VCC with the membrane lipid bilayer of Asolectin-cholesterol liposomes determined by the SPR-based assay. (A)** Real-time binding sensogram plots at the pH conditions of 7, 8, 9, and 10 are shown. **(B)** Plot of end-point response units against the protein concentration is shown to reflect the extent of VCC binding to the liposome membranes at the respective pH conditions.

The results obtained from this experiment suggested that with an increase in pH from 7 to 10, interaction of VCC to the liposomes membrane decreased severely, both in term of the real time binding and irreversible binding with the membrane lipid bilayer. At pH 8, the association was affected moderately while at pH 9 and pH 10 interaction efficacies were abrogated to a severe extent.

Overall, these data indicated that the elevated pH above the physiological condition of pH critically abrogated the association of VCC with the erythrocytes and the membrane lipid bilayer of the Asolectin-cholesterol liposomes.

### 5.4.4 Membrane-bound fraction of toxin remains trapped in the state of an abortive oligomeric assembly

Previous studies suggested that the water-soluble monomeric form of VCC exhibits an atypical propensity to associate with the detergent-rich phase of Triton X-114. Such property is commonly associated to the high level of global amphipathicity of a protein molecule in aqueous solution and is it generally observed with the integral membrane proteins (218). Based on such observation it has been suggested that VCC could spontaneously associate with the membrane lipid bilayer of the target membrane.

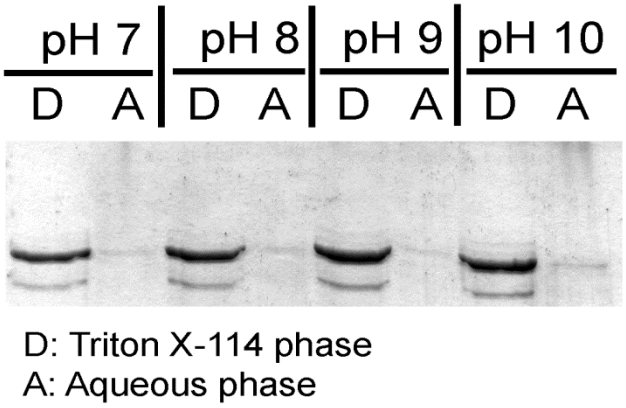


**Figure 5.9: Partitioning of VCC in the detergent-rich phase of Triton X-114 under different pH conditions, as analyzed by SDS-PAGE/Coomassie staining.**

In this study, we observed that the partitioning of VCC to the detergent-rich phase of Triton X-114 was not significantly affected at different elevated pH conditions, when examined in the pH range of 7 to 10 (Figure 5.9). Hence, we probed whether at elevated pH conditions VCC could show any basal-level association with the membranes of the human erythrocytes and liposome vesicles. Indeed, a pull-down-based experiment suggested that VCC, even at pH 9 and pH 10,

could display significant extent of association with the membrane fractions of the human erythrocytes and Asolectin-cholesterol liposomes. This experimental data was in significant contrast to the data we obtained from our flow-cytometry and SPR based experiment, where a critical abrogation in membrane interaction was observed at the high pH conditions of pH 9 and pH 10. Notably, in the flow cytometry-based assay hydrophobicity-driven association was marginal, as the experiment was done at the low temperature. SPR-based experiment also appeared to reflect that specific mode of the membrane interaction of VCC towards the liposome membranes, as the protein molecules were in constant flow during its association with the target membranes over a short duration of 600 seconds only, thus reducing its non-specific association towards lipid bilayer. In contrast, during the pull-down based experiment protein was allowed to co-sediment with the target membrane system of liposomes and human erythrocytes, where non-specific factors regulating the membrane interaction of the toxin were not removed. Hence, it could be suggested that the elevated pH conditions of pH 9 and pH 10, VCC toxin could interact with the target membranes through the non-specific amphipathicity-driven partitioning to the membrane lipid bilayer.

Notably, pull-down-based experiment suggested that the membrane-bound fraction of VCC, even in pH 9 and pH 10, could generate SDS-stable oligomeric species; oligomerization efficacy at pH 9 was found to be marginally reduced, while the extent of the oligomerization appeared to be less at pH 10 as compared to that at pH 7. Quantitative analysis of the pull-down data suggested that the extent of oligomerization at pH 9 varied from ~65% (in human erythrocytes), to ~90% (in the Asolectin-cholesterol liposomes), as compared to those at pH 7. Oligomerization efficacies at pH 10 were observed in the range of ~40-50% (in erythrocytes and liposomes) to those observed at pH 7. However, the membrane-permeabilization data showed that VCC could display less than ~25% pore-forming activity at pH 9 and nearly 10% of the membrane pore-forming activity at pH 10, in comparison to that at pH 7 (Figure 5.10).

This observation suggested that at elevated pH conditions of 9 and 10 membrane-associated fraction of toxin could form SDS-stable oligomers, which were probably abortive, and represented inactive oligomeric species of the toxin.

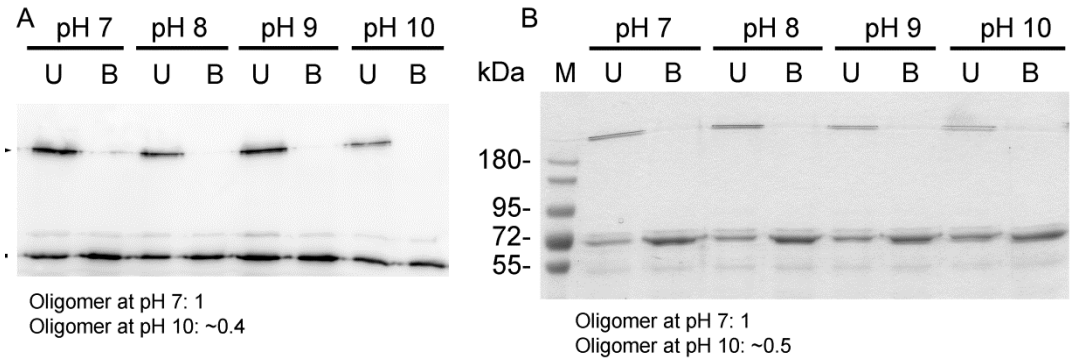


**Figure 5.10: Membrane-oligomerization of the membrane-bound fraction of VCC in the human erythrocyte and the Asolectin-cholesterol liposome membranes under different pH conditions. (A)** Oligomerization of the VCC in the human erythrocyte membranes under different pH conditions, as monitored by the pull-down-based assay, coupled with immunoblotting. Normalized oligomer band intensities are indicated. **(B)** Oligomerization of the membrane-bound fraction of VCC in the Asolectin-cholesterol liposome membranes under different pH conditions, as monitored by the pull-down-based assay, coupled with SDS-PAGE/Coomassie staining.

Such non-functional oligomers were SDS-stable, and therefore did not represent the pre-pore oligomeric intermediates (as reported in the process of pore-formation of archetypical β-PFTs), as the pre-pore oligomers are typically reported as the SDS-labile assembly (212). It, therefore, appeared from our experimental results that the physicochemical constraints(s) of high pH condition (pH 9 and pH 10) trapped toxin in the state of an abortive oligomeric intermediate, which probably represented a distinct and more advanced oligomeric assembly than the pre-pore assembly in the process of the functional membrane pore-formation.

### 5.4.5 Membrane insertion of the stem-loop of VCC critically compromises at elevated pH conditions

Membrane pore-formation process of VCC involves the insertion of its pore-forming 'stem-loop' into the membrane to generate the transmembrane β-barrel structure. Under high pH conditions above the pH 7, VCC showed abrogated membrane interaction. In these conditions, toxin could bind with the lipid bilayer of the membranes, and could generate an oligomeric assembly that appeared to be inactive. We, therefore, monitored whether the membrane-associated fraction of VCC at high pH conditions could insert its pore-forming stem-loop into the membrane towards the functional membrane pore-formation (Figure 5.11). We recorded the FRET from the tryptophan residue (Trp318) positioned within the stem region to the hydrophobic fluorophore DPH embedded in the membrane lipid bilayer of the Asolectin-cholesterol liposomes. A

significant time-dependent increase in tryptophan-to-DPH FRET signal during the VCC-liposomes interaction would indicate the membrane insertion of the stem-loop.

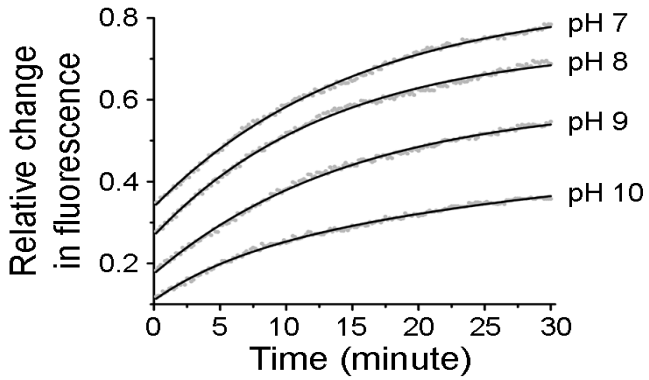


**Figure 5.11: Membrane insertion efficacies of the pore-forming stem region of VCC at different pH conditions were determined by monitoring the time-dependent relative change in the tryptophan-to-DPH FRET signal.**

In this study, we observed that with the elevated pH condition of the assay, time-dependent increase of the tryptophan-to-DPH FRET was severely affected. The data thus indicated critically compromised membrane insertion event of the membrane-associated VCC fractions under the elevated pH conditions, particularly at pH 9 and pH 10.

### 5.4.6 Membrane-associated abortive state of VCC trapped at elevated pH condition regain activity upon reversal to the physiological pH

The abortive oligomeric assembly of the membrane-associated VCC molecule trapped at the high pH (pH 10) was found to regain their membrane pore-forming ability when brought back to the physiological pH 7. When human erythrocyte, incubated with toxin at pH 10 for a period of 1 hour, were washed and re-suspended in buffer of pH 7, membrane-associated fraction of the toxin could trigger noticeable extent of the lysis of the human erythrocytes (Figure 5.12).

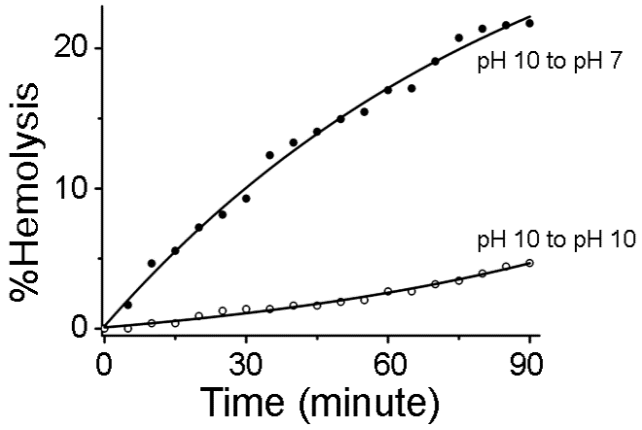


**Figure 5.12: Non-functional oligomeric form of VCC trapped on the human erythrocytes membrane at elevated pH condition (pH 10) regains its activity upon reversal to the physiological condition of pH 7.** The abortive oligomeric form of VCC trapped on the human erythrocytes at elevated pH condition (pH 10) regains its activity upon reversal to the physiological condition of pH 7.

This result suggested that the high pH condition abrogated the interaction of VCC with the target cell membranes, and trapped VCC in the state of abortive oligomeric assembly, and, such trapping could be partly released upon removal of the physicochemical constraint(s) imposed by the elevated pH condition.

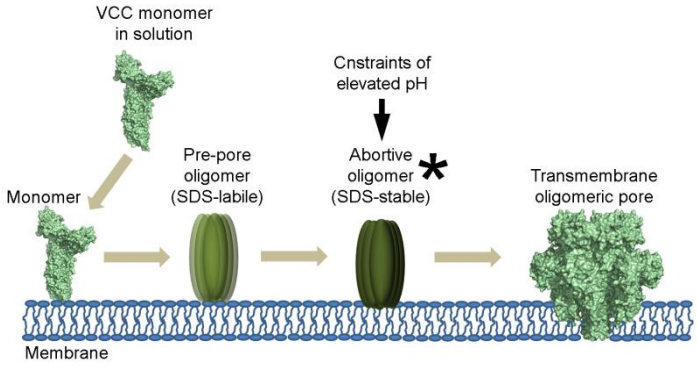


**Figure 5.13: Schematic presentation of the proposed modified model of membrane pore formation by VCC.** Proposed modified scheme of membrane pore formation by VCC. The water-soluble monomeric form of VCC binds to the target membranes and forms the pre-pore oligomeric assembly. Conversion of the pre-pore into the functional transmembrane pore presumably proceeds through an abortive oligomeric intermediate (*), that can be artificially trapped by imposing the physicochemical constraint of the elevated pH condition. Structural models of monomeric and oligomeric forms of VCC were generated using the PDB entries 1XEZ and 3O44, respectively.

## 5.5 Conclusion

This study elucidates the implications of the physicochemical constraint(s) imposed under elevated pH conditions, for regulating the functional membrane pore-formation mechanism by the toxin. At high pH conditions up to pH 10, VCC toxin remained stable in terms of its structural integrity in solution. However, under such conditions, In particular at pH 9 and pH 10, the functional membrane pore-forming ability of the toxin was found to be completely abolished. When examined for its membrane interaction efficacy, VCC showed severely inhibited membrane binding ability. Interestingly, however, even at pH 9 and pH 10, VCC toxin displayed a significant association with the target membranes, presumably through the non-specific amphipathicity-driven partitioning of the protein with the membranes. At the elevated pH conditions examined in our study, membrane-bound fractions of VCC were found to generate the typical SDS-stable oligomeric species to a noticeable extent, albeit significantly less compared to that generated at the physiological pH 7. The membrane-associated oligomers generated at the high pH conditions represent an abortive inactive assembly of the protein (probably, a distinct and more advanced intermediate assembly than the pre-pore assembly) and were found to be inefficient in terms of the membrane insertion of the pore-forming 'stem-loop' of the toxin. On the basis of our results, we propose that the physicochemical constraints of the high pH conditions affect an efficient binding of the protein with the target membrane components. Elevated pH would affect the overall surface charge distribution on protein, as well as those of the membrane components. Such modified charge distribution could be the reason of resulted abortive membrane interaction and abrogated pore-formation mechanism of the toxin under high pH conditions. Presumably, the more complicated mechanism involves the regulation of pore-formation under the elevated pH conditions. It is clear from our experimental data that the pore-forming mechanism of VCC is compromised under high pH condition through the abrogation of the membrane interaction step of the toxin that subsequently inhibited the functional membrane oligomerization and membrane insertion of the toxin. In this study, a compromised membrane-assocoation process at the elevated pH condition enabled us to trap an abortive oligomeric intermediate of the membrane-bound VCC. This inactive SDS-stable oligomeric species represented neither the pre-pore (SDS-labile) nor the functional oligomeric pore structure. Such oligomeric assembly could be considered as an advanced intermediate, formed at a following step after the SDS-labile pre-pore generation. The results obtained from our study indicated that

this oligomeric species could be released from its trapped abortive configuration upon elimination of the constraints of the elevated pH condition. Overall results obtained from our study allow us to propose modified scheme for the functional pore-formation employed by VCC on the lipid bilayer of the target cell membranes (Figure 5.13): (i) association of VCC to the target membranes, (ii) generation of the pre-pore oligomeric assembly, (iii) generation of an advanced and structurally more robust oligomeric intermediate, and finally (iv) formation of the functional heptameric pore structure. Overall, this study provides a novel insights towards the role of the physicochemical constraints governing the functionality of the membrane pore-formation mechanism of VCC.

# Summary

Pore-forming toxins (PFTs) represent a unique class of membrane-damaging proteins that act by killing their target host cells by generating pores in the cell membranes (233,242). PFTs are produced by many organisms such as bacteria, fungi, primitive metazoans, plants, and humans. The toxins are mostly produced as water-soluble molecules destined to generate pores in the membrane lipid bilayer of the target host cells (129,243). In the mode of action of the PFTs, the proteins first associate with the membrane lipid bilayer of the target cells, subsequently they undergo structural reorganization and self-assembly, and finally make pores in the membranes (95,128). This pore formation allows free diffusion of the solutes across the membranes and trigger osmotic imbalance, which further leads to cell swelling and lysis of the cells. Depending on the particular members of the PFTs, the membrane-inserted pore diameters can vary from less than 1 nm up to 50 nm (244).

PFTs follow common mechanism of pore-formation, which involves four distinct steps: (i) secretion of the toxin from the bacterial pathogen, (ii) interaction of the toxin with target cell membrane, (iii) self-assembly of the toxin on the membrane surface and (iv) membrane insertion of the toxin to generate the transmembrane pore (105,243).

*Vibrio cholerae* cytolysin (VCC) is a pore-forming toxin secreted by many pathogenic strains of the Gram-negative bacteria, *V. cholerae,* the causative pathogen of the diarrheal disease cholera. VCC belongs to the family of β-barrel pore-forming toxins (β-PFTs). VCC displays potent cytotoxic activity against the erythrocytes and the mammalian cells. VCC is secreted as a ~79 kDa inactive precursor (Pro-VCC), which upon proteolytic removal of the ~15 kDa N-terminal Pro-domain, converts into the functionally active form of the toxin with the potential to generate oligomeric pores in the target host cell membranes (181,187). Consistent with the archetypical β-PFT structural models, the central motif of the VCC molecule highlights presence of a core cytolysin domain that harbors ‘pre-stem’ loop (containing two β-strands). In the process of transmembrane oligomeric pore formation, the pre-stem loop from each toxin protomer contributes toward the generation of the transmembrane β-barrel segment. Apart from the cytolysin domain, VCC possesses two additional C-terminal domains showing the structural

features of the lectin-like folds: a β-Trefoil lectin-like domain, followed by a β-Prism lectin-like domain with potential functional implications (187).

The presence of unique structural features in VCC makes it different from other PFTs, and yet at the same time, represents it as a suitable model system for addressing the questions related to molecular mechanism of the toxin-membrane interactions and membrane pore-formation. In this direction, the present study explored the implications of distinct structural domains in VCC mode of action, particularly, in the process of its membrane binding, oligomerization and membrane insertion of the pore-forming stem loop of the toxin. Specifically, the present thesis work investigated the structure-function mechanisms of VCC with particular emphasis on the following four objectives:

A. To investigate the molecular mechanism of membrane interaction and to identify the specific structural motif responsible for binding of the toxin to the membrane lipid bilayer of target host cells.
B. To explore the implications of the β-Prism domain-mediated lectin property of the toxin.
C. To delineate the sequence of events in the pore-formation mechanism of VCC.
D. To elucidate the importance of the physicochemical constraints on the membrane pore-formation mechanism of the toxin.

**Membrane interaction mechanism of *Vibrio cholerae* cytolysin**

Membrane binding of the water-soluble toxin monomers is a crucial step in the membrane pore-formation mechanism of the toxin. VCC has been shown to associate with the target membranes via amphipathicity-driven spontaneous partitioning into the membrane environment (218). However, functional oligomeric pore formation by VCC requires more specific interactions of the toxin molecules with the membrane components (180,228). To explore the specific association events of VCC with the membrane lipid bilayer of the target cells, we have studied the structural basis of the lipid-mediated membrane binding mechanism of VCC.

Analysis of the transmembrane oligomeric pore assembly of VCC identifies two distinct regions that are making intimate interactions with the membrane lipid bilayer: (i) a ‘rim region’ that makes direct contacts to the membrane, and (ii) a ‘stem region’ that inserts through the membrane lipid bilayer. The ‘rim region’ of VCC oligomeric pore is constituted by the three loop sequences $^{236}$TTL$^{238}$, $^{359}$DALW$^{362}$, and $^{420}$YYVVGA$^{425}$. In this study, we have explored the

roles of the three loop sequences present in VCC structure for the membrane binding, and oligomeric pore formation of the toxin.

The three loop sequences, $^{236}$TTL$^{238}$, $^{359}$DALW$^{362}$, and $^{420}$YYVVGA$^{425}$, were replaced, one at a time, with a flexible linker repeat. To further investigate, one or more of the residues from each loop was mutated (T237A, L238A, W362A, W362Y, W362F and Y421A mutants).

We probed the pore-forming activity of the VCC variants, and the results obtained from lysis activity against human erythrocytes and calcein release assay against the liposome vesicles suggested that alterations of the loop sequences severely abrogated the pore-forming activity of the toxin. Also, the point mutations drastically reduced the pore-forming activity; only in case of the mutant T237A, the effect was found to be less severe. VCC variants were examined for their ability to bind to the human erythrocytes. A flow cytometry-based assay was used to monitor the erythrocytes binding of the VCC variants. The results of this assay showed a severely compromised erythrocyte-binding profile for all the VCC variants as compared to the wild-type toxin. The T237A mutant showed ~56% of the wild-type binding, whereas for all the other mutants, binding was in the range of 25% or less to that of the wild-type binding activity. Interestingly, all the VCC variants showed wild-type-like lectin activity.

Further, we tested binding efficacies of the VCC variants to the membrane lipid bilayer using a surface plasmon resonance (SPR)-based assay. It was observed that all the variants showed drastically reduced binding to the liposomes as compared to the wild-type VCC, thus suggesting that the alterations of the loop sequences critically affected binding of the VCC variants to the lipid components of the liposome membranes. All the VCC variants showed wild-type like ability to partition into the detergent-rich phase of Triton X-114, suggesting that the mutations did not affect the global amphipathicity of the toxin molecule. We also employed a pull-down-based assay to monitor whether the VCC variants could associate with the Asolectin-cholesterol liposomes in the absence of the specific interactions with the membrane lipid components. It was observed that all the VCC variants displayed the significant extent of association with the liposome vesicles, presumably facilitated by their high global amphipathic property. We further examined the membrane oligomerization and membrane insertion properties of the VCC variants. It was observed that the VCC variants severely abrogated the oligomerization and membrane insertion steps of the membrane-associated toxin molecules, presumably by blocking the specific intimate mode of interaction of VCC with the membrane lipid components. This is

the first report showing the implications of the membrane-proximal loop sequences in VCC for its functional membrane interaction and pore-formation mechanism.

**Implication of the C-terminal β-Prism lectin domain on the pore-formation mechanism of VCC**

Apart from the central core cytolysin domain, VCC also contains two extra C-terminal domains: namely, a β-Prism lectin-like domain and a β-trefoil lectin-like domain, which are structurally similar to many carbohydrate-binding proteins (174,187). However, the precise role of these lectin-like domains for lectin property of VCC remained unclear. In this part of the study, we have characterized the physiological implication of the β-Prism domain of VCC. For this, we generated the truncated variant of VCC lacking the β-Prism domain (VCC-Δβ-Prism). VCC-Δβ-Prism protein exhibited less than 10% of the hemolytic activity as displayed by the wild-type VCC against human erythrocytes. To examine the potential role of the β-Prism domain in the lectin-like property of VCC, we employed an ELISA-based assay to examine the interaction ability of the VCC-Δβ-Prism variant towards the immobilized β-1-galactosyl-terminated glycoprotein asialofetuin. We found, wild-type VCC displayed prominent interaction with the immobilized asialofetuin with a dissociation constant ($K_d$) of 16 nM. In contrast, VCC-Δβ-Prism showed no noticeable binding with the immobilized asialofetuin. The result, therefore, suggested that the β-Prism domain of VCC acts as a structural scaffold supporting the lectin activity of VCC.

We also examined whether the β-Prism domain in isolation could retain its lectin-like activity. To test this, we generated a histidine-tag containing β-Prism domain VCC variant. It was observed that the β-Prism domain protein displayed significant binding with the immobilized asialofetuin, with a dissociation constant $K_d$ in the range of 2 μM in the ELISA-based assay. This result, therefore, suggested that the β-Prism domain of VCC even in isolation was able to show the lectin-like activity.

Further, we also explored the presence the specific binding sites within the β-Prism domain of VCC. The crystal structure of the monomeric form of VCC displayed that the β-Prism domain of VCC in its solvent-exposed area harbors a potential binding pocket that interacts to the β-octyl glucoside (βOG), a detergent molecule. Interestingly, the similar binding pocket has been

reported in the other member of the β-Prism lectin family, including jacalin and *Maclura pomifera* agglutinin (MPA) (200,201). On the basis of the structural similarity with the carbohydrate-binding site of MPA and jacalin, we explored the possibility whether the presence of the amino acid triad containing Asp-617, Tyr-654 and Tyr-679 in the β-Prism domain would play any critical role in the lectin activity of VCC. For this, we generated three point mutations of Asp-617, Tyr-654 and Tyr-679 within the β-Prism domain of VCC and examined their ability to bind to the immobilized glycans by employing the ELISA-based assay. Notably, alteration of Y654A and Y679A caused almost 30% to 40% inhibition in its binding propensity towards the immobilized glycans, whereas D617A mutation resulted in 100% inhibition of its binding propensity towards the immobilized glycans as compared to the wild-type β-Prism domain protein. We also confirmed the lectin activity of the wild-type β-Prism domain protein and D617A mutant by employing ITC-based experiment. Altogether, the results confirmed the specific site within the β-Prism domain of VCC responsible for the β-1-galactosyl-terminated glycoconjugate-specific lectin activity of VCC. In the flow cytometry-based assay VCC-Δβ-Prism protein displayed significant inhibition of interaction ability toward the human erythrocytes membrane, as compared to the full-length wild-type VCC protein. The result, therefore, confirmed that the removal of the β-Prism domain of VCC critically compromised the binding of VCC towards the human erythrocytes cell membrane. Further, we examined the effects of D617A mutation in the full-length VCC protein. Interestingly, VCC protein harboring the D617A mutation displayed severely compromised pore-forming activity, and critically abrogated lectin activity. We also observed severely compromised binding ability of the D671A mutant towards the human erythrocytes. These data again confirmed the specific role of the β-Prism domain-mediated lectin activity and its role in the functional association with the erythrocytes cell membrane. Interestingly, the D617A mutant protein could not generate SDS-stable oligomeric assembly in the human erythrocytes membrane. From this study, it appears that the D617A mutation affected the interaction of VCC with the cell surface glycan receptor(s) presumably via abrogating its lectin activity. This effect, in turn, blocked the structural rearrangement of the β-Prism domain, thus ultimately abrogating the membrane oligomerization of VCC.

**Trapping of VCC in the membrane-bound monomeric state abrogates oligomerization, membrane insertion and functional pore-formation**

The mechanism of membrane pore formation by VCC is proposed to follow three distinct steps: interaction of the toxin monomers onto the target cell membrane, formation of pre-pore oligomeric intermediates on the membrane, and conversion of the pre-pore oligomers into the transmembrane oligomeric β-barrel pores (245). In this study, we elucidated the molecular mechanism of the oligomeric membrane pore-formation process of VCC. Analysis of the interprotomer interfaces of VCC oligomer shows the presence of an aspartate residue at position 214 (Asp-214), an arginine residue at position 330 (Arg-330), and a phenylalanine residue at position 581 (Phe-581). These residues, Asp-214, Arg-330, and Phe-581, are found to be highly conserved in the related cytolysin proteins of Vibrionaceae bacteria.

To examine the role of these three conserved residues, Asp-214, Arg-330, and Phe-581 in regulating the membrane oligomerization mechanism of VCC, we generated three recombinant variants of the toxin harboring the single point mutation of D214A, R330A and F581A. The pore-forming properties of the VCC variants were examined by assaying their ability to induce cytotoxic activity against human erythrocytes. We observed that, F581A-VCC showed only about 30% of the wild-type lytic activity, D214A-VCC displayed nearly 55% of lytic activity whereas R330A-VCC could not show any noticeable lytic activity. Further, we monitored the interaction of the VCC variants with human erythrocytes by using a flow cytometry-based assay. Our data showed that all three mutants, bound to the human erythrocytes with equal efficiency as compared to the wild-type VCC toxin. Together, these data suggested that the single point mutations of D214A, R330A, and F581A in VCC abrogated the membrane pore formation ability of the toxin without significantly affecting the membrane interaction ability of the protein.

Further, we examined the ability of the membrane-bound VCC variants to generate an SDS-stable oligomeric assembly. VCC variants F581A-VCC and D214A-VCC display a reduced ability to generate SDS-stable oligomers. Notably, R330A-VCC did not form any detectable amount of SDS-stable oligomeric assembly.

We also monitored whether the VCC variants could insert their pore-forming stem region into the membrane lipid bilayer in the absence of efficient membrane oligomerization, For this, we monitored FRET from the tryptophane residue located within the stem-loop of VCC to the DPH fluorophore embedded within the liposomes. D214A-VCC and F581A-VCC showed a

considerably reduced FRET signal, suggesting that the mutations of D214A and F581A not only reduced the efficacy of membrane oligomerization but also affected the membrane insertion step to a moderate extent. Interestingly, no significant time-dependent increase in the tryptophan-to-DPH FRET signal was observed for the R330A-VCC variant. These data, therefore, suggested that the mutation of R330A could not only block membrane oligomerization of VCC but also arrested the membrane insertion. Our study, for the first time, revealed the interactions and some of the associated key residues implicated in the membrane oligomerization process of VCC. Our study also showed the sequence of events in the membrane pore-formation process of VCC.

**Physicochemical constraints of elevated pH abrogate efficient membrane interaction and trap an abortive membrane-bound oligomeric intermediate of VCC**

Further, we explored the effect of the physicochemical constraint(s), imposed by the elevated pH conditions (in the pH range up to 10), on the membrane binding and pore-formation process of VCC. We monitored the membrane pore-forming activity of VCC under elevated pH conditions starting from the physiological pH of 7. In the hemolytic activity and the calcein release-assay, we observed that at an elevated pH condition of pH 9 and pH 10, membrane pore-forming activity of VCC was drastically reduced. Toward exploring the effects of elevated pH on the structure-function mechanism of VCC, we compared the structural integrity of the toxin in solution at different pH conditions in the range of 7-10. The protein displayed almost overlapping intrinsic tryptophan fluorescence emission and far-UV CD spectra profile in different pH conditions indicating no major structural changes under elevated pH conditions. We also examined any change in the solution state of VCC at different elevated pH, using sedimentation velocity analytical ultracentrifugation (AUC)-based study. Analysis of the sedimentation velocity AUC profile of VCC at pH 7 and pH 10 showed overlapping distribution of sedimentation coefficients, with the peaks at around 4.17 Svedberg units that corresponded to the monomeric state of the protein in solution. Altogether, these data indicated that under the elevated pH conditions, VCC lost functionality without compromising its overall structural integrity.

In flow cytometry-based assay and the surface plasmon resonance (SPR)-based assay we found, that the binding of VCC with human erythrocytes and liposome membranes decreased with increase in pH, above the physiological condition of pH 7, respectively. In particular, binding of

VCC was found to be significantly affected at pH 9, while at pH 10 the effect was found to be more severe.

Interestingly, pull-down assay showed that the membrane-associated fractions of VCC, even at pH 9 and 10, could form SDS-stable oligomeric assembly; oligomerization efficiency at pH 9 was found to be marginally reduced, while the extent of oligomerization appeared to be significantly less at pH 10 as compared to that at pH 7. The membrane-bound oligomers formed at the elevated pH state appeared to represent a distinct and more advanced assembly than the pre-pore state, in the process of membrane pore-formation of VCC.

## References


1. Los, F. C., Randis, T. M., Aroian, R. V., and Ratner, A. J. (2013) Role of pore-forming toxins in bacterial infectious diseases. *Microbiol Mol Biol Rev* 77, 173-207.
2. Bhakdi, S., and Tranum-Jensen, J. (1987) Damage to mammalian cells by proteins that form transmembrane pores. *Rev Physiol Biochem Pharmacol* 107, 147-223.
3. Alouf, J. E., and Popoff, M. R. (2006) *The Comprehensive Sourcebook of Bacterial Protein Toxins.*, Third Edition ed., Academic Press.
4. Berube, B. J., and Bubeck Wardenburg, J. (2013) Staphylococcus aureus alpha-toxin: nearly a century of intrigue. *Toxins (Basel)* 5, 1140-1166.
5. Laohachai, K. N., Bahadi, R., Hardo, M. B., Hardo, P. G., and Kourie, J. I. (2003) The role of bacterial and non-bacterial toxins in the induction of changes in membrane transport: implications for diarrhea. *Toxicon : official journal of the International Society on Toxinology* 42, 687-707.
6. Kloft, N., Busch, T., Neukirch, C., Weis, S., Boukhallouk, F., Bobkiewicz, W., Cibis, I., Bhakdi, S., and Husmann, M. (2009) Pore-forming toxins activate MAPK p38 by causing loss of cellular potassium. *Biochem Biophys Res Commun* 385, 503-506.
7. Parker, M. W., and Feil, S. C. (2005) Pore-forming protein toxins: from structure to function. *Prog Biophys Mol Biol* 88, 91-142.
8. Iacovache, I., van der Goot, F. G., and Pernot, L. (2008) Pore formation: An ancient yet complex form of attack. *Biochimica et Biophysica Acta (BBA) - Biomembranes* 1778, 1611-1623.
9. Ratner, A. J., Hippe, K. R., Aguilar, J. L., Bender, M. H., Nelson, A. L., and Weiser, J. N. (2006) Epithelial cells are sensitive detectors of bacterial pore-forming toxins. *The Journal of biological chemistry* 281, 12994-12998.
10. Schiavo, G., and van der Goot, F. G. (2001) The bacterial toxin toolkit. *Nat Rev Mol Cell Biol* 2, 530-537.
11. Provoda, C. J., and Lee, K. D. (2000) Bacterial pore-forming hemolysins and their use in the cytosolic delivery of macromolecules. *Adv Drug Deliv Rev* 41, 209-221.
12. Bhakdi, S., Valeva, A., Walev, I., Zitzer, A., and Palmer, M. (1998) Pore-forming bacterial cytolysins. *Symp Ser Soc Appl Microbiol* 27, 15S-25S.

13. Gonzalez, M., Bischofberger, M., Pernot, L., van der Goot, F., and Frêche, B. (2008) Bacterial pore-forming toxins: The (w)hole story? *Cellular and Molecular Life Sciences* 65, 493-507.
14. Hang'ombe, M. B., Mukamoto, M., Kohda, T., Sugimoto, N., and Kozaki, S. (2004) Cytotoxicity of Clostridium septicum alpha-toxin: its oligomerization in detergent resistant membranes of mammalian cells. *Microbial pathogenesis* 37, 279-286.
15. Xiong, G., Struckmeier, M., and Lutz, F. (1994) Pore-forming Pseudomonas aeruginosa cytotoxin. *Toxicology* 87, 69-83.
16. Tilley, S. J., and Saibil, H. R. (2006) The mechanism of pore formation by bacterial toxins. *Current Opinion in Structural Biology* 16, 230-236.
17. Kaneko, J., and Kamio, Y. (2004) Bacterial two-component and hetero-heptameric pore-forming cytolytic toxins: structures, pore-forming mechanism, and organization of the genes. *Biosci Biotechnol Biochem* 68, 981-1003.
18. Cossart, P., and Sansonetti, P. J. (2004) Bacterial invasion: the paradigms of enteroinvasive pathogens. *Science (New York, N.Y* 304, 242-248.
19. Rojko, N., Kristan, K. C., Viero, G., Zerovnik, E., Macek, P., Dalla Serra, M., and Anderluh, G. (2013) Membrane damage by an alpha-helical pore-forming protein, Equinatoxin II, proceeds through a succession of ordered steps. *J Biol Chem* 288, 23704-23715.
20. Iacovache, I., Bischofberger, M., and van der Goot, F. G. (2010) Structure and assembly of pore-forming proteins. *Current Opinion in Structural Biology* 20, 241-246.
21. Mueller, M., Grauschopf, U., Maier, T., Glockshuber, R., and Ban, N. (2009) The structure of a cytolytic alpha-helical toxin pore reveals its assembly mechanism. *Nature* 459, 726-730.
22. Kennedy, C. L., Lyras, D., Cordner, L. M., Melton-Witt, J., Emmins, J. J., Tweten, R. K., and Rood, J. I. (2009) Pore-forming activity of alpha-toxin is essential for clostridium septicum-mediated myonecrosis. *Infect Immun* 77, 943-951.
23. Gurcel, L., Abrami, L., Girardin, S., Tschopp, J., and van der Goot, F. G. (2006) Caspase-1 activation of lipid metabolic pathways in response to bacterial pore-forming toxins promotes cell survival. *Cell* 126, 1135-1145.

24. Nguyen, V. T., Higuchi, H., and Kamio, Y. (2002) Controlling pore assembly of staphylococcal gamma-haemolysin by low temperature and by disulphide bond formation in double-cysteine LukF mutants. *Mol Microbiol* 45, 1485-1498.
25. Bakrac, B., and Anderluh, G. (2010) Molecular mechanism of sphingomyelin-specific membrane binding and pore formation by actinoporins. *Advances in experimental medicine and biology* 677, 106-115.
26. Geny, B., and Popoff, M. R. (2006) Bacterial protein toxins and lipids: pore formation or toxin entry into cells. *Biol Cell* 98, 667-678.
27. Musse, A. A., and Merrill, A. R. (2003) The molecular basis for the pH-activation mechanism in the channel-forming bacterial colicin E1. *The Journal of biological chemistry* 278, 24491-24499.
28. Delcour, A. H. (2002) Structure and function of pore-forming beta-barrels from bacteria. *J Mol Microbiol Biotechnol* 4, 1-10.
29. Zhao, G., and London, E. (2005) Behavior of diphtheria toxin T domain containing substitutions that block normal membrane insertion at Pro345 and Leu307: control of deep membrane insertion and coupling between deep insertion of hydrophobic subdomains. *Biochemistry* 44, 4488-4498.
30. Collier, R. J. (2001) Understanding the mode of action of diphtheria toxin: a perspective on progress during the 20th century. *Toxicon : official journal of the International Society on Toxinology* 39, 1793-1803.
31. Pohl, E., Holmes, R. K., and Hol, W. G. (1999) Crystal structure of a cobalt-activated diphtheria toxin repressor-DNA complex reveals a metal-binding SH3-like domain. *J Mol Biol* 292, 653-667.
32. Louie, G. V., Yang, W., Bowman, M. E., and Choe, S. (1997) Crystal structure of the complex of diphtheria toxin with an extracellular fragment of its receptor. *Mol Cell* 1, 67-78.
33. Gouaux, E., Hobaugh, M., and Song, L. (1997) alpha-Hemolysin, gamma-hemolysin, and leukocidin from Staphylococcus aureus: distant in sequence but similar in structure. *Protein science : a publication of the Protein Society* 6, 2631-2635.
34. Bell, C. E., and Eisenberg, D. (1997) Crystal structure of nucleotide-free diphtheria toxin. *Biochemistry* 36, 481-488.

35. Choe, S., Bennett, M. J., Fujii, G., Curmi, P. M., Kantardjieff, K. A., Collier, R. J., and Eisenberg, D. (1992) The crystal structure of diphtheria toxin. *Nature* 357, 216-222.
36. Tamm, L. K., Arora, A., and Kleinschmidt, J. H. (2001) Structure and assembly of beta-barrel membrane proteins. *The Journal of biological chemistry* 276, 32399-32402.
37. Heuck, A. P., Tweten, R. K., and Johnson, A. E. (2001) Beta-barrel pore-forming toxins: intriguing dimorphic proteins. *Biochemistry* 40, 9065-9073.
38. Zitzer, A., Zitzer, O., Bhakdi, S., and Palmer, M. (1999) Oligomerization of Vibrio cholerae cytolysin yields a pentameric pore and has a dual specificity for cholesterol and sphingolipids in the target membrane. *J Biol Chem* 274, 1375-1380.
39. Rossjohn, J., Feil, S. C., McKinstry, W. J., Tsernoglou, D., van der Goot, G., Buckley, J. T., and Parker, M. W. (1998) Aerolysin--a paradigm for membrane insertion of beta-sheet protein toxins? *Journal of Structural Biology* 121, 92-100.
40. Benson, E. L., Huynh, P. D., Finkelstein, A., and Collier, R. J. (1998) Identification of residues lining the anthrax protective antigen channel. *Biochemistry* 37, 3941-3948.
41. Sellman, B. R., Kagan, B. L., and Tweten, R. K. (1997) Generation of a membrane-bound, oligomerized pre-pore complex is necessary for pore formation by Clostridium septicum alpha toxin. *Molecular microbiology* 23, 551-558.
42. Rossjohn, J., Buckley, J. T., Hazes, B., Murzin, A. G., Read, R. J., and Parker, M. W. (1997) Aerolysin and pertussis toxin share a common receptor-binding domain. *The EMBO journal* 16, 3426-3434.
43. Zitzer, A., Walev, I., Palmer, M., and Bhakdi, S. (1995) Characterization of Vibrio cholerae El Tor cytolysin as an oligomerizing pore-forming toxin. *Med Microbiol Immunol* 184, 37-44.
44. Eisele, J. L., and Rosenbusch, J. P. (1990) In vitro folding and oligomerization of a membrane protein. Transition of bacterial porin from random coil to native conformation. *J Biol Chem* 265, 10217-10220.
45. Bann, J. G. (2012) Anthrax toxin protective antigen--insights into molecular switching from prepore to pore. *Protein science : a publication of the Protein Society* 21, 1-12.
46. Nguyen, V. T., and Kamio, Y. (2004) Cooperative assembly of beta-barrel pore-forming toxins. *J Biochem* 136, 563-567.

47. Montoya, M., and Gouaux, E. (2003) Beta-barrel membrane protein folding and structure viewed through the lens of alpha-hemolysin. *Biochimica et biophysica acta* 1609, 19-27.
48. Fahie, M., Romano, F. B., Chisholm, C., Heuck, A. P., Zbinden, M., and Chen, M. (2013) A non-classical assembly pathway of Escherichia coli pore-forming toxin cytolysin A. *J Biol Chem* 288, 31042-31051.
49. Duche, D., Parker, M. W., Gonzalez-Manas, J. M., Pattus, F., and Baty, D. (1994) Uncoupled steps of the colicin A pore formation demonstrated by disulfide bond engineering. *J Biol Chem* 269, 6332-6339.
50. Pardo-Lopez, L., Gomez, I., Munoz-Garay, C., Jimenez-Juarez, N., Soberon, M., and Bravo, A. (2006) Structural and functional analysis of the pre-pore and membrane-inserted pore of Cry1Ab toxin. *J Invertebr Pathol* 92, 172-177.
51. Soberon, M., Pardo, L., Munoz-Garay, C., Sanchez, J., Gomez, I., Porta, H., and Bravo, A. (2010) Pore formation by Cry toxins. *Advances in experimental medicine and biology* 677, 127-142.
52. Bravo, A., Gill, S. S., and Soberon, M. (2007) Mode of action of Bacillus thuringiensis Cry and Cyt toxins and their potential for insect control. *Toxicon : official journal of the International Society on Toxinology* 49, 423-435.
53. Pardo-Lopez, L., Soberon, M., and Bravo, A. (2013) Bacillus thuringiensis insecticidal three-domain Cry toxins: mode of action, insect resistance and consequences for crop protection. *FEMS Microbiol Rev* 37, 3-22.
54. Galitsky, N., Cody, V., Wojtczak, A., Ghosh, D., Luft, J. R., Pangborn, W., and English, L. (2001) Structure of the insecticidal bacterial delta-endotoxin Cry3Bb1 of Bacillus thuringiensis. *Acta crystallographica. Section D, Biological crystallography* 57, 1101-1109.
55. Bravo, A., Gomez, I., Conde, J., Munoz-Garay, C., Sanchez, J., Miranda, R., Zhuang, M., Gill, S. S., and Soberon, M. (2004) Oligomerization triggers binding of a Bacillus thuringiensis Cry1Ab pore-forming toxin to aminopeptidase N receptor leading to insertion into membrane microdomains. *Biochimica et biophysica acta* 1667, 38-46.
56. Valeva, A., Weisser, A., Walker, B., Kehoe, M., Bayley, H., Bhakdi, S., and Palmer, M. (1996) Molecular architecture of a toxin pore: a 15-residue sequence lines the

transmembrane channel of staphylococcal alpha-toxin. *The EMBO journal* 15, 1857-1864.

57. Gouaux, J. E., Braha, O., Hobaugh, M. R., Song, L., Cheley, S., Shustak, C., and Bayley, H. (1994) Subunit stoichiometry of staphylococcal alpha-hemolysin in crystals and on membranes: a heptameric transmembrane pore. *Proc Natl Acad Sci U S A* 91, 12828-12831.
58. Menestrina, G., Serra, M. D., and Prevost, G. (2001) Mode of action of beta-barrel pore-forming toxins of the staphylococcal alpha-hemolysin family. *Toxicon : official journal of the International Society on Toxinology* 39, 1661-1672.
59. Kaneko, J., Tomita, T., and Kamio, Y. (2001) [Structure and mode of action of staphylococcal bi-component pore-forming toxins]. *Tanpakushitsu Kakusan Koso* 46, 497-505.
60. Dinges, M. M., Orwin, P. M., and Schlievert, P. M. (2000) Exotoxins of Staphylococcus aureus. *Clin Microbiol Rev* 13, 16-34, table of contents.
61. Guillet, V., Roblin, P., Werner, S., Coraiola, M., Menestrina, G., Monteil, H., Prevost, G., and Mourey, L. (2004) Crystal structure of leucotoxin S component: new insight into the Staphylococcal beta-barrel pore-forming toxins. *The Journal of biological chemistry* 279, 41028-41037.
62. Menestrina, G., Dalla Serra, M., Comai, M., Coraiola, M., Viero, G., Werner, S., Colin, D. A., Monteil, H., and Prevost, G. (2003) Ion channels and bacterial infection: the case of beta-barrel pore-forming protein toxins of Staphylococcus aureus. *FEBS letters* 552, 54-60.
63. Prevost, G., Mourey, L., Colin, D. A., and Menestrina, G. (2001) Staphylococcal pore-forming toxins. *Curr Top Microbiol Immunol* 257, 53-83.
64. Pedelacq, J. D., Maveyraud, L., Prevost, G., Baba-Moussa, L., Gonzalez, A., Courcelle, E., Shepard, W., Monteil, H., Samama, J. P., and Mourey, L. (1999) The structure of a Staphylococcus aureus leucocidin component (LukF-PV) reveals the fold of the water-soluble species of a family of transmembrane pore-forming toxins. *Structure* 7, 277-287.
65. Olson, R., Nariya, H., Yokota, K., Kamio, Y., and Gouaux, E. (1999) Crystal structure of staphylococcal LukF delineates conformational changes accompanying formation of a transmembrane channel. *Nat Struct Biol* 6, 134-140.

66. Song, L., Hobaugh, M. R., Shustak, C., Cheley, S., Bayley, H., and Gouaux, J. E. (1996) Structure of staphylococcal alpha-hemolysin, a heptameric transmembrane pore. *Science* 274, 1859-1866.

67. Wilke, G. A., and Bubeck Wardenburg, J. (2010) Role of a disintegrin and metalloprotease 10 in Staphylococcus aureus alpha-hemolysin-mediated cellular injury. *Proc Natl Acad Sci U S A* 107, 13473-13478.

68. Gouaux, E., Hobaugh, M., and Song, L. (2008) α-Hemolysin, γ-hemolysin, and leukocidin from Staphylococcus aureus: Distant in sequence but similar in structure. *Protein Science* 6, 2631-2635.

69. Uhlen, P., Laestadius, A., Jahnukainen, T., Soderblom, T., Backhed, F., Celsi, G., Brismar, H., Normark, S., Aperia, A., and Richter-Dahlfors, A. (2000) Alpha-haemolysin of uropathogenic E. coli induces Ca2+ oscillations in renal epithelial cells. *Nature* 405, 694-697.

70. Valeva, A., Hellmann, N., Walev, I., Strand, D., Plate, M., Boukhallouk, F., Brack, A., Hanada, K., Decker, H., and Bhakdi, S. (2006) Evidence that clustered phosphocholine head groups serve as sites for binding and assembly of an oligomeric protein pore. *J Biol Chem* 281, 26014-26021.

71. Hermoso, J. A., Mancheno, J. M., and Pebay-Peyroula, E. (2006) X-ray and neutron diffraction approaches to the structural analysis of protein lipid interactions. in *Protein-Lipid Interactions* (Mateo, C. R., Gomez, J., Villalain, J., and Gonzalez Ros, J. M. eds.), 1st Ed. pp 63-110.

72. Valeva, A., Schnabel, R., Walev, I., Boukhallouk, F., Bhakdi, S., and Palmer, M. (2001) Membrane insertion of the heptameric staphylococcal alpha-toxin pore. A domino-like structural transition that is allosterically modulated by the target cell membrane. *The Journal of biological chemistry* 276, 14835-14841.

73. Huang, J., Buboltz, J. T., and Feigenson, G. W. (1999) Maximum solubility of cholesterol in phosphatidylcholine and phosphatidylethanolamine bilayers. *Biochim Biophys Acta* 1417, 89-100.

74. Hotze, E. M., Wilson-Kubalek, E. M., Rossjohn, J., Parker, M. W., Johnson, A. E., and Tweten, R. K. (2001) Arresting pore formation of a cholesterol-dependent cytolysin by

disulfide trapping synchronizes the insertion of the transmembrane beta-sheet from a prepore intermediate. *The Journal of biological chemistry* 276, 8261-8268.

75. Fang, Y., Cheley, S., Bayley, H., and Yang, J. (1997) The heptameric prepore of a staphylococcal alpha-hemolysin mutant in lipid bilayers imaged by atomic force microscopy. *Biochemistry* 36, 9518-9522.
76. Walker, B., Braha, O., Cheley, S., and Bayley, H. (1995) An intermediate in the assembly of a pore-forming protein trapped with a genetically-engineered switch. *Chem Biol* 2, 99-105.
77. Hildebrand, A., Pohl, M., and Bhakdi, S. (1991) Staphylococcus aureus alpha-toxin. Dual mechanism of binding to target cells. *The Journal of biological chemistry* 266, 17195-17200.
78. Collier, R. J. (2009) Membrane translocation by anthrax toxin. *Mol Aspects Med* 30, 413-422.
79. Scobie, H. M., and Young, J. A. (2005) Interactions between anthrax toxin receptors and protective antigen. *Curr Opin Microbiol* 8, 106-112.
80. Lacy, D. B., Wigelsworth, D. J., Melnyk, R. A., Harrison, S. C., and Collier, R. J. (2004) Structure of heptameric protective antigen bound to an anthrax toxin receptor: a role for receptor in pH-dependent pore formation. *Proceedings of the National Academy of Sciences of the United States of America* 101, 13147-1315.
81. Petosa, C., Collier, R. J., Klimpel, K. R., Leppla, S. H., and Liddington, R. C. (1997) Crystal structure of the anthrax toxin protective antigen. *Nature* 385, 833-838.
82. Abrami, L., Fivaz, M., Decroly, E., Seidah, N. G., Jean, F., Thomas, G., Leppla, S. H., Buckley, J. T., and van der Goot, F. G. (1998) The pore-forming toxin proaerolysin is activated by furin. *J Biol Chem* 273, 32656-32661.
83. Mogridge, J., Mourez, M., and Collier, R. J. (2001) Involvement of domain 3 in oligomerization by the protective antigen moiety of anthrax toxin. *J Bacteriol* 183, 2111-2116.
84. Rosovitz, M. J., Schuck, P., Varughese, M., Chopra, A. P., Mehra, V., Singh, Y., McGinnis, L. M., and Leppla, S. H. (2003) Alanine-scanning mutations in domain 4 of anthrax toxin protective antigen reveal residues important for binding to the cellular receptor and to a neutralizing monoclonal antibody. *J Biol Chem* 278, 30936-30944.

85. Degiacomi, M. T., Iacovache, I., Pernot, L., Chami, M., Kudryashev, M., Stahlberg, H., van der Goot, F. G., and Dal Peraro, M. (2013) Molecular assembly of the aerolysin pore reveals a swirling membrane-insertion mechanism. *Nat Chem Biol* 9, 623-629.
86. Fivaz, M., Abrami, L., Tsitrin, Y., and van der Goot, F. G. (2001) Aerolysin from Aeromonas hydrophila and Related Toxins. 257, 35-52.
87. Nelson, K. L., and Buckley, J. T. (2000) Channel formation by the glycosylphosphatidylinositol-anchored protein binding toxin aerolysin is not promoted by lipid rafts. *J Biol Chem* 275, 19839-19843.
88. Parker, M. W., van der Goot, F. G., and Buckley, J. T. (1996) Aerolysin--the ins and outs of a model channel-forming toxin. *Molecular microbiology* 19, 205-212.
89. Hardie, K. R., Schulze, A., Parker, M. W., and Buckley, J. T. (1995) Vibrio spp. secrete proaerolysin as a folded dimer without the need for disulphide bond formation. *Molecular microbiology* 17, 1035-1044.
90. Parker, M. W., Buckley, J. T., Postma, J. P., Tucker, A. D., Leonard, K., Pattus, F., and Tsernoglou, D. (1994) Structure of the Aeromonas toxin proaerolysin in its water-soluble and membrane-channel states. *Nature* 367, 292-295.
91. van der Goot, F. G., Lakey, J., Pattus, F., Kay, C. M., Sorokine, O., Van Dorsselaer, A., and Buckley, J. T. (1992) Spectroscopic study of the activation and oligomerization of the channel-forming toxin aerolysin: identification of the site of proteolytic activation. *Biochemistry* 31, 8566-8570.
92. Klimpel, K. R., Molloy, S. S., Thomas, G., and Leppla, S. H. (1992) Anthrax toxin protective antigen is activated by a cell surface protease with the sequence specificity and catalytic properties of furin. *Proceedings of the National Academy of Sciences of the United States of America* 89, 10277-10281.
93. Abrami, L., Fivaz, M., and van der Goot, F. G. (2000) Surface dynamics of aerolysin on the plasma membrane of living cells. *Int J Med Microbiol* 290, 363-367.
94. Diep, D. B., Lawrence, T. S., Ausio, J., Howard, S. P., and Buckley, J. T. (1998) Secretion and properties of the large and small lobes of the channel-forming toxin aerolysin. *Mol Microbiol* 30, 341-352.

95. Cowell, S., Aschauer, W., Gruber, H. J., Nelson, K. L., and Buckley, J. T. (1997) The erythrocyte receptor for the channel-forming toxin aerolysin is a novel glycosylphosphatidylinositol-anchored protein. *Mol Microbiol* 25, 343-350.

96. MacKenzie, C. R., Hirama, T., and Buckley, J. T. (1999) Analysis of receptor binding by the channel-forming toxin aerolysin using surface plasmon resonance. *J Biol Chem* 274, 22604-22609.

97. Krause, K. H., Fivaz, M., Monod, A., and van der Goot, F. G. (1998) Aerolysin induces G-protein activation and Ca2+ release from intracellular stores in human granulocytes. *J Biol Chem* 273, 18122-18129.

98. Abrami, L., Fivaz, M., Glauser, P. E., Parton, R. G., and van der Goot, F. G. (1998) A pore-forming toxin interacts with a GPI-anchored protein and causes vacuolation of the endoplasmic reticulum. *J Cell Biol* 140, 525-540.

99. Sakai, H., and Tsukihara, T. (1998) Structures of membrane proteins determined at atomic resolution. *J Biochem* 124, 1051-1059.

100. Heuck, A. P., Moe, P. C., and Johnson, B. B. (2010) The cholesterol-dependent cytolysin family of gram-positive bacterial toxins. *Sub-cellular biochemistry* 51, 551-577.

101. Rosado, C. J., Kondos, S., Bull, T. E., Kuiper, M. J., Law, R. H., Buckle, A. M., Voskoboinik, I., Bird, P. I., Trapani, J. A., Whisstock, J. C., and Dunstone, M. A. (2008) The MACPF/CDC family of pore-forming toxins. *Cellular microbiology* 10, 1765-1774.

102. Soltani, C. E., Hotze, E. M., Johnson, A. E., and Tweten, R. K. (2007) Structural elements of the cholesterol-dependent cytolysins that are responsible for their cholesterol-sensitive membrane interactions. *Proc Natl Acad Sci U S A* 104, 20226-20231.

103. Soltani, C. E., Hotze, E. M., Johnson, A. E., and Tweten, R. K. (2007) Specific protein-membrane contacts are required for prepore and pore assembly by a cholesterol-dependent cytolysin. *J Biol Chem* 282, 15709-15716.

104. Tweten, R. K. (2005) Cholesterol-dependent cytolysins, a family of versatile pore-forming toxins. *Infect Immun* 73, 6199-6209.

105. Hotze, E. M., and Tweten, R. K. (2012) Membrane assembly of the cholesterol-dependent cytolysin pore complex. *Biochim Biophys Acta* 1818, 1028-1038.

106. Dowd, K. J., Farrand, A. J., and Tweten, R. K. (2012) The cholesterol-dependent cytolysin signature motif: a critical element in the allosteric pathway that couples membrane binding to pore assembly. *PLoS Pathog* 8, e1002787.
107. Gilbert, R. J. (2010) Cholesterol-dependent cytolysins. *Advances in experimental medicine and biology* 677, 56-66.
108. Birmingham, C. L., Canadien, V., Kaniuk, N. A., Steinberg, B. E., Higgins, D. E., and Brumell, J. H. (2008) Listeriolysin O allows Listeria monocytogenes replication in macrophage vacuoles. *Nature* 451, 350-354.
109. Schnupf, P., and Portnoy, D. A. (2007) Listeriolysin O: a phagosome-specific lysin. *Microbes Infect* 9, 1176-1187.
110. Bavdek, A., Gekara, N. O., Priselac, D., Gutierrez Aguirre, I., Darji, A., Chakraborty, T., Macek, P., Lakey, J. H., Weiss, S., and Anderluh, G. (2007) Sterol and pH interdependence in the binding, oligomerization, and pore formation of Listeriolysin O. *Biochemistry* 46, 4425-4437.
111. Schuerch, D. W., Wilson-Kubalek, E. M., and Tweten, R. K. (2005) Molecular basis of listeriolysin O pH dependence. *Proceedings of the National Academy of Sciences of the United States of America* 102, 12537-12542.
112. Zitzer, A., Westover, E. J., Covey, D. F., and Palmer, M. (2003) Differential interaction of the two cholesterol-dependent, membrane-damaging toxins, streptolysin O and Vibrio cholerae cytolysin, with enantiomeric cholesterol. *FEBS Lett* 553, 229-231.
113. Giddings, K. S., Johnson, A. E., and Tweten, R. K. (2003) Redefining cholesterol's role in the mechanism of the cholesterol-dependent cytolysins. *Proc Natl Acad Sci U S A* 100, 11315-11320.
114. Zitzer, A., Bittman, R., Verbicky, C. A., Erukulla, R. K., Bhakdi, S., Weis, S., Valeva, A., and Palmer, M. (2001) Coupling of cholesterol and cone-shaped lipids in bilayers augments membrane permeabilization by the cholesterol-specific toxins streptolysin O and Vibrio cholerae cytolysin. *J Biol Chem* 276, 14628-14633.
115. Tweten, R. K., Parker, M. W., and Johnson, A. E. (2001) The cholesterol-dependent cytolysins. *Curr Top Microbiol Immunol* 257, 15-33.
116. Shepard, L. A., Shatursky, O., Johnson, A. E., and Tweten, R. K. (2000) The mechanism of pore assembly for a cholesterol-dependent cytolysin: formation of a large prepore

complex precedes the insertion of the transmembrane beta-hairpins. *Biochemistry* 39, 10284-10293.

117. Palmer, M., Harris, R., Freytag, C., Kehoe, M., Tranum-Jensen, J., and Bhakdi, S. (1998) Assembly mechanism of the oligomeric streptolysin O pore: the early membrane lesion is lined by a free edge of the lipid membrane and is extended gradually during oligomerization. *EMBO J* 17, 1598-1605.

118. Johnson, B. B., and Heuck, A. P. (2014) Perfringolysin O structure and mechanism of pore formation as a paradigm for cholesterol-dependent cytolysins. *Sub-cellular biochemistry* 80, 63-81.

119. Harris, J. R., Bhakdi, S., Meissner, U., Scheffler, D., Bittman, R., Li, G., Zitzer, A., and Palmer, M. (2002) Interaction of the Vibrio cholerae cytolysin (VCC) with cholesterol, some cholesterol esters, and cholesterol derivatives: a TEM study. *J Struct Biol* 139, 122-135.

120. Farrand, A. J., LaChapelle, S., Hotze, E. M., Johnson, A. E., and Tweten, R. K. (2010) Only two amino acids are essential for cytolytic toxin recognition of cholesterol at the membrane surface. *Proc Natl Acad Sci U S A* 107, 4341-4346.

121. Rossjohn, J., Polekhina, G., Feil, S. C., Morton, C. J., Tweten, R. K., and Parker, M. W. (2007) Structures of perfringolysin O suggest a pathway for activation of cholesterol-dependent cytolysins. *Journal of molecular biology* 367, 1227-1236.

122. Polekhina, G., Giddings, K. S., Tweten, R. K., and Parker, M. W. (2005) Insights into the action of the superfamily of cholesterol-dependent cytolysins from studies of intermedilysin. *Proc Natl Acad Sci U S A* 102, 600-605.

123. Jamin, N., Neumann, J. M., Ostuni, M. A., Vu, T. K., Yao, Z. X., Murail, S., Robert, J. C., Giatzakis, C., Papadopoulos, V., and Lacapere, J. J. (2005) Characterization of the cholesterol recognition amino acid consensus sequence of the peripheral-type benzodiazepine receptor. *Mol Endocrinol* 19, 588-594.

124. Ballard, J., Crabtree, J., Roe, B. A., and Tweten, R. K. (1995) The primary structure of Clostridium septicum alpha-toxin exhibits similarity with that of Aeromonas hydrophila aerolysin. *Infect Immun* 63, 340-344.

125. Epand, R. F., Thomas, A., Brasseur, R., Vishwanathan, S. A., Hunter, E., and Epand, R. M. (2006) Juxtamembrane protein segments that contribute to recruitment of cholesterol into domains. *Biochemistry* 45, 6105-6114.

126. Nelson, L. D., Johnson, A. E., and London, E. (2008) How interaction of perfringolysin O with membranes is controlled by sterol structure, lipid structure, and physiological low pH: insights into the origin of perfringolysin O-lipid raft interaction. *J Biol Chem* 283, 4632-4642.

127. Rossjohn, J., Feil, S. C., McKinstry, W. J., Tweten, R. K., and Parker, M. W. (1997) Structure of a cholesterol-binding, thiol-activated cytolysin and a model of its membrane form. *Cell* 89, 685-692.

128. Bayley, H., Jayasinghe, L., and Wallace, M. (2005) Prepore for a breakthrough. *Nat Struct Mol Biol* 12, 385-386.

129. Gouaux, E. (1997) Channel-forming toxins: tales of transformation. *Curr Opin Struct Biol* 7, 566-573.

130. Jafurulla, M., Tiwari, S., and Chattopadhyay, A. (2011) Identification of cholesterol recognition amino acid consensus (CRAC) motif in G-protein coupled receptors. *Biochem Biophys Res Commun* 404, 569-573.

131. Palmer, M. (2004) Cholesterol and the activity of bacterial toxins. *FEMS Microbiol Lett* 238, 281-289.

132. Tsou, A. M., and Zhu, J. (2010) Quorum sensing negatively regulates hemolysin transcriptionally and posttranslationally in Vibrio cholerae. *Infect Immun* 78, 461-467.

133. Pichel, M., Rivas, M., Chinen, I., Martin, F., Ibarra, C., and Binsztein, N. (2003) Genetic diversity of Vibrio cholerae O1 in Argentina and emergence of a new variant. *J Clin Microbiol* 41, 124-134.

134. Yamamoto, K., Wright, A. C., Kaper, J. B., and Morris, J. G., Jr. (1990) The cytolysin gene of Vibrio vulnificus: sequence and relationship to the Vibrio cholerae E1 Tor hemolysin gene. *Infection and immunity* 58, 2706-2709.

135. Yamamoto, K., Ichinose, Y., Nakasone, N., Tanabe, M., Nagahama, M., Sakurai, J., and Iwanaga, M. (1986) Identity of hemolysins produced by Vibrio cholerae non-O1 and V. cholerae O1, biotype El Tor. *Infect Immun* 51, 927-931.

136. Kaper, J. B., Morris, J. G., Jr., and Levine, M. M. (1995) Cholera. *Clinical microbiology reviews* 8, 48-86.

137. Kaper, J., Fasano, A., and Trucksis, M. (1994) Toxins of Vibrio cholerae. *Vibrio cholerae*, 145-176.

138. Trucksis, M., Galen, J. E., Michalski, J., Fasano, A., and Kaper, J. B. (1993) Accessory cholera enterotoxin (Ace), the third toxin of a Vibrio cholerae virulence cassette. *Proceedings of the National Academy of Sciences of the United States of America* 90, 5267-5271.

139. Saha, P. K., Koley, H., Mukhopadhyay, A. K., Bhattacharya, S. K., Nair, G. B., Ramakrishnan, B. S., Krishnan, S., Takeda, T., and Takeda, Y. (1996) Nontoxigenic Vibrio cholerae 01 serotype Inaba biotype El Tor associated with a cluster of cases of cholera in southern India. *Journal of clinical microbiology* 34, 1114-1117.

140. Bharati, K., and Ganguly, N. K. (2011) Cholera toxin: a paradigm of a multifunctional protein. *The Indian journal of medical research* 133, 179-187.

141. Vanden Broeck, D., Horvath, C., and De Wolf, M. J. (2007) Vibrio cholerae: cholera toxin. *Int J Biochem Cell Biol* 39, 1771-1775.

142. Iredell, J. R., and Manning, P. A. (1994) The toxin-co-regulated pilus of Vibrio cholerae O1: a model for type 4 pilus biogenesis? *Trends Microbiol* 2, 187-192.

143. Trucksis, M., Conn, T. L., Fasano, A., and Kaper, J. B. (1997) Production of Vibrio cholerae accessory cholera enterotoxin (Ace) in the yeast Pichia pastoris. *Infect Immun* 65, 4984-4988.

144. Silva, A. J., Leitch, G. J., Camilli, A., and Benitez, J. A. (2006) Contribution of hemagglutinin/protease and motility to the pathogenesis of El Tor biotype cholera. *Infection and immunity* 74, 2072-2079.

145. Datta-Roy, K., Banerjee, K., De, S. P., and Ghose, A. C. (1986) Comparative study of expression of hemagglutinins, hemolysins, and enterotoxins by clinical and environmental isolates of non-O1 Vibrio cholerae in relation to their enteropathogenicity. *Appl Environ Microbiol* 52, 875-879.

146. Olivier, V., Haines, G. K., 3rd, Tan, Y., and Satchell, K. J. (2007) Hemolysin and the multifunctional autoprocessing RTX toxin are virulence factors during intestinal infection of mice with Vibrio cholerae El Tor O1 strains. *Infect Immun* 75, 5035-5042.

147. Sheahan, K. L., Cordero, C. L., and Satchell, K. J. (2007) Autoprocessing of the Vibrio cholerae RTX toxin by the cysteine protease domain. *The EMBO journal* 26, 2552-2561.

148. Chow, K. H., Ng, T. K., Yuen, K. Y., and Yam, W. C. (2001) Detection of RTX toxin gene in Vibrio cholerae by PCR. *Journal of clinical microbiology* 39, 2594-2597.

149. Zampini, M., Canesi, L., Betti, M., Ciacci, C., Tarsi, R., Gallo, G., and Pruzzo, C. (2003) Role for Mannose-Sensitive Hemagglutinin in Promoting Interactions between Vibrio cholerae El Tor and Mussel Hemolymph. *Appl Environ Microbiol* 69, 5711-5715.

150. Chiavelli, D. A., Marsh, J. W., and Taylor, R. K. (2001) The mannose-sensitive hemagglutinin of Vibrio cholerae promotes adherence to zooplankton. *Appl Environ Microbiol* 67, 3220-3225.

151. Peumans, W. J., Hause, B., and Van Damme, E. J. (2000) The galactose-binding and mannose-binding jacalin-related lectins are located in different sub-cellular compartments. *FEBS Lett* 477, 186-192.

152. Pal, S., Guhathakurta, B., Sasmal, D., Mallick, R., and Datta, A. (1997) Purification and characterisation of a hemolysin with phospholipase C activity from Vibrio cholerae O139. *FEMS Microbiol Lett* 147, 115-120.

153. Watnick, P. I., Fullner, K. J., and Kolter, R. (1999) A role for the mannose-sensitive hemagglutinin in biofilm formation by Vibrio cholerae El Tor. *Journal of bacteriology* 181, 3606-3609.

154. Peterson, K. M. (2002) Expression of Vibrio cholerae virulence genes in response to environmental signals. *Curr Issues Intest Microbiol* 3, 29-38.

155. Weber, G. G., and Klose, K. E. (2011) The complexity of ToxT-dependent transcription in Vibrio cholerae. *The Indian journal of medical research* 133, 201-206.

156. Lutfullah, G., Azhar, N., Amin, F., Khan, Z., Azim, M. K., Shouqat, K., Noor, S., and Ali, R. (2009) Structural bioinformatics of Vibrio cholerae aminopeptidase A (PepA) monomer. *Protein Pept Lett* 16, 36-45.

157. Edwin, A., Grundström, C., Wai, S. N., Öhman, A., Stier, G., and Sauer-Eriksson, A. E. (2014) Domain isolation, expression, purification and proteolytic activity of the metalloprotease PrtV from Vibrio cholerae. *Protein Expression and Purification* 96, 39-47.

158. Vaitkevicius, K., Rompikuntal, P. K., Lindmark, B., Vaitkevicius, R., Song, T., and Wai, S. N. (2008) The metalloprotease PrtV from Vibrio cholerae. *The FEBS journal* 275, 3167-3177.

159. Gutierrez, M. G., Saka, H. A., Chinen, I., Zoppino, F. C., Yoshimori, T., Bocco, J. L., and Colombo, M. I. (2007) Protective role of autophagy against Vibrio cholerae cytolysin, a pore-forming toxin from V. cholerae. *Proc Natl Acad Sci U S A* 104, 1829-1834.

160. Cinar, H. N., Kothary, M., Datta, A. R., Tall, B. D., Sprando, R., Bilecen, K., Yildiz, F., and McCardell, B. (2010) Vibrio cholerae hemolysin is required for lethality, developmental delay, and intestinal vacuolation in Caenorhabditis elegans. *PLoS One* 5, e11558.

161. Vidal, J. E., Enriquez-Rincon, F., Giono-Cerezo, S., Ribas-Aparicio, R. M., and Figueroa-Arredondo, P. (2009) Culture supernatants from V. cholerae O1 El Tor strains isolated from different geographic areas induce cell vacuolation and cytotoxicity. *Salud Publica Mex* 51, 39-47.

162. Debellis, L., Diana, A., Arcidiacono, D., Fiorotto, R., Portincasa, P., Altomare, D. F., Spirli, C., and de Bernard, M. (2009) The Vibrio cholerae cytolysin promotes chloride secretion from intact human intestinal mucosa. *PLoS One* 4, e5074.

163. Saka, H. A., Bidinost, C., Sola, C., Carranza, P., Collino, C., Ortiz, S., Echenique, J. R., and Bocco, J. L. (2008) Vibrio cholerae cytolysin is essential for high enterotoxicity and apoptosis induction produced by a cholera toxin gene-negative V. cholerae non-O1, non-O139 strain. *Microb Pathog* 44, 118-128.

164. Mukherjee, G., Biswas, A., Banerjee, K. K., and Biswas, T. (2008) Vibrio cholerae hemolysin is apoptogenic to peritoneal B-1a cells but its oligomer shepherd the cells for IgA response. *Mol Immunol* 45, 266-270.

165. Arcidiacono, D., Odom, S., Frossi, B., Rivera, J., Paccani, S. R., Baldari, C. T., Pucillo, C., Montecucco, C., and de Bernard, M. (2008) The Vibrio cholerae cytolysin promotes activation of mast cell (T helper 2) cytokine production. *Cell Microbiol* 10, 899-907.

166. Moschioni, M., Tombola, F., de Bernard, M., Coelho, A., Zitzer, A., Zoratti, M., and Montecucco, C. (2002) The Vibrio cholerae haemolysin anion channel is required for cell vacuolation and death. *Cell Microbiol* 4, 397-409.

167. Figueroa-Arredondo, P., Heuser, J. E., Akopyants, N. S., Morisaki, J. H., Giono-Cerezo, S., Enriquez-Rincon, F., and Berg, D. E. (2001) Cell vacuolation caused by Vibrio cholerae hemolysin. *Infect Immun* 69, 1613-1624.

168. Scott, M., and Sandkvist, M. (2006) Toxin secretion systems. in *The comprehensive sourcebook of bacterial protein toxins* (Alouf, J. E., and Popoff, M. R. eds.), 3rd Ed., Academic Press. pp 83-105.

169. Zitzer, A., Wassenaar, T. M., Walev, I., and Bhakdi, S. (1997) Potent membrane-permeabilizing and cytocidal action of Vibrio cholerae cytolysin on human intestinal cells. *Infect Immun* 65, 1293-1298.

170. McCardell, B. A., Kothary, M. H., and Madden, J. M. (1999) Two-step purification and partial characterization of a variant of the Vibrio cholerae non-O1 hemolysin. *FEMS Microbiol Lett* 180, 177-182.

171. Sathyamoorthy, V., Huntley, J. S., Hall, A. C., and Hall, R. H. (1997) Biochemical and physiological characteristics of HlyA, a pore-forming cytolysin of Vibrio cholerae serogroup O1. *Toxicon* 35, 515-527.

172. Nagamune, K., Yamamoto, K., Naka, A., Matsuyama, J., Miwatani, T., and Honda, T. (1996) In vitro proteolytic processing and activation of the recombinant precursor of El Tor cytolysin/hemolysin (pro-HlyA) of Vibrio cholerae by soluble hemagglutinin/protease of V. cholerae, trypsin, and other proteases. *Infect Immun* 64, 4655-4658.

173. Hall, R. H., and Drasar, B. S. (1990) Vibrio cholerae HlyA hemolysin is processed by proteolysis. *Infect Immun* 58, 3375-3379.

174. De, S., and Olson, R. (2011) Crystal structure of the Vibrio cholerae cytolysin heptamer reveals common features among disparate pore-forming toxins. *Proc Natl Acad Sci U S A* 108, 7385-7390.

175. He, Y., and Olson, R. (2010) Three-dimensional structure of the detergent-solubilized Vibrio cholerae cytolysin (VCC) heptamer by electron cryomicroscopy. *Journal of Structural Biology* 169, 6-13.

176. Mukherjee, G., Banerjee, K. K., and Biswas, T. (2008) Oligomerization of Vibrio cholerae hemolysin induces CXCR3 upregulation and activation of B-1a cell. *Cell Mol Immunol* 5, 231-234.

177. Ray, A., Chattopadhyay, K., Banerjee, K. K., and Biswas, T. (2003) Macrophage distinguishes Vibrio cholerae hemolysin from its protease insensitive oligomer by time dependent and selective expression of CD80-CD86. *Immunol Lett* 89, 143-147.

178. Chattopadhyay, K., and Banerjee, K. K. (2003) Unfolding of Vibrio cholerae hemolysin induces oligomerization of the toxin monomer. *J Biol Chem* 278, 38470-38475.

179. Ikigai, H., Ono, T., Iwata, M., Nakae, T., and Shimamura, T. (1997) El Tor hemolysin of Vibrio cholerae O1 forms channels in planar lipid bilayer membranes. *FEMS Microbiol Lett* 150, 249-254.

180. Saha, N., and Banerjee, K. K. (1997) Carbohydrate-mediated regulation of interaction of Vibrio cholerae hemolysin with erythrocyte and phospholipid vesicle. *J Biol Chem* 272, 162-167.

181. Rai, A. K., and Chattopadhyay, K. (2015) Vibrio cholerae Cytolysin: Structure-Function Mechanism of an Atypical beta-Barrel Pore-Forming Toxin. *Adv Exp Med Biol* 842, 109-125.

182. Lohner, S., Walev, I., Boukhallouk, F., Palmer, M., Bhakdi, S., and Valeva, A. (2009) Pore formation by Vibrio cholerae cytolysin follows the same archetypical mode as {beta}-barrel toxins from gram-positive organisms. *Faseb J* 23, 2521-2528.

183. Zitzer, A., Harris, J. R., Kemminer, S. E., Zitzer, O., Bhakdi, S., Muething, J., and Palmer, M. (2000) Vibrio cholerae cytolysin: assembly and membrane insertion of the oligomeric pore are tightly linked and are not detectably restricted by membrane fluidity. *Biochim Biophys Acta* 1509, 264-274.

184. Nelson, K. L., Raja, S. M., and Buckley, J. T. (1997) The glycosylphosphatidylinositol-anchored surface glycoprotein Thy-1 is a receptor for the channel-forming toxin aerolysin. *J Biol Chem* 272, 12170-12174.

185. Huntley, J. S., Sathyamoorthy, V., Hall, R. H., and Hall, A. C. (1997) Membrane attack induced by HlyA, a pore-forming toxin of Vibrio cholerae. *Hum Exp Toxicol* 16, 101-105.

186. Krasilnikov, O. V., Muratkhodjaev, J. N., and Zitzer, A. O. (1992) The mode of action of Vibrio cholerae cytolysin. The influences on both erythrocytes and planar lipid bilayers. *Biochim Biophys Acta* 1111, 7-16.

187. Olson, R., and Gouaux, E. (2005) Crystal structure of the Vibrio cholerae cytolysin (VCC) pro-toxin and its assembly into a heptameric transmembrane pore. *J Mol Biol* 350, 997-1016.

188. Dutta, S., Banerjee, K. K., and Ghosh, A. N. (2013) Cryo-electron microscopy reveals the membrane insertion mechanism of V. cholerae hemolysin. *J Biomol Struct Dyn.*

189. Dutta, S., Mazumdar, B., Banerjee, K. K., and Ghosh, A. N. (2009) Three-dimensional structure of different functional forms of the Vibrio cholerae hemolysin oligomer: a cryo-electron microscopic study. *J Bacteriol* 192, 169-178.

190. Olson, R., and Gouaux, E. (2003) Vibrio cholerae cytolysin is composed of an alpha-hemolysin-like core. *Protein Sci* 12, 379-383.

191. Ikigai, H., Ono, T., Nakae, T., Otsuru, H., and Shimamura, T. (1999) Two forms of Vibrio cholerae O1 El Tor hemolysin derived from identical precursor protein. *Biochim Biophys Acta* 1415, 297-305.

192. Valeva, A., Walev, I., Boukhallouk, F., Wassenaar, T. M., Heinz, N., Hedderich, J., Lautwein, S., Mocking, M., Weis, S., Zitzer, A., and Bhakdi, S. (2005) Identification of the membrane penetrating domain of Vibrio cholerae cytolysin as a beta-barrel structure. *Mol Microbiol* 57, 124-131.

193. Valeva, A., Walev, I., Weis, S., Boukhallouk, F., Wassenaar, T. M., Endres, K., Fahrenholz, F., Bhakdi, S., and Zitzer, A. (2004) A cellular metalloproteinase activates Vibrio cholerae pro-cytolysin. *J Biol Chem* 279, 25143-25148.

194. Paul, K., and Chattopadhyay, K. (2014) Pre-pore oligomer formation by Vibrio cholerae cytolysin: insights from a truncated variant lacking the pore-forming pre-stem loop. *Biochem Biophys Res Commun* 443, 189-193.

195. Yamamoto, K., Ichinose, Y., Shinagawa, H., Makino, K., Nakata, A., Iwanaga, M., Honda, T., and Miwatani, T. (1990) Two-step processing for activation of the cytolysin/hemolysin of Vibrio cholerae O1 biotype El Tor: nucleotide sequence of the structural gene (hlyA) and characterization of the processed products. *Infect Immun* 58, 4106-4116.

196. Nagamune, K., Yamamoto, K., and Honda, T. (1997) Intramolecular chaperone activity of the pro-region of Vibrio cholerae El Tor cytolysin. *J Biol Chem* 272, 1338-1343.

197. Alm, R. A., Stroeher, U. H., and Manning, P. A. (1988) Extracellular proteins of Vibrio cholerae: nucleotide sequence of the structural gene (hlyA) for the haemolysin of the haemolytic El Tor strain 017 and characterization of the hlyA mutation in the non-haemolytic classical strain 569B. *Mol Microbiol* 2, 481-488.

198. Paul, K., and Chattopadhyay, K. (2011) Unfolding distinguishes the Vibrio cholerae cytolysin precursor from the mature form of the toxin. *Biochemistry* 50, 3936-3945.

199. Rutenber, E., Ready, M., and Robertus, J. D. (1987) Structure and evolution of ricin B chain. *Nature* 326, 624-626.

200. Lee, X., Thompson, A., Zhang, Z., Ton-that, H., Biesterfeldt, J., Ogata, C., Xu, L., Johnston, R. A., and Young, N. M. (1998) Structure of the complex of Maclura pomifera agglutinin and the T-antigen disaccharide, Galbeta1,3GalNAc. *The Journal of biological chemistry* 273, 6312-6318.

201. Sankaranarayanan, R., Sekar, K., Banerjee, R., Sharma, V., Surolia, A., and Vijayan, M. (1996) A novel mode of carbohydrate recognition in jacalin, a Moraceae plant lectin with a beta-prism fold. *Nat Struct Biol* 3, 596-603.

202. Dutta, S., Mazumdar, B., Banerjee, K. K., and Ghosh, A. N. (2010) Three-dimensional structure of different functional forms of the Vibrio cholerae hemolysin oligomer: a cryo-electron microscopic study. *J Bacteriol* 192, 169-178.

203. Menzl, K., Maier, E., Chakraborty, T., and Benz, R. (1996) HlyA hemolysin of Vibrio cholerae O1 biotype E1 Tor. Identification of the hemolytic complex and evidence for the formation of anion-selective ion-permeable channels. *Eur J Biochem* 240, 646-654.

204. Ikigai, H., Akatsuka, A., Tsujiyama, H., Nakae, T., and Shimamura, T. (1996) Mechanism of membrane damage by El Tor hemolysin of Vibrio cholerae O1. *Infect Immun* 64, 2968-2973.

205. Zhang, D., Takahashi, J., Seno, T., Tani, Y., and Honda, T. (1999) Analysis of receptor for Vibrio cholerae El tor hemolysin with a monoclonal antibody that recognizes glycophorin B of human erythrocyte membrane. *Infect Immun* 67, 5332-5337.

206. Harris, J. R., and Palmer, M. (2010) Cholesterol specificity of some heptameric beta-barrel pore-forming bacterial toxins: structural and functional aspects. *Subcell Biochem* 51, 579-596.

207. Krasilnikov, O. V., Merzlyak, P. G., Lima, V. L., Zitzer, A. O., Valeva, A., and Yuldasheva, L. N. (2007) Pore formation by Vibrio cholerae cytolysin requires cholesterol in both monolayers of the target membrane. *Biochimie* 89, 271-277.

208. Yuldasheva, L. N., Merzlyak, P. G., Zitzer, A. O., Rodrigues, C. G., Bhakdi, S., and Krasilnikov, O. V. (2001) Lumen geometry of ion channels formed by Vibrio cholerae EL Tor cytolysin elucidated by nonelectrolyte exclusion. *Biochim Biophys Acta* 1512, 53-63.

209. Huang, J., and Feigenson, G. W. (1999) A microscopic interaction model of maximum solubility of cholesterol in lipid bilayers. *Biophys J* 76, 2142-2157.

210. Zitzer, A., Palmer, M., Weller, U., Wassenaar, T., Biermann, C., Tranum-Jensen, J., and Bhakdi, S. (1997) Mode of primary binding to target membranes and pore formation induced by Vibrio cholerae cytolysin (hemolysin). *Eur J Biochem* 247, 209-216.

211. Ichinose, Y., Yamamoto, K., Nakasone, N., Tanabe, M. J., Takeda, T., Miwatani, T., and Iwanaga, M. (1987) Enterotoxicity of El Tor-like hemolysin of non-O1 Vibrio cholerae. *Infect Immun* 55, 1090-1093.

212. Paul, K., and Chattopadhyay, K. (2012) Single point mutation in Vibrio cholerae cytolysin compromises the membrane pore-formation mechanism of the toxin. *FEBS J* 279, 4039-4051.

213. Ikigai, H., Otsuru, H., Yamamoto, K., and Shimamura, T. (2006) Structural requirements of cholesterol for binding to Vibrio cholerae hemolysin. *Microbiol Immunol* 50, 751-757.

214. Rai, A. K., and Chattopadhyay, K. (2015) Revisiting the membrane interaction mechanism of a membrane-damaging beta-barrel pore-forming toxin Vibrio cholerae cytolysin. *Molecular microbiology*.

215. Lomize, M. A., Pogozheva, I. D., Joo, H., Mosberg, H. I., and Lomize, A. L. (2012) OPM database and PPM web server: resources for positioning of proteins in membranes. *Nucleic Acids Res* 40, D370-376.

216. Lakowicz, J. R. (2006) *Principles of Fluorescence Spectroscopy*, 3rd ed., Springer, New York.

217. Mazumdar, B., Ganguly, S., Ghosh, A. N., and Banerjee, K. K. (2011) The role of C-terminus carbohydrate-binding domain of Vibrio cholerae haemolysin/cytolysin in the

conversion of the pre-pore beta-barrel oligomer to a functional diffusion channel. *Indian J Med Res* 133, 131-137.

218. Chattopadhyay, K., Bhattacharyya, D., and Banerjee, K. K. (2002) Vibrio cholerae hemolysin. Implication of amphiphilicity and lipid-induced conformational change for its pore-forming activity. *Eur J Biochem* 269, 4351-4358.
219. Rai, A. K., and Chattopadhyay, K. (2014) Trapping of Vibrio cholerae cytolysin in the membrane-bound monomeric state blocks membrane insertion and functional pore formation by the toxin. *The Journal of biological chemistry* 289, 16978-16987.
220. Valeva, A., Palmer, M., and Bhakdi, S. (1997) Staphylococcal alpha-toxin: formation of the heptameric pore is partially cooperative and proceeds through multiple intermediate stages. *Biochemistry* 36, 13298-13304.
221. Bhakdi, S., Bayley, H., Valeva, A., Walev, I., Walker, B., Kehoe, M., and Palmer, M. (1996) Staphylococcal alpha-toxin, streptolysin-O, and Escherichia coli hemolysin: prototypes of pore-forming bacterial cytolysins. *Arch Microbiol* 165, 73-79.
222. Levan, S., De, S., and Olson, R. (2013) Vibrio cholerae cytolysin recognizes the heptasaccharide core of complex N-glycans with nanomolar affinity. *J Mol Biol* 425, 944-957.
223. Ramachandran, S., Kota, P., Ding, F., and Dokholyan, N. V. (2011) Automated minimization of steric clashes in protein structures. *Proteins* 79, 261-270.
224. Martner, A., Dahlgren, C., Paton, J. C., and Wold, A. E. (2008) Pneumolysin released during Streptococcus pneumoniae autolysis is a potent activator of intracellular oxygen radical production in neutrophils. *Infect Immun* 76, 4079-4087.
225. Walker, B., Krishnasastry, M., Zorn, L., and Bayley, H. (1992) Assembly of the oligomeric membrane pore formed by Staphylococcal alpha-hemolysin examined by truncation mutagenesis. *J Biol Chem* 267, 21782-21786.
226. Loris, R. (2002) Principles of structures of animal and plant lectins. *Biochimica et biophysica acta* 1572, 198-208.
227. Li, J. D., Carroll, J., and Ellar, D. J. (1991) Crystal structure of insecticidal delta-endotoxin from Bacillus thuringiensis at 2.5 A resolution. *Nature* 353, 815-821.

228. Rai, A. K., Paul, K., and Chattopadhyay, K. (2013) Functional mapping of the lectin activity site on the beta-prism domain of vibrio cholerae cytolysin: implications for the membrane pore-formation mechanism of the toxin. *J Biol Chem* 288, 1665-1673.

229. Wiseman, T., Williston, S., Brandts, J. F., and Lin, L. N. (1989) Rapid measurement of binding constants and heats of binding using a new titration calorimeter. *Anal Biochem* 179, 131-137.

230. Arnold, K., Bordoli, L., Kopp, J., and Schwede, T. (2006) The SWISS-MODEL workspace: a web-based environment for protein structure homology modelling. *Bioinformatics* 22, 195-201.

231. Emsley, P., Lohkamp, B., Scott, W. G., and Cowtan, K. (2010) Features and development of Coot. *Acta Crystallogr D Biol Crystallogr* 66, 486-501.

232. Ganguly, S., Mukherjee, A., Mazumdar, B., Ghosh, A. N., and Banerjee, K. K. (2014) The beta-Prism Lectin Domain of Vibrio cholerae Hemolysin Promotes Self-assembly of the beta-Pore-forming Toxin by a Carbohydrate-independent Mechanism. *J Biol Chem* 289, 4001-4008.

233. Iacovache, I., van der Goot, F. G., and Pernot, L. (2008) Pore formation: an ancient yet complex form of attack. *Biochim Biophys Acta* 1778, 1611-1623.

234. Collier, R. J. (1975) Diphtheria toxin: mode of action and structure. *Bacteriol Rev* 39, 54-85.

235. Lohner, S., Walev, I., Boukhallouk, F., Palmer, M., Bhakdi, S., and Valeva, A. (2009) Pore formation by Vibrio cholerae cytolysin follows the same archetypical mode as beta-barrel toxins from gram-positive organisms. *FASEB J* 23, 2521-2528.

236. Subramaniam, S. (1998) The Biology Workbench--a seamless database and analysis environment for the biologist. *Proteins* 32, 1-2.

237. Thompson, J. D., Higgins, D. G., and Gibson, T. J. (1994) CLUSTAL W: improving the sensitivity of progressive multiple sequence alignment through sequence weighting, position-specific gap penalties and weight matrix choice. *Nucleic Acids Res* 22, 4673-4680.

238. Gouet, P., Courcelle, E., Stuart, D. I., and Metoz, F. (1999) ESPript: analysis of multiple sequence alignments in PostScript. *Bioinformatics* 15, 305-308.

239. Han, J. H., Lee, J. H., Choi, Y. H., Park, J. H., Choi, T. J., and Kong, I. S. (2002) Purification, characterization and molecular cloning of Vibrio fluvialis hemolysin. *Biochimica et biophysica acta* 1599, 106-114.

240. Rader, A. E., and Murphy, J. R. (1988) Nucleotide sequences and comparison of the hemolysin determinants of Vibrio cholerae El Tor RV79(Hly+) and RV79(Hly-) and classical 569B(Hly-). *Infect Immun* 56, 1414-1419.

241. CCP4 (Collaborative Computational Project, N. (1994) The CCP4 suite: programs for protein crystallography. *Acta Crystallogr D Biol Crystallogr* 50, 760-763.

242. Gonzalez, M. R., Bischofberger, M., Pernot, L., van der Goot, F. G., and Freche, B. (2008) Bacterial pore-forming toxins: the (w)hole story? *Cell Mol Life Sci* 65, 493-507.

243. Iacovache, I., Bischofberger, M., and van der Goot, F. G. (2010) Structure and assembly of pore-forming proteins. *Curr Opin Struct Biol* 20, 241-246.

244. Tilley, S. J., and Saibil, H. R. (2006) The mechanism of pore formation by bacterial toxins. *Current opinion in structural biology* 16, 230-236.

245. Hotze, E. M., Wilson-Kubalek, E., Farrand, A. J., Bentsen, L., Parker, M. W., Johnson, A. E., and Tweten, R. K. (2012) Monomer-monomer interactions propagate structural transitions necessary for pore formation by the cholesterol-dependent cytolysins. *J Biol Chem* 287, 24534-24543.